ABSTRACT

SENSORIMOTOR CONTENT OF MULTI-UNIT ACTIVITY RECORDED IN THE PARAMEDIAN LOBULE OF THE CEREBELLUM USING CARBON FIBER MICROELECTRODE ARRAYS

by
Esma Cetinkaya

Based on Center for Disease Control and Prevention report 2016, around 39.5 million people in the United States suffer from motor disabilities. These disabilities are due to traumatic conditions like traumatic brain injury (TBI), neurological diseases such as amyotrophic lateral sclerosis (ALS), or congenital conditions. One of the approaches for restoring the lost motor function is to extract the volitional information from the central nervous system (CNS) and control a mechanical device that can replace the function of a paralyzed limb through systems called Brain-Computer Interfaces (BCI).

One of the major challenges being faced in BCIs and also in general neural recording field is the limitations of the microelectrodes. In this study, as the first aim, a custom-made micro-electrode array (MEA) using carbon fibers is developed. After *ex vivo* testing, they are implanted into the paramedian lobule (PML) of the rat cerebellum to record the multi-unit activity from its cortex. Following animal termination, tissue samples are examined with histological techniques for the assessment of tissue damage caused by the electrodes.

Another challenge in the BCI field is extracting the control information regarding the intended motor function from the CNS. The way the cerebellar cortex encodes sensorimotor information and contributes to motor coordination has been a topic of discussion for decades. Recent studies have revealed high correlations between Purkinje cell simple spikes and the forelimb kinematics in experimental animals. However, tracking single spike activity in long-term implants with multi-channel electrodes has well-known challenges. Therefore, as the second aim of this study, the correlation of multi-unit neural signals from the paramedian lobule (PML) of the cerebellar cortex to the forelimb muscle activities (EMG) in rats during behavior was investigated. Linear regression is performed to predict the EMG signal envelopes using the cerebellar activity for various time shifts of the data (±10, ±50, ±100, and ±200 ms) to determine if the neural signals are primarily motor or sensory. The highest correlations (~0.6 on average) between neural and EMG envelopes are observed when the EMG signals are either shifted only about ±10 ms or not shifted at all with respect to the neural signals. There were however still correlations above the chance level for larger shifts in time. The results suggest that PML cortex contains both motor and sensory information in relation to the forelimb activity, and also that the extraction of motor information is feasible from multi-unit neural recordings from the cerebellar cortex. Increased prediction success was observed in reaching and retrieval phases compared to grasping phase when predictions were tested on three phases of the behavior separately. When EMG and neural signal envelopes were clustered, they showed patterns of surges of activity in all three phases. The neural signals showed higher activity in the reaching phase. The 300-1000Hz components of neural signals contributed to the predictions more than the other frequency bands. The results of this study supports the feasibility of a BCI based on MUA extracted from the cerebellar cortex using MEAs.

SENSORIMOTOR CONTENT OF MULTI-UNIT ACTIVITY IN THE PARAMEDIAN LOBULE OF THE CEREBELLUM

by
Esma Cetinkaya

A Dissertation
Submitted to the Faculty of
New Jersey Institute of Technology
And Rutgers Biomedical and Health Sciences
in Partial Fulfillment of the Requirements for the Degree of
Doctor of Philosophy in Biomedical Engineering

Department of Biomedical Engineering

August 2022

APPROVAL PAGE

SENSORIMOTOR CONTENT OF MULTI-UNIT ACTIVITY IN THE PARAMEDIAN LOBULE OF THE CEREBELLUM

Esma Cetinkaya

Dr. Mesut Sahin, Dissertation Advisor Date
Professor of Biomedical Engineering, NJIT

Dr. Bryan J. Pfister, Committee Member Date
Chair and Professor of Biomedical Engineering, NJIT

Dr. Stella Elkabes, Committee Member Date
Professor of Neuroendocrinology, Rutgers University, Newark, NJ

Dr. Eric Lang, Committee Member Date
Associate Professor of Department of Neuroscience and Physiology,
New York University, New York, NY

Dr. Ozlem Gunal, Committee Member Date
Assistant Professor of Department of Psychiatry, Rutgers University, Newark, NJ

BIOGRAPHICAL SKETCH

Author: Esma Cetinkaya

Degree: Doctor of Philosophy

Date: August 2022

Undergraduate and Graduate Education:

- Doctor of Philosophy in Biomedical Engineering,
  New Jersey Institute of Technology, New Jersey, Newark, 2022

- Master of Science in Medical Physics,
  Istanbul University, Istanbul, Turkey, 2013

- Bachelor of Science in Physics Engineering,
  Gaziantep University, Gaziantep, Turkey, 2009

Major: Biomedical Engineering

Presentations and Publications:

Journal Paper:

Ordek, G., Asan, A. S., Cetinkaya, E., Skotak, M., Kakulavarapu, V. R., Chandra, N., and Sahin, M. (2018). "Electrophysiological Correlates of Blast-Wave Induced Cerebellar Injury" Nature Scientific Reports 8(1): 13633.

Conference Proceedings:

Cetinkaya, E., Gok, S., and Sahin, M. (2018). “Carbon Fiber Electrodes for In Vivo Spinal Cord Recordings" Proceedings of the 40th Annual International Conference of the Institute of Electrical and Electronics Engineers (IEEE) Engineering in Medicine and Biology Society (EMBS), Honolulu, HI.

Cetinkaya, E., Gok, S., and Sahin, M. (2019). “Volitional Signals Recorded from the Cerebellar Cortex Using Carbon Fiber Electrodes” Proceedings of the 2019 Biomedical Engineering Society (BMES) Annual Meeting, Philadelphia.

Presentations:

Cetinkaya, E., Gok, S., and Sahin, M. (2018). “Carbon Fiber Electrodes for In Vivo Spinal Cord Recordings” Proceedings of the 40th Annual International Conference of the Institute of Electrical and Electronics Engineers (IEEE) Engineering in Medicine and Biology Society (EMBS), Honolulu, HI.

Cetinkaya, E., Gok, S., and Sahin, M. (2019). “Volitional Signals Recorded from the Cerebellar Cortex Using Carbon Fiber Electrodes” Proceedings of the 2019 Biomedical Engineering Society (BMES) Annual Meeting, Philadelphia.

Posters:

Cetinkaya, E. and Sahin, M. (2022). “Motor Correlates of Cerebellar Activity Recorded with Carbon Electrode Arrays” The Brain Initiative Meeting, Online Meeting.

Cetinkaya, E., Gok, S., and Sahin, M. (2017). “Carbon Fiber Electrodes for Recording Spinal Cord Activity in Rats” Biomedical Engineering Society (BMES), Phoenix.

Asan, A. S., Ordek, G., Cetinkaya, E., Skotak, M., Kakulavarapu, V., Chandra, N., and Sahin, M. (2017). “Assessment of Cerebellar Injury Using Micro EcoG Technique and a Behavior Paradigm in Rats” Biomedical Engineering Society (BMES), Phoenix.

Ali, A., Sahin, M., and Cetinkaya, E. (2016). “The Fabrication of a Novel Microelectrode for Interfacing with the Brain” 9th International Undergraduate Summer Research Symposium, New Jersey.

Uslu, N., Dizman, A., Cetinkaya, E., Oner, K., Arslan, S., Kaya, P., and Aksu, R. (2015). “Multimodal Treatment Approach for Infant Patient with Wilm`s Tumor” 21st National Cancer Congress, Antalya/Turkey.

Uslu, N., Soykut, E., Kucukpilakci, B., and Cetinkaya, E. (2014) “Case Study: Intensity Modulated Radiotherapy (IMRT) Application to a Patient with Recurred Skin Cancer Located at Medial Cantus with Dural Extension” 11th National Radiation Oncology Congress, Antalya/Turkey.

Oner, K. and Cetinkaya, E. (2013). “Comparing Conformal Radiotherapy Plans of Low Risk Prostate Cancer Patients: Analysis of Treatment Planning System Algorithms of Prowess Panther and CMS” 14th Medical Physics Congress, Antalya/Turkey.

“Let the beauty of what you love be what you do."

Rumi

ACKNOWLEDGMENT

First of all, I would like to express my deepest gratitude for my dissertation advisor, Dr. Mesut Sahin, for his support and help throughout my dissertation, particularly at times of difficulty and facing obstacles.

Also I would like to thank to my Committee Members: Drs. Bryan Pfister, Stella Elkabes, Eric Lang, and Ozlem Gunal for their guidance and advice during the writing stage of my dissertation. I had the opportunity to have access to laboratories of Dr. Elkabes and Dr. Pfister to perform the histological assays of the cerebellum. I am thankful to them for letting me use their facilities and give me a chance to learn from them. Especially Dr. Elkabes and her students accommodated me for months for me to learn various techniques of tissue staining, for which I am grateful. Dr. Gunal made me realize very important points I had overlooked in my discussions of the results. The detailed feedbacks I received from Dr. Lang on my writing have been extremely valuable for me to see the big picture.

I would also like to acknowledge The Republic of Turkey Ministry of Education and New Jersey Commission on Brain Injury Research Committee (Grant #: CBIR19FEL020) for providing financial support during my PhD.

Additionally, my thanks to all Neural Prosthetics Laboratory members, for their help when I needed, encouragement, and friendship that I will always cherish.

Last but not least, I would like to thank my dear mother and entire family for supporting, encouraging, and trusting me during this journey as they have in every stage of my life.

TABLE OF CONTENTS

TABLE OF CONTENTS
(Continued)

Chapter **Page**

TABLE OF CONTENTS
(Continued)

Chapter **Page**

TABLE OF CONTENTS
(Continued)

Chapter **Page**

LIST OF FIGURES

LIST OF FIGURES
(Continued)

LIST OF FIGURES
(Continued)

LIST OF FIGURES
(Continued)

LIST OF FIGURES
(Continued)

LIST OF FIGURES
(Continued)

LIST OF FIGURES
(Continued)

LIST OF FIGURES
(Continued)

LIST OF SYMBOLS

®	Registered
#	Number Sign
~	Approximately
µm	Micrometer
mm	Millimeter
sec	Second
ms	Millisecond
ºC	Celsius Degree
mV	Millivolt
µV	Microvolt
Hz	Hertz
kHz	Kilohertz
v/v	Volume/volume
GPa	Gigapascal
MPa	Megapascal
g	Gram
mN	Millinewton
Ω	Ohm

CHAPTER 1

INTRODUCTION

1.1 Objective

The main objective of this dissertation is to extract volitional motor information from the cerebellar signals by demonstrating the correlation between cerebellar neural signals and kinematic parameters.

The ultimate purpose of this work is to help patients with motor disability by making a contribution to our understanding of the volitional information contained in the cerebellar neural activity. We aim to investigate characteristics of cerebellar signals during motor behavior, and particularly the kinematic parameters of forelimb movement. The extracted volitional motor information can be potentially used for a brain-computer interface (BCI) system that can predict and substitute for the motor function based on neural signals from the cerebellum.

This project has two goals. The first one is to develop a novel carbon fiber microelectrode array (CFMEA) designed for the rat cerebellum. The second one is to understand the cerebellar neural activity of the paramedian lobule (PML) of the cerebellum during behavior, specifically during forelimb motor movements in the rat, and determine its correlation with electromyogram (EMG) and force signals.

1.2 Organization

This dissertation is divided into three chapters. This chapter presents the objectives, the clinical significance of this work, and theoretical background for this study. Chapter 2 presents the methodology developed for microelectrode array development and testing of the electrodes for their recording capabilities by chronically implanting them in the cerebellum and the spinal cord. Lastly, Chapter 3 includes the data collected and the results of data analysis towards exploring the presence of motor information in the cerebellum relevant to the forelimb muscle EMGs and the force signals.

1.3 Clinical Significance

1.3.1 Motor Disabilities and Clinical Significance of Brain Computer Interfaces

Either traumatic injuries, neurological diseases, or congenital conditions cause motor disabilities. Some of these conditions that result in motor disabilities are traumatic brain injury (TBI), cerebral palsy, multiple sclerosis, amyotrophic lateral sclerosis (ALS), Parkinson`s disease, and locked-in syndrome. Based on Center for Disease Control and Prevention (CDC) report in 2016 (Centers for Disease Control and Prevention 2016), the number of adults in United States (U.S.) with difficulties in physical functioning is 39.5 million. These people face various challenges of communication and motor impairments at different levels. Because of this reason, they need adaptive and personalized rehabilitation options. To this end, BCI systems have been developed to meet this need. BCIs record brain signals that generate a specific motor function and reconstruct the required signal to restore the missing or lost motor function which is what people with motor disabilities need. There have been human studies showing how a neurally controlled robotic arm can help people with tetraplegia to restore reach and grasp movement (Hochberg et al. 2012). However, in general, these systems still in the testing and development stages and not in standardized clinical practice due to problems encountered in obtaining volitional signals from the central nervous system (CNS) for the fine motor control.

1.4 Microelectrode Development

1.4.1 Microelectrodes

Carbon fiber (CF) microelectrodes have been widely used for neurotransmitter concentration measurements for a long time owing to carbon fiber`s unique properties (Huffman and Venton 2009). Recordings of extracellular neural activity with microelectrodes were first demonstrated in the 1950s and since then several types have been developed. Most common types are Michigan shank electrodes, wire electrodes, and the Utah array. There are companies such as BrainGate, NeuroNexus, and Tucker-Davis Technology that manufacture these types of electrodes according to customer specifications.

Microelectrodes for electrophysiology applications are of two types: recording and/or stimulation microelectrodes. Recording microelectrodes record single unit or multi-unit activity (MUA) or local field potentials (LFPs). Multi-unit recordings mostly show varying spike durations and amplitudes since they are the summation of activity from multiple neurons while the single unit spike durations and amplitudes are more consistent (Brookhart, Moruzzi, and Snider 1950). Stimulation electrodes on the other hand, activate neurons extracellularly by applying a current into the tissue.

1.4.2 Microelectrode Development Parameters

Four main parameters are crucial for electrode quality (Wellman et al. 2018): electrode material, insulation, electrode active area, and electrode size/geometry.

Electrode material determines electrode`s electrical, mechanical, and chemical stability. An ideal electrode material should have low electrical impedance, long-term functional durability, small cross-sectional area, and electrochemical/mechanical stability. CF is one of the most suitable electrode materials due to its strength, flexibility, small surface area, and high conductivity. Nickel-chrome (or Nichrome or NiCh) is another common material with high strength, high conductivity, chemical durability, and low cost.

Insulation material on the electrode surface works as a dielectric layer to prevent signal leak into the tissue. It is also important to limit cross talk between electrodes in multichannel designs, which deteriorates recordings especially in high-resolution array electrodes. If the electrode coating cracks, a short circuit forms, and also causes corrosion and failure of the electrode.

Deinsulating CF electrode’s active site is an important step that determines the electrode characteristics. For this process, various techniques are used by different groups such as a burning the insulation with a flame (Guitchounts et al. 2013), making a razor cut (Guitchounts et al. 2013), or using a laser beam to remove the insulation at the tip (Welle et al. 2020). In selection of these techniques, impedance variation, unwanted cracking, and delamination of the coating due to the technique selected should be considered.

The electrode geometry determines if a microelectrode can effectively stimulate neurons or record signals from. Densely placed electrodes in an array can record from more neurons in a local area, therefore a small distance between channels (pitch) is preferred. Simulations conducted to compare different pitch values show that the smallest inter-electrode distance to maximize the number of neurons recorded from is about 16 micrometer (Viswam et al. 2019). However, the volume of tissue displaced by the electrode arrays can induce a significant trauma to the surrounding neurons as the number of channels and the number of shanks are increasing. Moreover, even though electrodes with thousands of contacts on each shank can be fabricated, physically connecting so many channels to the recording amplifiers or telemetering the recorded neural signals to an extracorporeal unit becomes a technological bottleneck. Long electrode shanks are also desired sometimes to record from neurons in different layers of the cortex.

1.4.3 The Challenges in Microelectrode Technology

While microelectrodes are used in neuroscience research for neural signal recording or electrical stimulation of the nervous system in this study the focus will be given to neural signal recording with carbon microelectrodes.

Microelectrodes with variety of designs are commercially available, but the current technology is limited in a number of ways. Some of these limitations are long term stability (a challenge for chronic studies), difficulties in the fabrication process (need to use advanced technologies and facilities that not all laboratories can provide), and inducing significant tissue response due to mechanical mismatch of the electrode properties with neural tissue. The microelectrodes that will be implanted especially into the parts of the central nervous system that experience large displacements, like spinal cord and the cerebellum (or the peripheral nervous system) require more flexibility.

Thus, microelectrode development is an active and a popular research field. Improvements in microelectrode fabrication methods will help the BCI technology transition from research settings to clinical environment and allow more reliable and detailed brain mapping.

Two main goals of electrode technology are maximizing the electrode longevity and minimizing the tissue damage during implantation acutely and in the long term. These two goals are also the criteria for chronic *in vivo* validation of microelectrodes. Initial insertion of the electrode is the first traumatic damage to cellular network and vasculature and initiates an inflammatory tissue response.

Studies mostly point out that large electrode size, high electrode stiffness, and electrode-tissue mechanical mismatch are important, but they also highlight that the electrode size is the most effective factor (Patel et al. 2016). Macrophages migrate to the implant area to get rid of the microelectrode. Electrodes can cause neuronal cell death depending on their size and the physical properties of the electrode material. Glial cells (mostly astrocytes and microglia) are sent to form a scar tissue (encapsulation) around microelectrodes.

The amplitudes of the signals decrease because of the increased distance between electrodes and recorded neurons due to encapsulation. Thus, a major drawback of the encapsulation is the electrode failure over time that impedes chronic recordings and limits microelectrode longevity. After approximately two weeks, the thickness of encapsulation around the electrodes reaches a peak of ~200 μm, then the tightening starts, and finally 12 weeks later it stabilizes around 100 μm (Patel et al. 2015). If an electrode is still functioning after 12 weeks, the electrode will most likely stay liable in the long term because after this time point tissue response generally does not change substantially (Patel et al. 2016). The extracellular medium can limit the lifetime of an electrode by damaging the coating. Even if an electrode survives the mechanical stress induced by the micro motion of the surrounding tissue, its electrical properties, such as the impedance, may change and lead to decreased signal quality and eventually failure to record.

1.5 Sensorimotor Content of Multi-Unit Activity in The Paramedian Lobule of The Cerebellum

1.5.1 Information Extraction, Its Purpose, and The Role of Microelectrodes

Fritsch and Hitzig in 1870 with their groundbreaking article ‘The excitable cerebral cortex’ (G.Fritsch and E.Hitzig 1870) proved that the cerebral cortex is involved in various functions, and each of these functions are encoded in specific cerebral brain regions (Carlson and Devinsky 2009). During the course of many years using low-intensity surface stimulation, brain maps were generated (Schwartz 2007). However, more intensive studies showed that motor movements are in fact controlled by and represented in multiple cortical areas (Phillips and Porter 1977). Also, the neural control of coordinated muscle activity that occurs during volitional movement is more complicated than it was once thought (Schwartz 2007).

Understanding the signals underlying the motor process that creates behavior and to extract the volitional signals for potential therapeutic applications is one important goal of neural engineering (Schwartz 2007). This goal can be achieved by simultaneous recordings of various correlates of a motor function such as neural activity, muscle activity, position, and velocity to quantify the behavior. The choice of neural data type depends on the types of recording system used. For example, EEG recordings provide limited spatial resolution and signals generally in the frequency range of 1-30 Hz; with glass electrodes in acute experiments it is feasible to record single-unit activity, while in chronic studies signals are mostly local field potentials (LFPs) with some single-unit activity unless the electrode depth can be adjusted over time to relocate and track single cells. Therefore, multi-unit activity or LFP signals tend to be much more stable over time in chronic studies compared to single cell recording. In this study the primary neural signal types that we target to understand motor movement are LFPs and multi-unit activities. The reason for using the population activity instead of single unit activity is that the information contained in the activity of individual neurons is very noisy and the brain encodes information in populations of neurons (Averbeck, Latham, and Pouget 2006). Furthermore, maintaining single unit activity over the course of a chronic study is shown to be challenging.

Volitional components in neural signals can be demonstrated by testing the correlation between them and the motor function. This is done by simultaneous recordings of the neural activity and the output function such as the muscle activity or kinematic parameters (e.g., limb position or velocity). Although non-invasive technics like EEG is available, microelectrodes provide richer signals with higher spatial and temporal resolution and signal-to-noise ratio.

1.5.2 Cerebellar Anatomy and Functions

The word cerebellum is Latin for “little brain”. It is the largest part of the hind brain and located in the posterior cranial fossa. It has two hemispheres connected by the vermis and has outer grey and inner white matters.

The well-known functions of the cerebellum are maintenance of balance and posture. It is involved in precision in timing and smoothness of the movement. Motor learning is also one of the functions of the cerebellum. In general, the cerebellum`s contribution to the motor movement has been considered as limited to the coordination of the motor functions. However, in the last few decades, even higher order cognitive function has been reported to involve the cerebellum (Rapoport 2000).

Direct injury to the cerebellum is very rare because of its well protected anatomical position tugged underneath the cerebrum. However, indirect cerebellar injury due to trauma is very common (Potts, Adwanikar, and Noble-Haeusslein 2009). Cerebellar injury mostly causes coordination problems in movement. The cerebellar cortex has a highly organized canonical anatomy with molecular layer, Purkinje Cell (PC) layer, and granular layer (Figure 1.1 A) and zones (up to ~500 µm) / microzones (up to ~100 µm) (Figure 1.1 B).

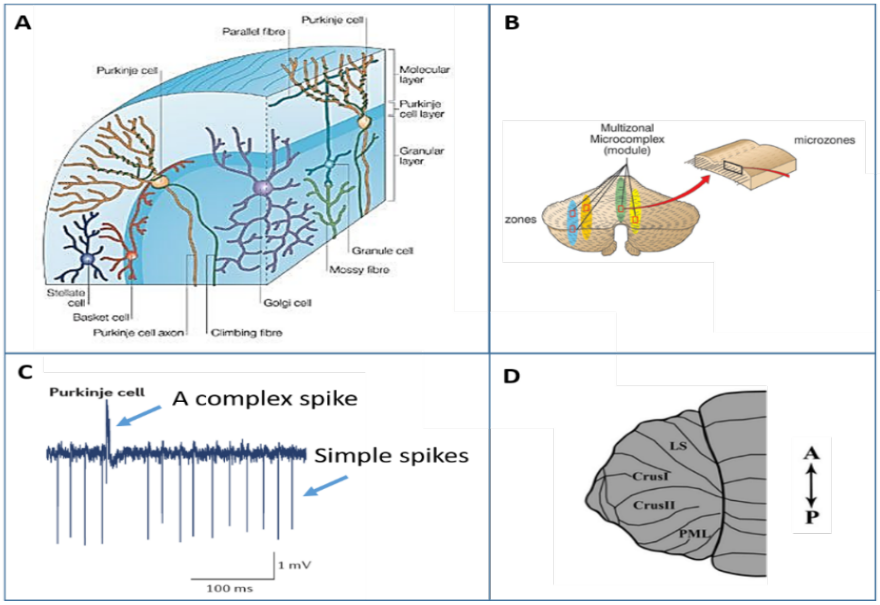

Figure 1.1 A) Layers of the cerebellar cortex. B) Cerebellum zones and microzones C) A Purkinje cell complex and simple spikes D) Anatomical structure of one cerebellar hemisphere and the location of the PML

Source: A) (Apps and Garwicz 2005) B) (D’Angelo and Casali 2012) C) (Zeeuw et al. 2011) D) (Rylkova, Crank, and Linden 2015)

1.5.3 Cerebellar Neurophysiology

Neuronal cell count in the cerebellum comprises about 80% of the total neurons in the brain (Herculano-Houzel 2010). On the other hand, glial cells as a percentage is lower in the cerebellum compared to the cerebral cortex, which lowers the cerebellum’s healing capacity after injury. The afferent pathways to the cerebellum are the climbing fibers and the mossy fibers. PCs are the main and only output neurons from the cerebellar cortex and together with deep cerebellar nuclei the cerebellar cortical networks are responsible for motor coordination, learning, and cognitive functions (Orozco et al. 2010).

Most of the computation in the cerebellar cortex occurs in the molecular layer. One type of afferents, parallel fibers to the molecular layer, originate in the granular layer, while the other afferent, climbing fibers, originate from the inferior olive (Armstrong and Drew 1980). Several studies pointed out that PCs are at the center of computation in the cerebellar cortex (Fernández-Guardiola et al. 1962). PCs are one of the largest neurons in the brain with a diameter of 25-40 µm (Herndon 1963) and have large dendritic trees to synapse an average of ~175,000 parallel fibers in the rat (Napper and Harvey 1988). PCs have two types of action potentials: 1) simple spikes (SSs) (20-187 Hz, (Chen, Augustine, and Chadderton 2016)), or up to 250 Hz (Zeeuw et al. 2011)) modulated by the activity of parallel fibers (excitation), molecular layer interneurons (inhibition), and Golgi cells indirectly, and 2) complex spikes (CSs) (0.5-3.3 Hz, (Chen, Augustine, and Chadderton 2016), (Zeeuw et al. 2011)) induced by the climbing fibers (Figure 1.C). SSs are spontaneously occurring single spikes in the PCs and can be modulated by synaptic input signals from the parallel fibers and the inhibitory neurons (Harmon et al. 2017) while complex spikes have an initial high-amplitude single spike followed by several low amplitude spikelet bursts followed by a characteristic pause (climbing fiber pause).

1.5.4 Spatiotemporal Coding

In recent years, new mechanisms about the brain`s information processing systems have been discovered. One well-known and established system, the rate coding, says that alternating firing rate is an information encoding method between brain regions. Recent studies introduced an additional communication paradigm, the spatiotemporal coding. Olivocerebellar system creates precise spatiotemporal patterns of CSs during motor movement acquisition (Zeeuw et al. 2011).

There are different opinions about the spatiotemporal coding. Some characteristics of these patterns are SS and CS synchrony and olivary neuron oscillations at 2-4 Hz or 6-9 Hz. SSs and CSs affect each other and cerebellar nuclei (PCs send inhibitory signals to the cerebellar nuclei). One hypothesis is that SS synchrony regulates the timing of the action potentials in the cerebellar nuclei and CS synchrony results in cerebellar nuclei “rebound firing” (Zeeuw et al. 2011).

The mechanism and the degree of cerebellum`s contribution to motor function has been investigated by many researchers. In this study, we also attempted to contribute to this field by developing and testing the feasibility of carbon fiber microelectrode arrays that can record both multi-unit activity and single unit activity that can be utilized to extract volitional information (Han et al. 2017). The developed microelectrode array (MEA) with under ten-micron individual electrode sizes offers less tissue disturbance/replacement and with the array design provides recording ability from a 3D volume. Correlation between different types of neural signals from various regions of the cerebellum and the kinetic/kinematic parameters during motor function has been shown. For example, Chen *et al.* observed correlation between SS firing rates and whisker position, but no correlation was found with CSs (Chen, Augustine, and Chadderton 2016). Since SSs have much higher firing frequencies than the CSs, changes in the SS spike frequency is a strong candidate for representing the cerebellar contribution to the motor function during execution. Spikelets in the complex spikes poorly transfer to the cerebellar nuclei, and thus they cannot reflect instantaneous changes in motor function (Hewitt, Popa, and Ebner 2015). Heck suggests SS synchrony in the paramedian lobule are related to reaching movements (Heck, Thach, and Keating 2007). Popa proposed that position, velocity, and position errors are the most important parameters which can be extracted from population SSs for long term feedback and feedforward modulations and ultimately error correction and working memory (Popa, Streng, and Ebner 2017).

1.5.5 Cerebellar Electrophysiological Recordings in Behaving Animals with Multielectrode Recordings

In 1911, Cajal studied the neural cytoarchitecture of the cerebellum using Nissl staining (Cajal 1911). Research by Holmes contributed to the general understanding of the cerebellar function substantially with his observation on the cerebellar injured patients between 1917 and 1922 (Holmes 1917) [For a review (Breatnach 1975)]. Thach in 1968 in his monkey studies showed the changes in purkinje discharges and DCN activity during arm movements (Thach 1968). Marr was the first neuroscientist to describe the cerebellum as a computational unit by providing a model to explain how two excitatory inputs mossy and climbing fibers, interact with purkinje cells (Marr 1969; Strata 2009; Glickstein, Strata, and Voogd 2009). Ebner, Hewitt, and Popa specifically studied the role of the cerebellum in reaching kinematics in their several studies around 1980s. Armstrong in 1980 recorded cerebellar signals using surface and penetrating micro electrodes at different cortical depths (Armstrong and Drew 1980).

Spiking activity recording from single cells has been the golden standard for a long time to tap into the neural function. However, after Donald Hebb`s assertion that “neural assemblies form basic functional unit of operation of the mammalian central nervous system”, recording extracellular electrical activity of neural populations gained traction (Hebb 1949). In 1950, Brookhart performed the first extracellular microelectrode study using fine, wire microelectrodes in decerebrated and anesthetized cats (Brookhart, Moruzzi, and Snider 1950). In recent years, it has been shown that population activity can be used in decoding brain function (Mirfathollahi et al. 2022; Khorasani et al. 2018).

There has been studies exploring the cerebellum`s involvement in motor functions like skilled tongue, stepping or saccade movements in behaving animals using spike activity (Welsh et al. 1995; Sauerbrei, Lubenov, and Siapas 2015; Sedaghat-Nejada et al. 2022; Lang et al. 1999). However, studies investigating specifically forelimb reaching representation in the cerebellar cortex, using chronic recordings of neural activity in behaving animals with multichannel implantable electrodes are scarce (Milak, Bracha, and Bloedel 1995) (cerebellar nuclei recording in cats during trained reaching movement with SU activity) (Kitazawa, Kimura, and Yin 1998) (lobule IV-VI recordings in monkeys during trained reaching movement with SU) (Streng, Popa, and Ebner 2017) (lobule IV-VI recording in monkey during pseudo-random manual tracking task with SU). [For a review see (Therrien and Bastian 2019; Lang 2015)].

CHAPTER 2

CARBON FIBER MICROELECTRODE ARRAY DEVELOPMENT

2.1 Introduction

Neuroprosthetic technology aims to develop devices that can restore or replace the neural function lost due to injury or disease. Successful implementation of these goals depends on the availability of recording devices that can provide signals with high spatial resolution and without significant trauma to the neural tissue. The signals collected by chronic implementation of these devices in experimental animals has the potential to reveal new information about the brain functions and guide the development of new diagnostic and treatment options for neurological disorders.

These recording devices, or microelectrodes, impose two significant challenges: minimal tissue damage and the mechanical/electrical stability of the electrode after implantation, also known as electrode longevity. Even though commercially available microelectrodes have been commonly used in neuroprosthetic applications, their limitations, such as lack of flexibility and low channel counts were also reported. Thus, there is a need to develop microelectrodes that can yield signals with better quality and longevity without causing significant tissue damage. To achieve this challenging task two important factors, electrode material and mechanical properties, play a key role.

Carbon fiber is one of the most promising electrode materials owing to its strength and flexibility even at micrometer dimensions (Grill, Norman, and

Bellamkonda 2009). Carbon fibers` high tensile strength and flexibility allow fabrication of micro-scale electrodes that can withstand mechanical stress within the central nervous system (CNS). Although there are studies showing that carbon fiber has superior qualities as a potential electrode material, these studies are mostly restricted to the cortical tissue (Kozai et al. 2012). There is a need for a microelectrode design that can survive long implantation times in parts of the CNS that experience much larger translational and rotational movements, such as the spinal cord and cerebellum.

In this study, we developed high spatial resolution carbon fiber microelectrode arrays (CFMEA) and carbon fiber micro electrode bundle (CFMEB) for *in vivo* chronic cerebellum recordings. The manufacturing process included simple fabrication steps and basic equipment making it easy for others to replicate. After testing them *in vitro*, the electrodes were implanted for *in vivo* evaluation. Key outcomes of this study are the ability to record local field potentials (LFP), multi-units, and single-units and lesser amounts of tissue displacement compared to other penetrating electrodes, such as microwires. *In vivo* chronic neural recordings were collected in trained animals in the cerebellum. The electrophysiological signals were then analyzed to detect LFPs and single spikes. Finally, the tissue response to the electrode was demonstrated with immunohistochemistry.

2.2 Methodology

2.2.1 Electrode Fabrication

2.2.1.1 Carbon Fiber Microelectrode Array for the Cerebellum.

Coating Bare Carbon Fibers: Uncoated 7 μm diameter carbon fiber wires (Goodfellow Cambridge Ltd., England) were purchased. They were wound around a spool, all in one bundle, held together with epoxy. They were cured at 400˚C for 6 hours to remove the epoxy and easily separate them. Then each carbon fiber wire was placed on a frame with ~1cm distance. On each frame, 20±3 carbon fiber filaments with ~7 cm length (depending on the frame size) were placed. A total of 10 frames were sent to Specialty Coating Systems for

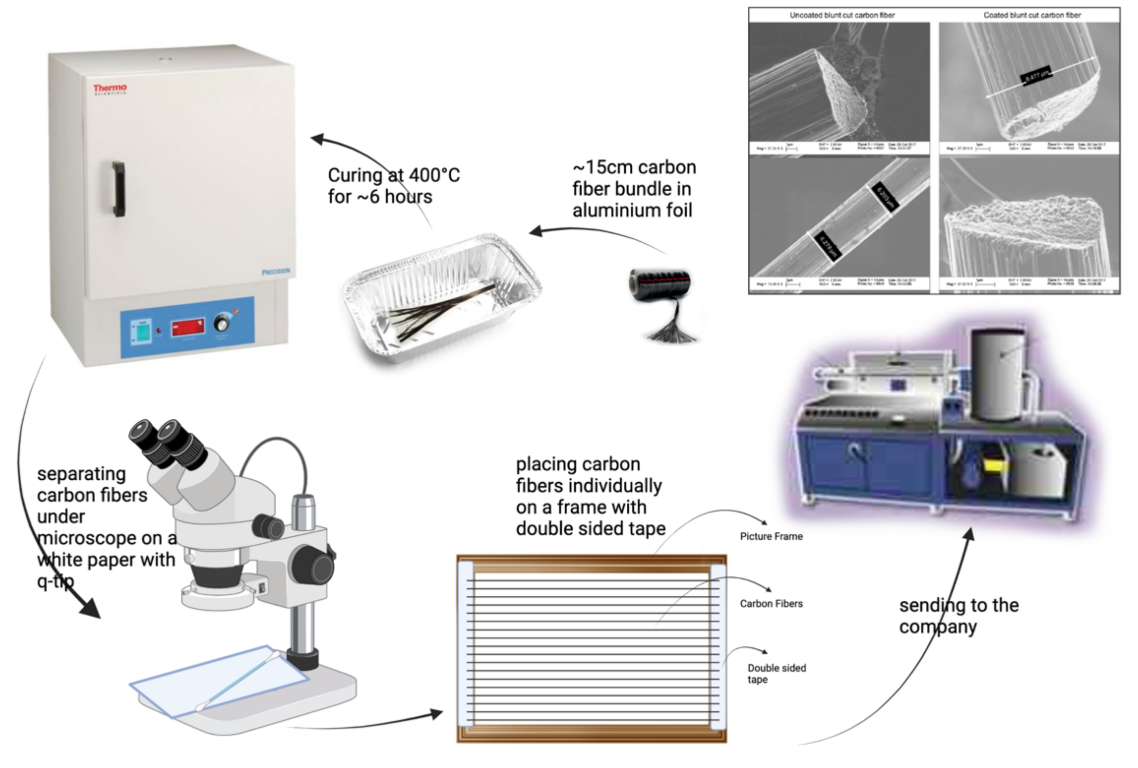

Figure 2.1 Carbon fiber coating procedure: Curing bundle carbon fibers, separating them, placing on frames, sending to the company.

approximately 1.5-micron thick parylene-C coating for the insulation purposes (The steps of this procedure can be seen in Figure 2.1).

A minimum thickness of a micron parylene-C coating should be targeted in order to ensure that there are no exposed electrode areas due to imperfections in the coating process (e.g. pinholes). In the first round of trials, 0.75 micron coating thickness was used by referring to other studies (Patel et al. 2016). Later experiments in our laboratory showed that for the technique we were using to desheath the coating, thicker insulation would be a better option for reproducible results.

Desheathing Carbon Fiber Tips: A glass slide with grid lines for each channel on the connector (from Channel 1 to 32) and a ~250 μm guideline to use as a reference to desheath carbon fiber tips at desired length was laser engraved

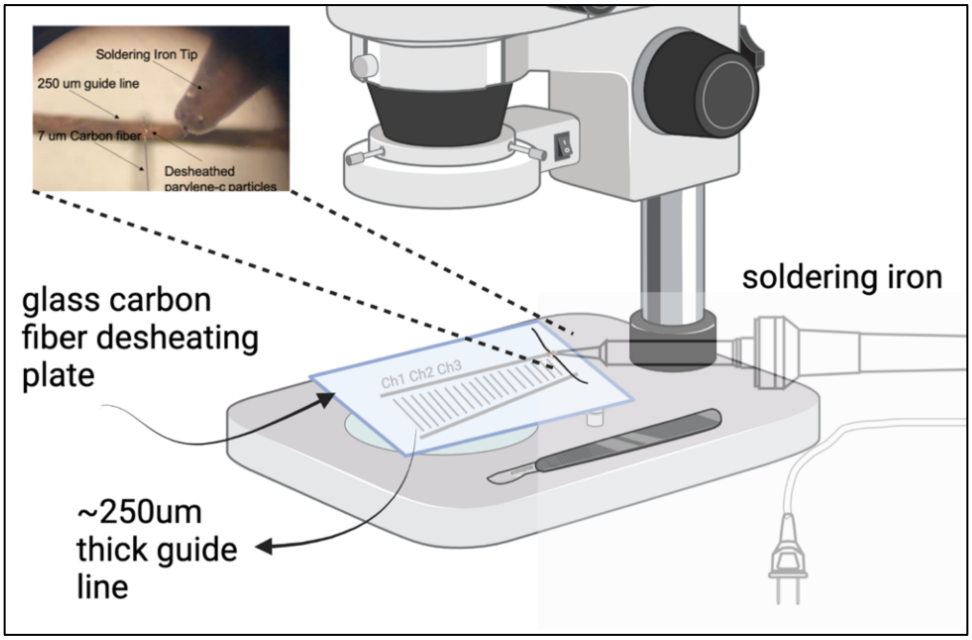

Figure 3.2 Carbon fiber desheathing setup using soldering iron. Small picture in the corner shows the desheated parylene-C particles after the desheathing method developed.

(Figure 2.2). Desheathing was performed with a soldering iron. The solder tip was customized by smoothening and sharpening it. The temperature during desheathing was kept at 290 ˚C, which is above the melting point for parylene-C. Desheathing parylene-C on the carbon fiber on a black surface allows visual confirmation of proper desheathing (The mechanism of this step can be seen in Figure 2.2).

Electrode holder: A connector holder apparatus is prepared to hold the connector during manufacturing process. A glass slide, stainless steel metal plates, a stainless-steel clip and dental acrylic are used to avoid deformation during heat curing in the heater that is required in later steps. In the Figure 2.3, “step” is used to assure that the carbon fibers are aligned exactly vertical in the array.

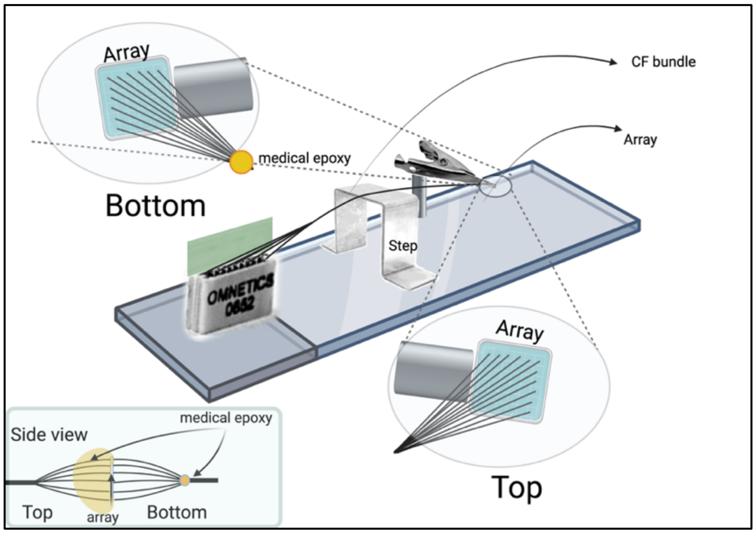

Figure 2.3 Electrode holder. The apparatus is made from heat resistive components to avoid deformation during curing process in the oven. Top view shows the array that is held by the metal clips, from the side closer to the connector and visualize how CFs are placed in the array mesh. Bottom view shows the array from the opposite side and shows how CFs that leaving the array bundled again to keep them straight. Small drawing in the left bottom shows the array from the side view to capture both top and bottom views together.

Electrode fabrication setup: A stand under the microscope to keep connector still during manufacturing was prepared. The stand has places to keep the electrode holder in three positions and it is fixed to the bench. The first position is to see the one side of the connector while connecting the carbon fiber and the second one is to see the other side. The third position is to place the connected carbon fibers to the designated positions on the array (Figure 2.4).

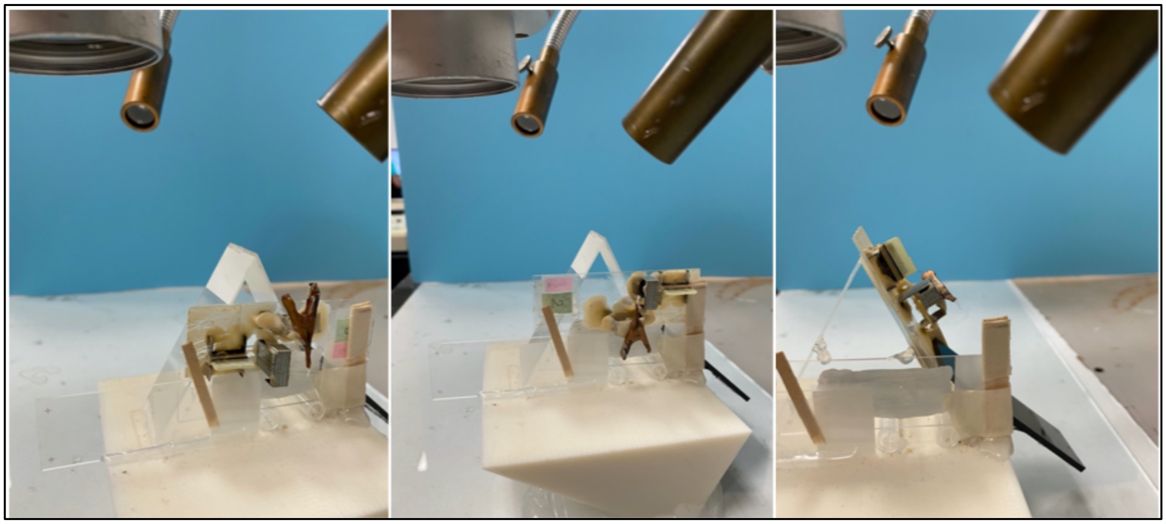

Figure 2.4 Electrode making setup. From left to right: 1: Positioning to connect CFs to one side of the connector. 2: Positioning to connect CFs to other side of the connector. 3: Positioning to place connected CFs to the designated position in the mesh array.

Preparing the connector and array: A 32-channels Omnetics connector with straight terminals is used. A piece of bare (nonconductive) laminate board is placed between the terminals. An array of 10 x 10 matrix (with a long extension on one side to hold with clips) was cut from nylon braided filter (CS Component Supply, TN, part number: U-CMN-18, mesh opening 18 μm, thread diameter 30 μm) (Figure 2.5).

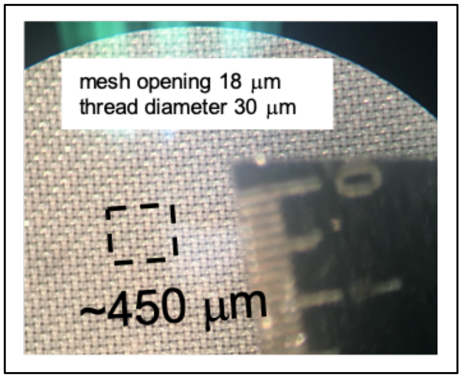

Figure 2.5 Cutting a 10 x 10 matrix substrate from the mesh for the array preparation.

Connecting carbon fibers to the connector: Electrical connection of carbon fibers to the connector is made by applying a small amount of silver epoxy (H20E, EpoTek, MA) to the terminals, placing carbon fibers (tips desheathed for around 0.25 mm) on top, and curing them in laboratory oven at ~200°C for ~7 minutes (Figure 2.6).

Reference and ground wires: For both reference and ground connections, around 1 cm, seven-strand stainless steel wires are used.

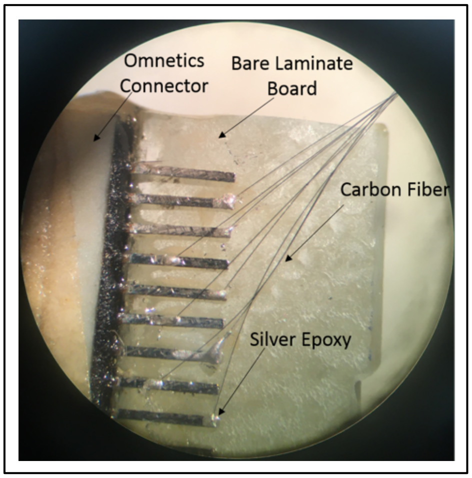

Figure 2.6 Attachment of the single carbon fibers to the Omnetics connector using silver conductive epoxy.

Reference and ground wires were also connected to the connector terminals in the same way that the carbon fiber were done and then their other ends were desheathed for about 3-4 mm for interfacing with the tissue.

Placing carbon fibers into the array: Each carbon fiber, after being connected, is inserted to the designated hole in the mesh. Electrode map is seen in Figure 2.7.

Covering the carbon fibers on the connector with medical epoxy: First a very small amount of medical epoxy is applied to the edge of the PCB to hold all carbon fibers together. Then all connector terminals with the PCB were entirely covered with medical epoxy.

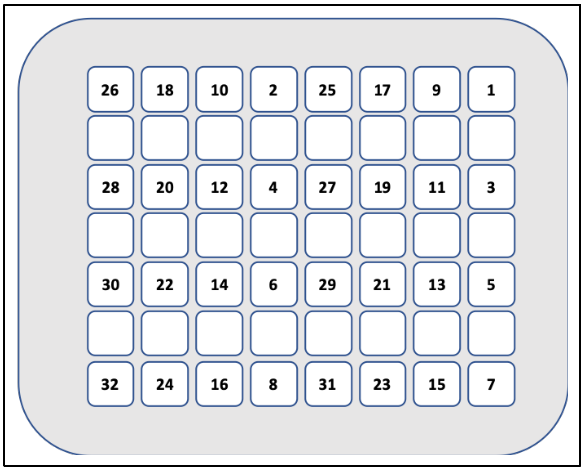

Figure 2.7 CFMEA array map shows the designated positions of the CFs based on their given channel numbers on the connector terminal.

Securing carbon fibers to the array: An extra amount of medical epoxy is applied on the array with 32g needle by making sure all carbon fibers are covered by medical epoxy and secured to the array. It is essential to apply the

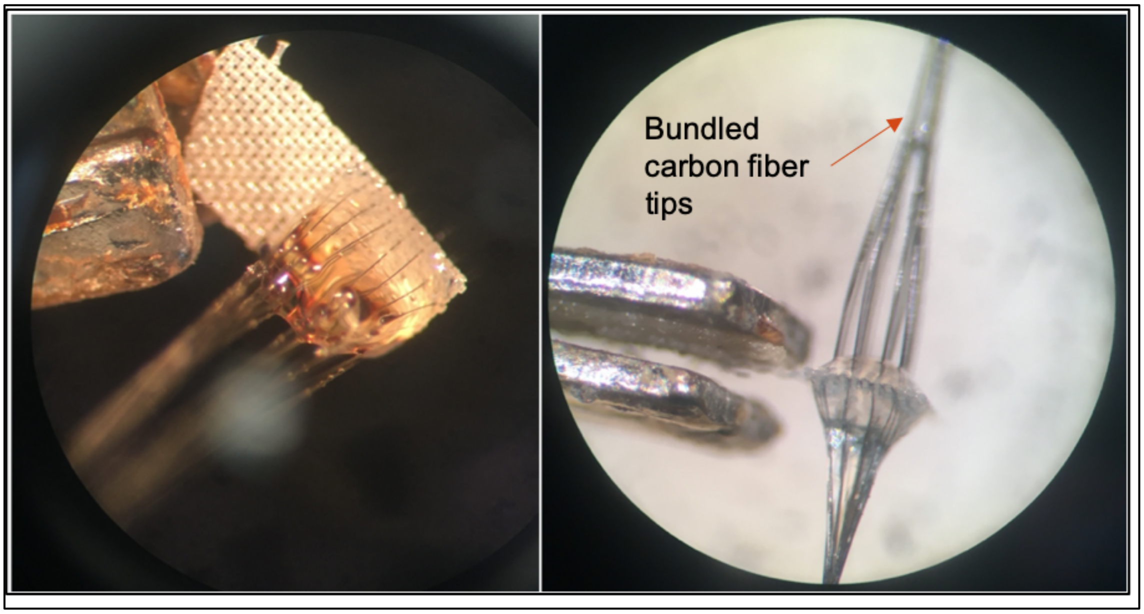

Figure 2.8 Array close-ups during making process. Left: The array with the medical epoxy applied on top of the mesh array. Right: Showing the re-bundling of carbon fibers that leave the mesh array to keep carbon fibers straight.

epoxy right after it is prepared, when it is least viscous. Also, the fast-curing epoxies are better choice for this step. After applying the epoxy, the electrode holder is positioned upside down during epoxy curing to avoid leaking of epoxy underneath the array.

Bundling carbon fibers underneath the array: The free ends of carbon fibers were bundled around 1 mm away from the array to avoid fanning out of carbon fibers underneath array (as shown in Figure 2.8-Right) and to keep them straight as they exit the mesh on the other side. Then, the electrode is transferred to another electrode holder that is designed for the laser system.

Laser Electrode Holder: Another electrode holder is made using a non-reflective black plexiglass, metal clips, and a metal plate (Figure 2.9). The metal plate is 200 micron thick and has a hole with the size of the footprint of the carbon fiber array. The array sits on this plate with the extensions around and only the carbon fibers go through the hole. The thickness of the metal plate determines the final length of the carbon fibers from laser cutting. The laser beam is sent towards the carbon fibers in the plane of the plate and the part of the carbon fibers extending beyond the thickness of the plate are burnt, resulting in ~400 μm long carbon fiber lengths. In Figure 2.9 left image shows the carbon fiber lengths (~400 μm) under the array which is the targeted recording depth in the cerebellum. The parts of the carbon fibers going to the connector are shadowed with another non-reflective plate (Protector in Figure 2.9).

Electrode Array Making with The Laser System: The Laser system is composed of a DAQ board controlling the laser beam through MATLAB by generating 5V pulses. The maximum power of the laser is 4W and its wavelength

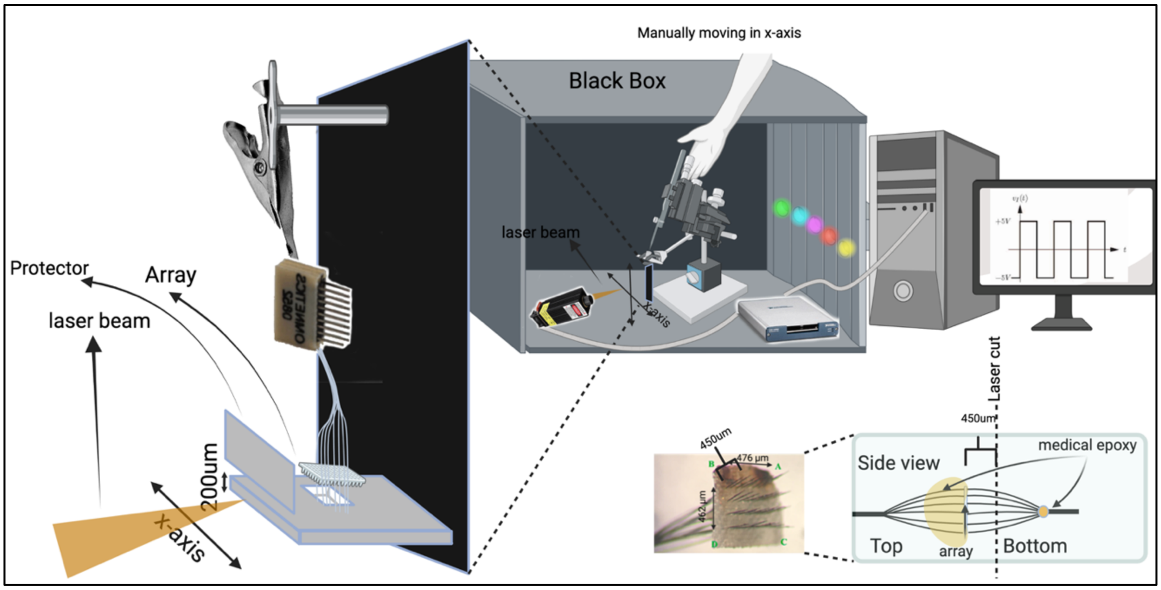

Figure 2.9 Laser setup. Carbon fiber tips were cut in the laser cutting box that is connected to the computer to run the laser. On the left, the enlarged view of the connector holder designed for laser cutting.

is 450 nm (blue light). The laser was tested at different duty cycles to determine the optimum power and concluded 0.75-1W is optimum. The cutting is performed by moving the electrode holder apparatus with a micromanipulator in 50 micron intervals and exposing the electrode to the laser 3-5 seconds. The laser cuts all the fibers in the array at the same time uniformly and sharpens the tips, which yields lower electrode impedances compared to a blunt cut.

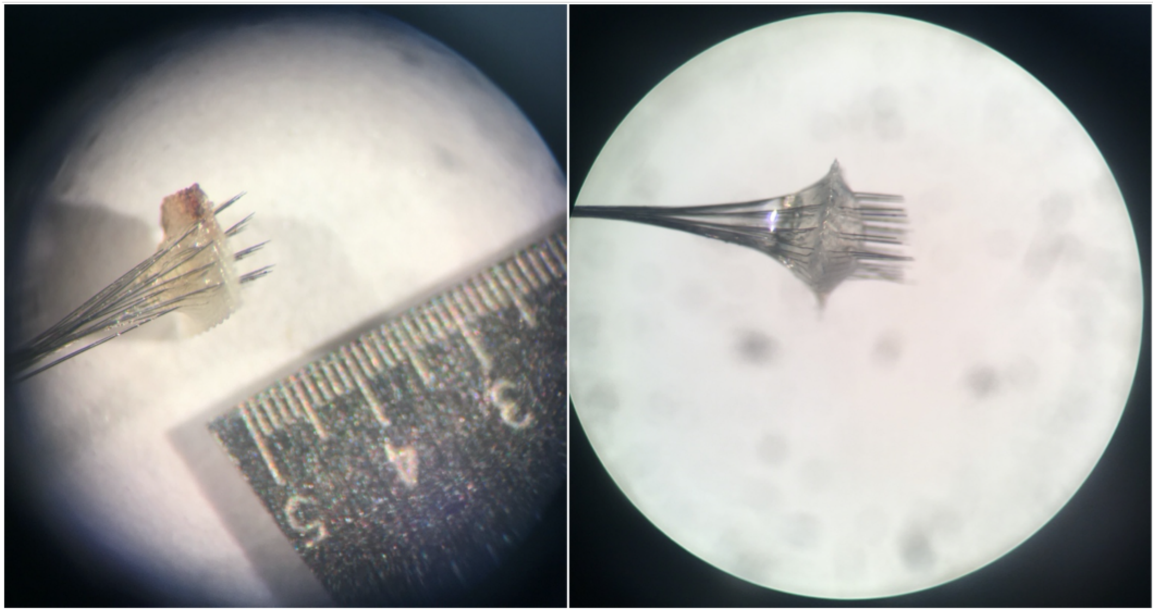

Figure 2.10 Arrays after their electrode tips were cut. The one on the right shows some leaking of the medical epoxy underneath the array. This problem was solved later with the techniques mentioned in the text.

2.2.1.2 Carbon Fiber Micro Electrode Bundle for the Spinal Cord.

The First Design: Thirty-two carbon fiber filaments were cut to a length of 3.5 cm. Under microscope approximately a 200 μm long coating was removed from

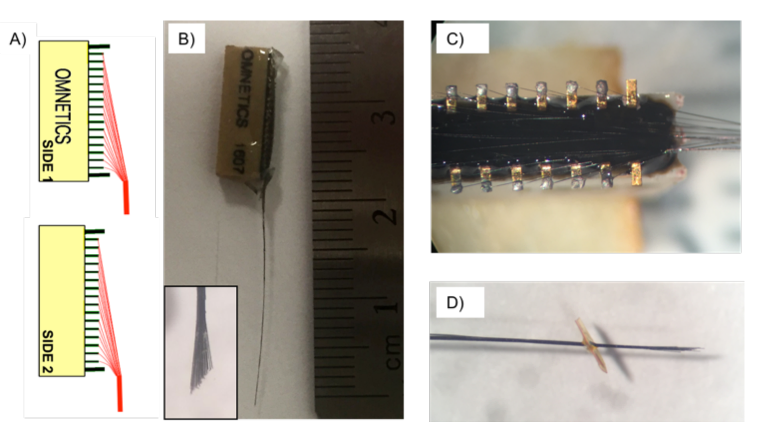

Figure 2.11 Spinal cord electrode design1.

one end of the filament by using a soldering iron heated up to 290˚C. Each filament was connected to a separate pin on the micro-connector using conductive silver epoxy (EpoTek, MA) (Figure 2.11-C) and heating in an oven at 200 °C for 7 minutes.

The Second Design: Plain non-conductive printed circuit board (PCB) was placed between two rows of the connector pins. The proximal ends of the filaments were desheathed with soldering iron as described above. Carbon fiber filaments were connected to the pins individually with silver epoxy in half the channels. Ten channels on one side of the connector had triple carbon fiber filaments at each contact side. Electrodes from each side of the PCB were gathered into a separate bundle, and each bundle was composed of 16 channels (Figure 2.12). Teflon-coated multi-strand stainless steel wires (50 µm diam.) were connected to two of the upper corner pins of the connector and used as the reference for recording. The connector contacts were secured and insulated with

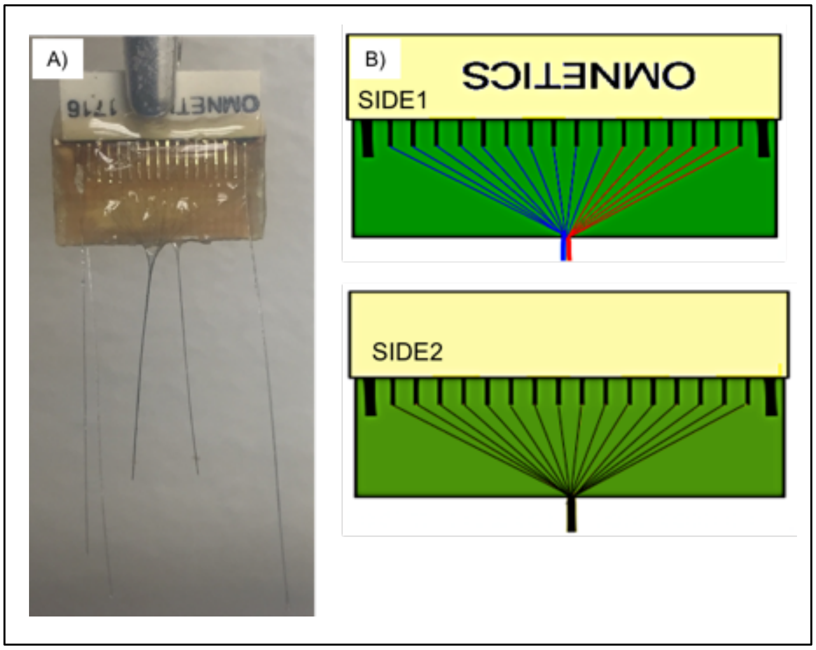

Figure 2.12 Spinal cord electrode design2.

clear medical epoxy (EpoTek, MA). The recording ends of the filaments were cut into staggered shape with a surgical blade at 2 cm from the PCB. A small piece (1 mm^2) of polyimide film (25 μm thick) was glued 1.5 mm above the recording tips to mark the length that will be inserted into the spinal cord. The tips of the fibers on one side of the connector (16 fibers) were desheathed about 75 μm of its length using a technique that was developed as a part of this study and as detailed in the next section below.

Desheathing Electrode Tips (Electrode Active Area Making): For this study, a system was built for desheathing fiber tips that were coated with parylene-C. This technique allowed us to remove the coating material in a controlled manner at the desired length without damaging the carbon electrodes.

This system is based on electrical heating and works like a miniature oven to increase the local temperature around the electrode tip (Figure 2.13).

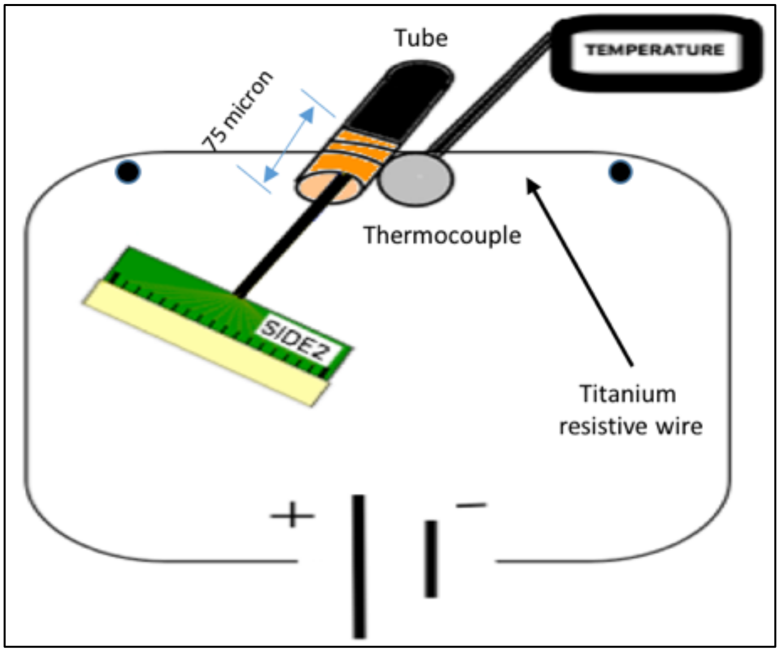

Figure 2.13 Carbon fiber desheathing setup for the spinal cord bundle electrode.

Briefly, it consisted of a simple circuit, a heating element (titanium resistance wire), a stainless steel hollow tube (1mm diameter), and a thermocouple. The resistance wire was wrapped around the metal tube a few times. The metal tube`s hollow part was 75 µm deep from the tip opening. The thermocouple under the tube monitored the temperature of the chamber during the heating process. The tip of the desired carbon fiber bundle was inserted into the metal tube. The current passing through the resistance wire was adjusted to obtain temperatures up to 290°C by varying the voltage supply. Carbon fiber filaments were left in the chamber for 1-2 minutes while the current was kept on to completely remove the parylene-C coating at the carbon fiber tips.

2.2.2 *In Vitro* Testing

2.2.2.1 Bubble Test. The bubble test was performed by passing a small (<1 μA) DC anodic current through the carbon fibers that was submerged into PBS solution (Dulbecco`s Phosphate Buffered Saline-DPBS, Ge Healthcare Life Sciences) to determine if the tips were exposed and the rest of the fiber remained insulated. Electrolysis of water occurred at the exposed parts of the carbon fiber and gas bubbles were formed when a current was passed through the electrode. Under microscope with 100x magnification, the entire length and tips of the electrode were inspected. Observing gas bubbles only at the tip of an electrode confirmed that the desheathing procedure was done successfully. Gas bubbles observed on the parylene-C coated parts of the fiber surface indicated coating defects.

2.2.2.2 Impedance Test. Electrode impedances were measured at 1 kHz to ensure that they are in the expected range (0.5-3 MΩ) prior to implantation.

2.2.2.3 Soak Test. Prior to implantation, the soak test was performed to measure the resistance of the electrodes. Electrodes were soaked in the saline 24 hours and the next day their impedances were measured again and visually checked if there is any deformation on the medical epoxy insulation or any other damage.

2.2.2.4 Scanning Electron Microscopy Imaging. SEM images were taken to confirm the intactness of the coating material, verify the desheathing technique, and measure the exposed area of the electrodes.

2.2.3 *In Vivo* Testing

Two Long Evans rats were implanted with the spinal cord electrodes, and eight Long Evans rats (~250g, male) were implanted with the cerebellum electrodes. The details of cerebellar implant surgeries were explained in Chapter3.

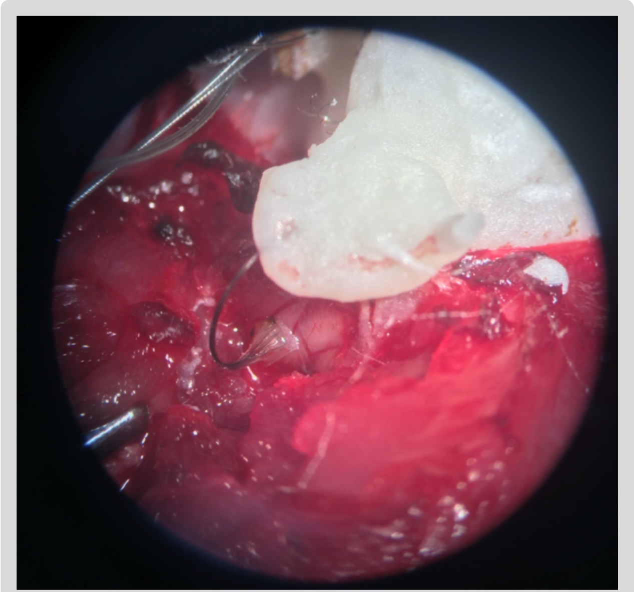

Figure 2.14 Electrode implantation on the cerebellum.

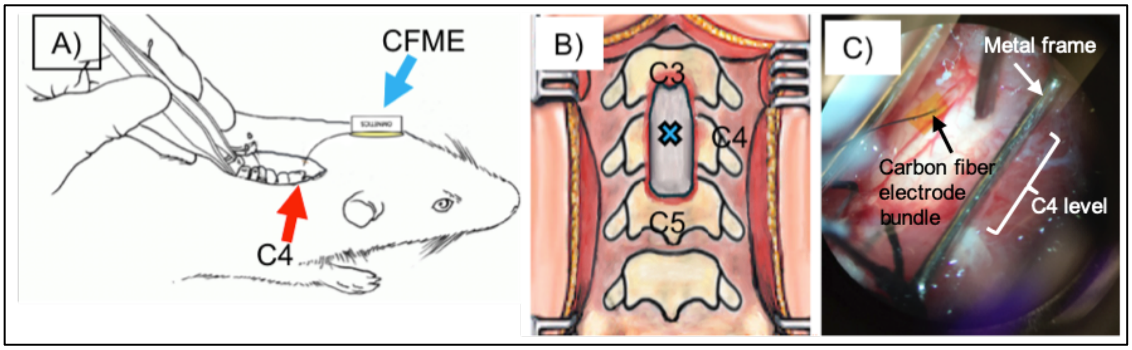

Figure 2.15 Spinal cord implantation. A) A laminectomy was performed at C4 level. B) An illustrative figure that shows the top view of the surgical area. From mid-C3 to mid-C5 vertebrae were removed. C) A picture of the implanted carbon fiber bundle with metal frames that hold the connector (the yellowish part on the spinal cord is the stopper).

Spinal Cord Surgery: The rats were initially anesthetized with 5% isoflurane (v/v) to shave the hair at the back of the neck. The head was mounted on a stereotaxic frame and anesthesia was maintained by administering 1-3% isoflurane during the surgery. Blood oxygenation level was monitored with a pulse-oximeter and the body temperature was controlled by a closed loop heating plate and a rectal temperature probe. Ointment was applied to the eyes to keep them moisturized. A dorsal laminectomy at the cervical level was performed (Figure 2.15 A and B) to assist resection of the dura and exposing the pia. The carbon fiber bundle was inserted vertically along the central fissure of the spinal cord into the dorsal column at the C4 level.

In both rats, the bundles were inserted (at a 45° angle) 1.5 mm of their length, using the polyimide attachment as a stopper (Figure 2.15 C). Then, the bundles were secured in place by applying trace amounts of cyano-acrylic glue on the pia. A metal wire frame was attached to the spinal vertebrae by tying it to C2 and C5 vertebral bones with 4.0 silk sutures. The Omnetics connector was attached to the frame with dental acrylic. The connector was protruding half-way through the skin to make connections with the multi-channel amplifier head-stage. Each microelectrode bundle had some slack to avoid any pulling on the spinal cord. Finally, the skin incision was closed with absorbable sutures. Following surgery, the animals were allowed to recover in three to five days. During recovery time, recordings were not taken and the animals received daily post-surgical care that includes monitoring of the animal for sufficient feeding, cleaning surgical incisions from blood and detached sutures, and applying triple ointment (Neosporin) to the surgical incisions to protect from infection. If animal shows itching behavior, Lidocaine gel was applied topically, and if sutures become loose Gluture (WPI Inc.) was applied on the incision.

2.2.4 Data Recording and Analysis

Cerebellum Electrode: A detailed data analysis was performed for the cerebellum electrodes which was explained in Chapter3. Here for the sake of showing electrode performance and capability some sample data will be shown in Results in this Chapter.

Spinal Cord Electrode: Neural signals were recorded using a multichannel amplifier (Ripple, UT) and a custom software written in MATLAB (Mathworks, Inc.). A video camera was used to record (30fps) animal movements and for offline determination of animal behavior (awake vs. anesthetized, active vs. quiet). Signals were recorded during face cleaning activity since this task involved cyclic forelimb movements and did not require training. *In vivo* impedance measurements were performed before each recording session.

Signal processing was performed in MATLAB. Raw data from three sessions of Rat1 that consisted of multiple trials of 32-channel recordings were band-pass filtered between 300 and 1200 Hz. Channels that had passed the *in vitro* bubble test and had low impedances were selected. Using a simple thresholding technique, the spikes were detected, and raster plots were drawn for the trials that captured the face cleaning activity. Firing rates for the selected trials and channels were reported. Using k-means clustering algorithm, spikes were sorted based on their amplitude and width. For Rat2, our aim was to determine how *in vivo* impedance values and signal-to-noise ratio (SNR) changed according to the desheathing of carbon fiber tips and the number of carbon fiber filaments attached on individual channels. The channels with previously mentioned configurations were compared to control channels which had blunt-cut single carbon fiber filaments. Comparative analysis was done in terms of impedances, baseline noise, and SNR values for each group. Groups were formed as blunt-cut single CF filaments (group1), blunt-cut triple CF filaments (group2), and desheathed-tip single CF filaments (group3).

Signal Quality: It was measured with three metrics:

1. Average of correlations between channels: In the cerebellum high correlations between channels were one of the challenges. To eliminate this, the differential configuration was used in data analysis, which significantly decreased average correlations from ~0.6 to ~0.2. As a metric, absolute values of correlations between all differential channels were averaged. Then the mean of absolute correlations from all animals and sessions were averaged to obtain an overall measure of inter-channel correlations in the data.

2. Mean of RMS values of the signals were calculated for all animals and sessions.

3. Mean SNR: Signal-to-noise ratios were defined as the RMS of the signal when there is neural activity present divided by the RMS of the baseline.

In vivo impedances: The changes in electrode impedances were tracked over time with measurements made at 1 kHz.

2.2.5 Dissection and Histology

Visually confirming intactness of electrode tails: First aim of the dissection was to visually confirm the tail of the electrodes were intact since it is solely composed of carbon fibers which can be fragile.

Dissecting tissue samples carbon fibers inside: The second purpose of the dissection was dissecting tissue samples electrodes inside. Spinal cord samples were easily dissected with the electrode but for the cerebellum electrodes were required to remove the cerebellum with the bone because electrodes were adhered to the bone.

Perfusion: Eight weeks (cerebellum electrodes) - four weeks (spinal cord electrodes) after implantation, animals were terminated with lethal dose ketamine-xylazine cocktail (Ketamine (80mg/kg, IP) and xylazine (12mg/mg, IP) and fixated by perfusion transcardially using 10% formalin (10% Neutral Buffered Formalin). After 48 hours, samples were transferred to 10% sucrose solution.

Approaches to section tissue with electrodes inside:

1. ***Using Tape Transfer System:*** The CryoJane Tape-Transfer System (Leica Biosystems, IL) is used for spinal cord samples. This system helps to keep sectioned small carbon fiber pieces on the slide.

2. ***EDTA decalcification:*** Due to difficulty of sectioning hard bone tissue, decalcification protocol was used (Rolls 2022). As decalcifying agent, chelating agent EDTA (prepared at pH 7.0) was used. The protocol involves keeping samples in EDTA for 12-24-48-96-192 hours and changing used EDTA with the fresh EDTA at every time point.

Histology: Frozen cerebellum samples in Tissue-Tek O.C.T. compound were sagittally sectioned using cryostat microtome at 50 μm section thickness (thicker sections were chosen due to the need to section the entire implant area and collecting all sections to be able to confirm the location of the implanted electrode. For example, for each cerebellum sample, the entire 10 mm (5mm from midline medio laterally into both hemispheres) around 200 sectioned were made. Collected sections were mounted on glass slides and kept at -80°C till staining.

The sections were then double stained with CD68 (mouse, Bio-rad) (1:200 concentration), NeuN (anti-rabbit, Sigma Millipore) (1:500 concentration), Calbindin (anti-rabbit, D-28k, Calbiochem) (1:1000 concentration), Calbindin (anti-mouse, Sigma Millipore) (1:300 concentration) iba1 (anti-rabbit, Fujifilm Wako) (1:500 concentration), GFAP (anti-rabbit, Dako) (1:1000 concentration) and DAPI (Invitrogen). As secondary Alexa 488 (mouse) (1:1000 concentration), 594 (rabbit) (1:1000 concentration), and Sigma 488(rabbit) (1:1000 concentration), and as blocking serum and medium to prepare antibodies normal goat serum (Vector Lab) were used. Sections were kept at -20°C for 10 minutes in methanol, and then washed three times in 1x PBS for 5 minutes at each wash. Following drawing borders around sections with hydrophobic PAP pen (Abcam), sections were blocked with 10% goat serum in 1x PBS-Triton (0.1%) at 4°C for one hour. The blocking serums were disposed and sections were incubated with primary antibodies that were prepared in 1% goat serum in 1x PBS-Triton(0.1%) at 4°C overnight. Next day primary antibodies were disposed and slides were washed three times in 1xPBS-Triton (0.1%) for 10 minutes each wash. Following steps were performed in a dark room. The sections were incubated with secondary antibodies that were prepared in 2% goat serum in 1xPBS-Triton(0.1%) at room temperature for one hour. Lastly, the slides were washed three times in 1xPBS-Triton (0.1%), for 10 minutes at each wash, and PAP pen traces were cleaned with nail polish remover, 1-2 drops of DAPI was added on each section, covered with cover slips, and after drying they were sealed applying nail polish to the edges of cover slips.

CD68 was used to visualize macrophages, NeuN for neurons, Calbindin for Purkinje cells, iba1 for microglia, and DAPI for cell nuclei. Spinal cord samples were stained with LFB (Luxol fast blue) for myelin, H&E for structural analysis, GFAP for astrocytes and also with CD68 and DAPI.

2.3 Results

2.3.1 *In Vitro* Testing

2.3.1.1 Scanning Electron Microscopy Images. The outcome of desheathing

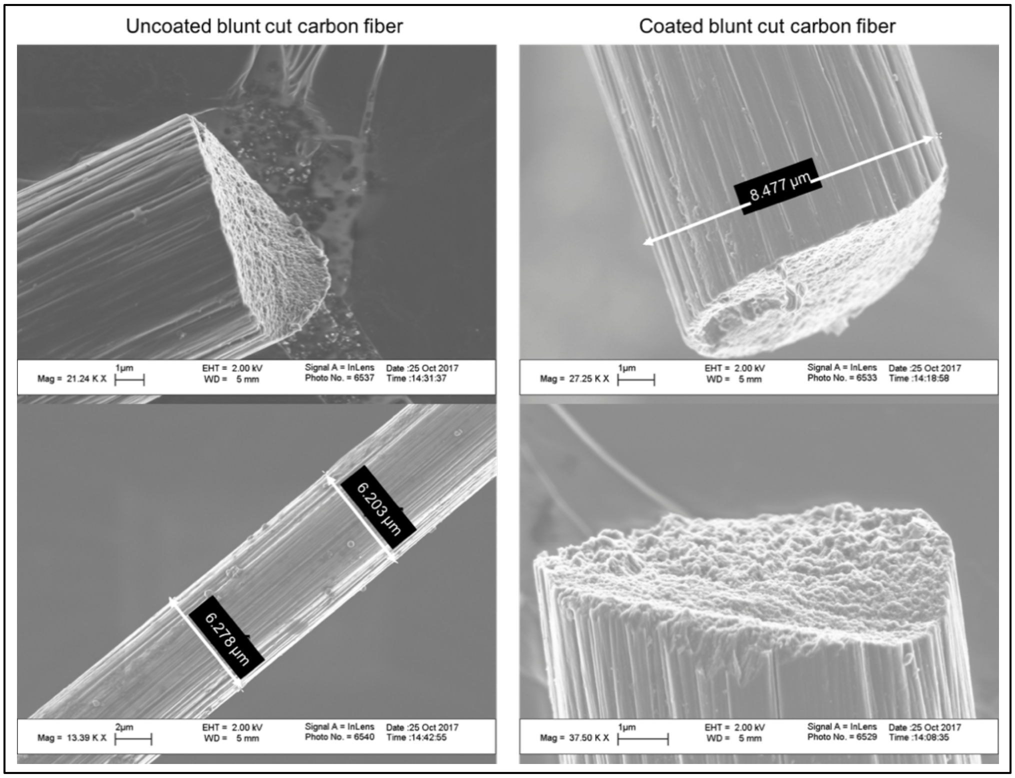

Figure 2.16 SEM images of uncoated blunt cut carbon fiber and coated blunt cut carbon fiber.

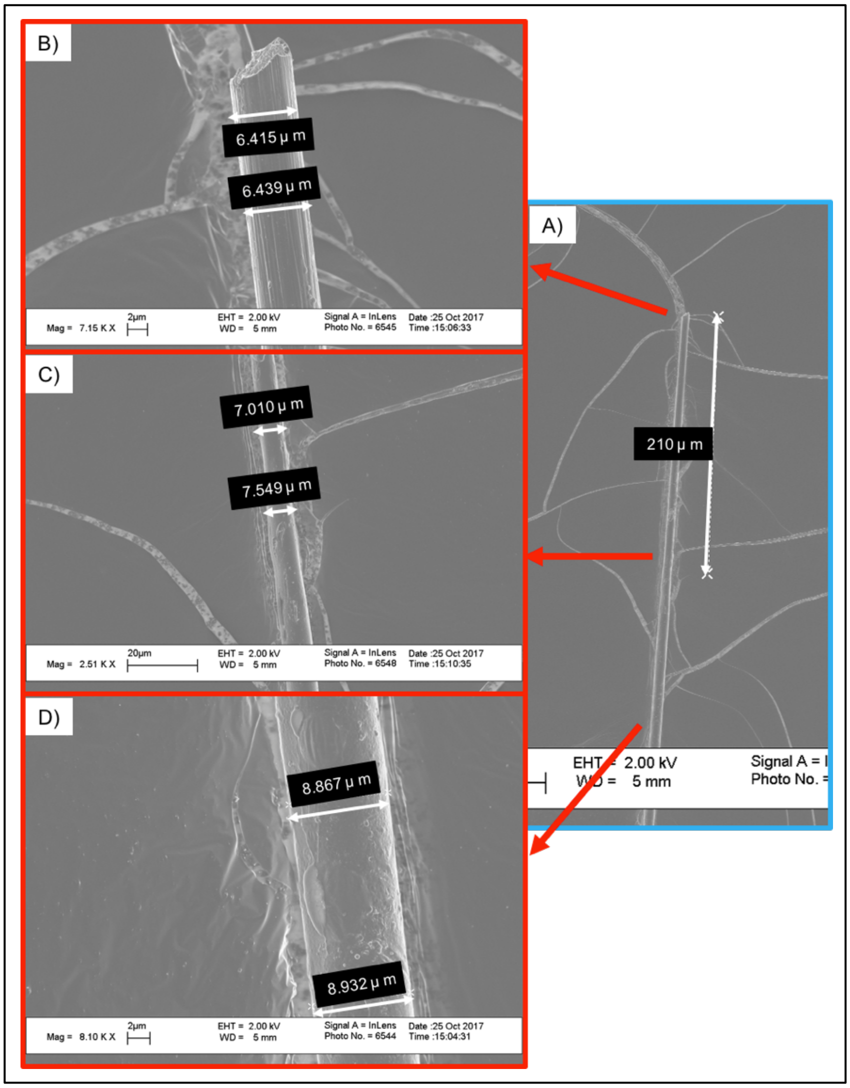

Figure 2.17 SEM images of soldering iron desheathed carbon fiber. A) shows the entire desheathed length. The thickness measurement at the tip is approximately 6.42 µm (B), at the end of desheathing length the average is 7.28 µm (C), and at the remaining part of the carbon fiber filament it is 8.90 µm (D).

technique was evaluated by examining the SEM images of the fibers with

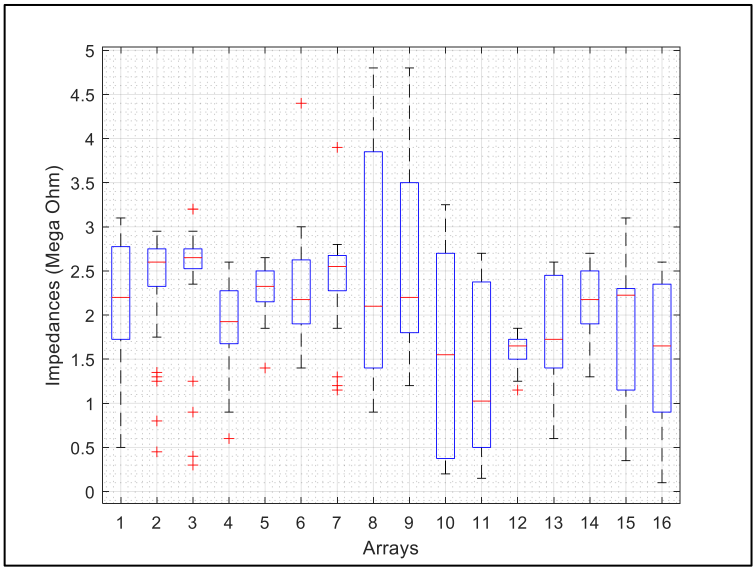

Figure 2.18 *In vitro* impedances of 16 cerebellum arrays with 32 electrodes. The median (red horizontal mark) and the second and third quartiles are shown (rectangular boxes). Plus-signs indicate outliers.

parylene-C coating and the desheathed fibers. The diameter of undesheathed fibers were around 8.4 μm indicating a coating thickness of a little more than 1 μm (These SEM images were taken for the first set of carbon fibers that were tested, which were coated with ~750 μm parylene-C). The diameters of desheathed fibers were measured around 6.2 μm.

2.3.1.2 *In Vitro* Impedances.

2.3.1.2.1 Cerebellum Electrode In vitro impedance measurements showed for most of the arrays tested an average of ~2.2 MΩ with relatively narrow distributions (Figure 2.18). The arrays with higher standard deviations were not implanted.

2.3.2 *In Vivo* Testing

2.3.2.1 In Vivo Impedances.

2.3.2.1.1 Cerebellum Electrode

***In Vivo* Impedances:** Average impedances of all electrodes were increased over sessions as a result of increased individual electrode impedances. Median was raised from hundreds of kΩ to ~3.9 MΩ by the end of the chronic study, i.e. the 8th recording session ~1.5 months after implantation. There was a decrease in impedance distributions on the 4th session despite the increasing trend in impedance (Figure 2.19).

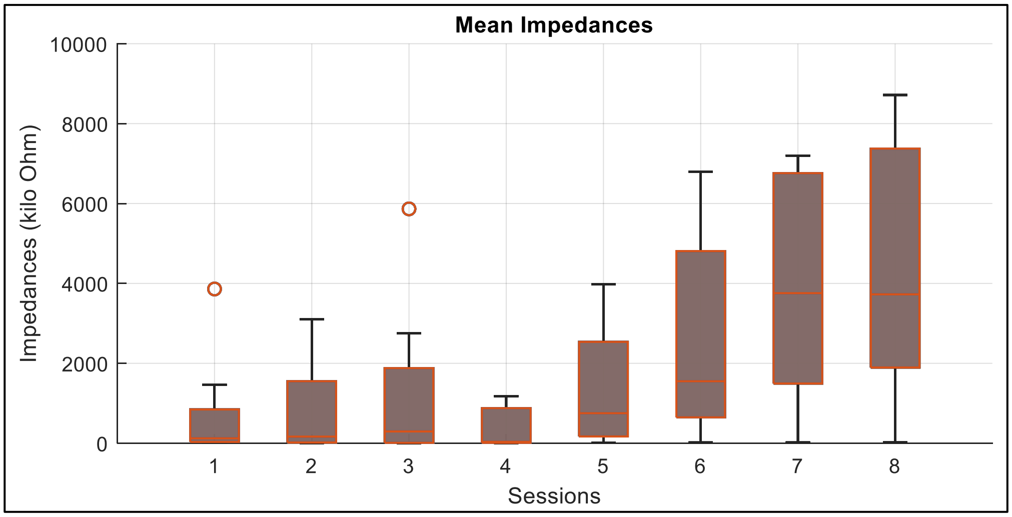

Figure 2.19 *In vivo* impedances of carbon electrodes and their change over sessions, average of all electrode arrays in all animals.

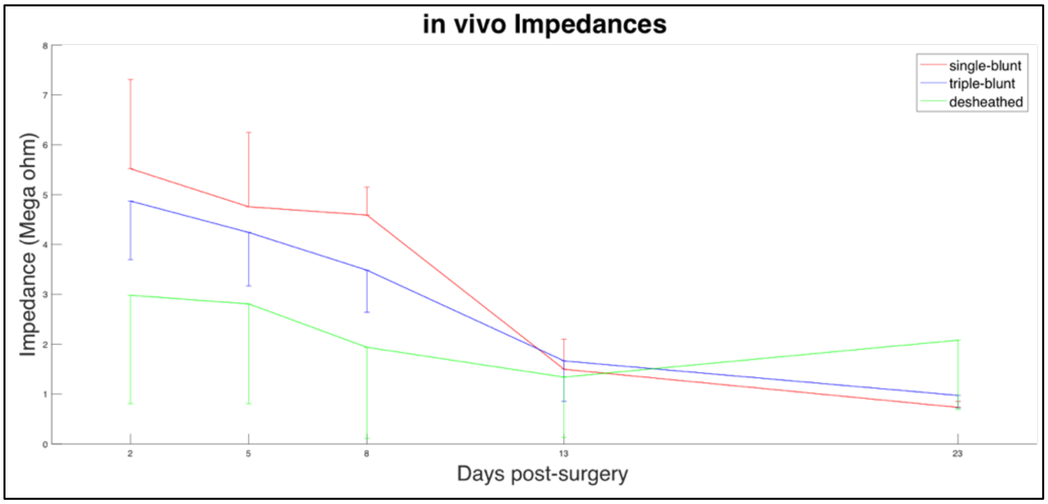

Figure 2.20 *In vivo* impedances of spinal cord electrodes. Mean impedances of all electrodes in the array and std (vertical bars) are shown.

2.3.2.1.2 Spinal Cord Electrode All impedance values decreased over time. Figure 2.20 shows that impedances were very small after the 2nd week compared to initial sessions. Signals of all sessions were recorded and analyzed but specifically signals from the first three sessions on days 2, 5, and 8 were used for further signal analysis. The drop of the impedance was interpreted as electrode failure due to breakage or damage to the insulation, thus the signals after the 4th session were excluded from further analysis.

2.3.2.2 Spike Activity.

2.3.2.2.1 Cerebellum Electrode The data below shows a single unit activity recorded from the cerebellum in a rat. Single spikes were seen in the same animal over several sessions (Figure 2.21). The time width of the spikes was <1 ms. Based on amplitudes (~100-150 μV), spike width (1-2 ms), and the shape of the spikes in raw data they were characterized as single unit activity. More detailed spike analysis and additional confirmation methods like firing rate testing were not applied since it was out of the scope of the project. Complex spike pauses were not studied.

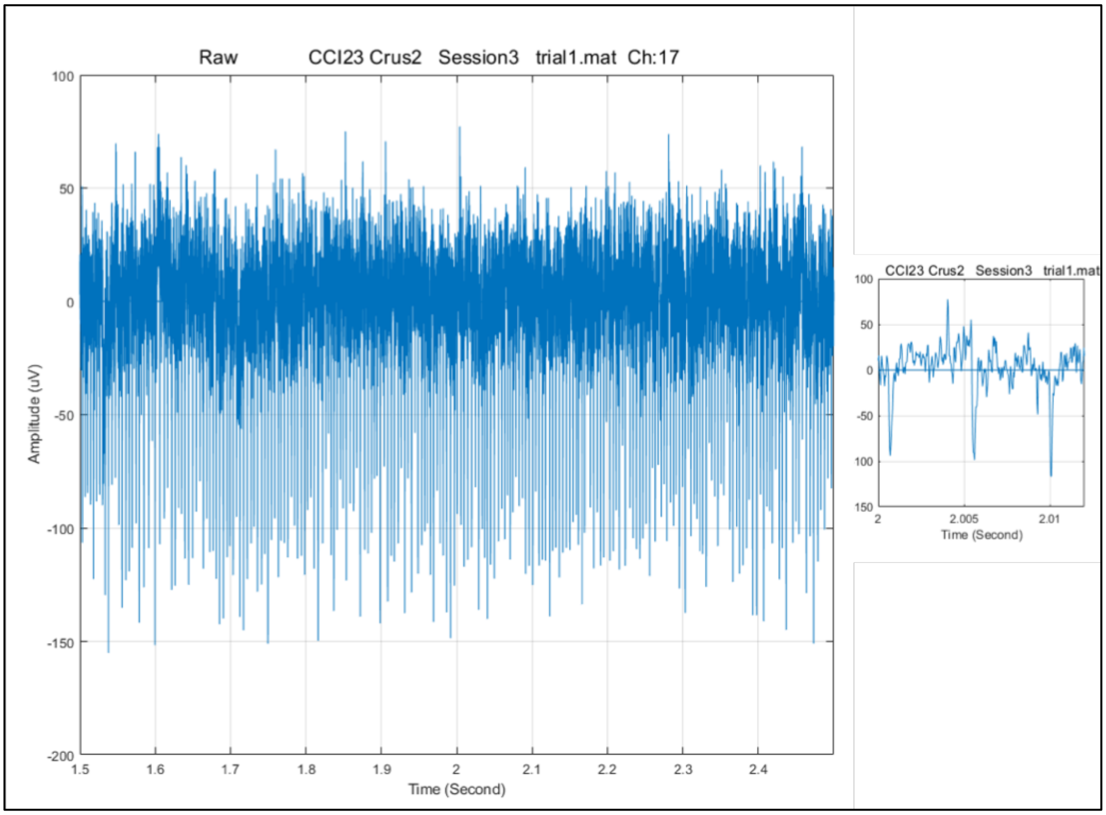

Figure 2.21 Sample single spike recording with the carbon electrode array in the rat cerebellum.

2.3.2.2.2 Spinal Cord Electrode The data below shows a single unit activity recorded from the cervical spinal cord (C5) in a rat. The raster plot in Figure 2.22 demonstrates the spiking activity of two different channels from all trials in a

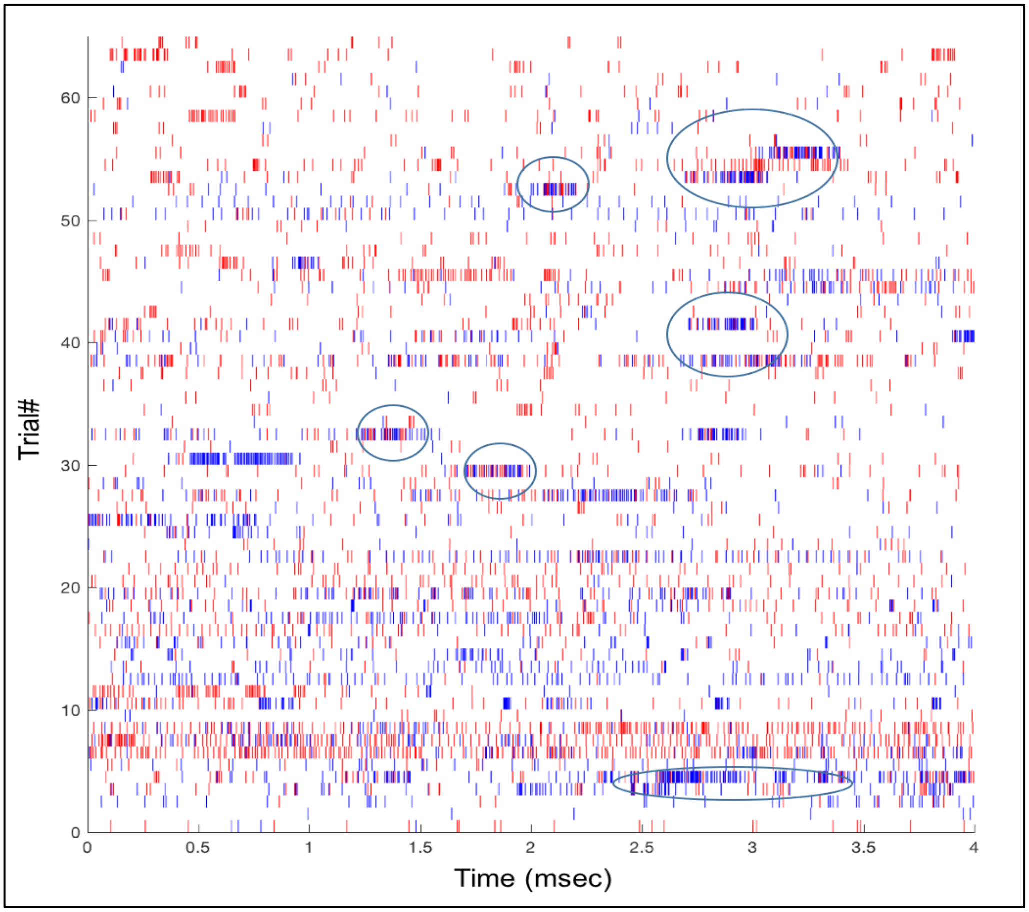

Figure 2.22 Raster plots from two CFME channels of the first design shown in red and blue. Simultaneous recordings in each of the 65 trials are plotted one above the other in rows for comparison. Areas marked with circles indicate some of the time intervals when both channels (blue and red) record similar pattern of activity occasionally.

single session (3rd session, day 8). The figure shows that each channel was able to record uncorrelated signals in most of the trials containing activity of the neurons in their vicinity. Additionally, the figure highlights that both channels recorded coinciding bursts in some trials as marked by the circles (Figure 22). Figure 2.23 shows the same animal`s spike activity.

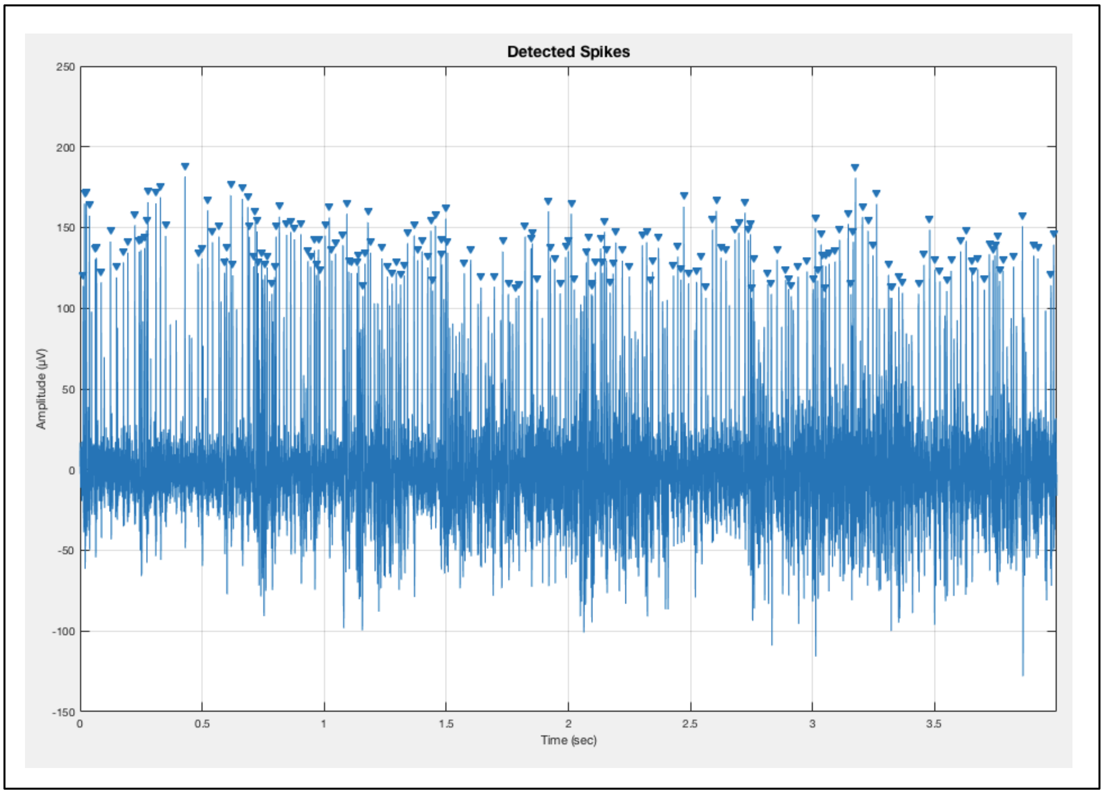

Figure 2.23 Spinal cord spikes recorded with carbon fiber electrodes.

Spike Sorting: A representative image of sorted spikes of a single trial from Rat1 is shown in Figure 2.25. After the spikes were detected using a thresholding method, the spikes were clustered based on their amplitudes and durations using

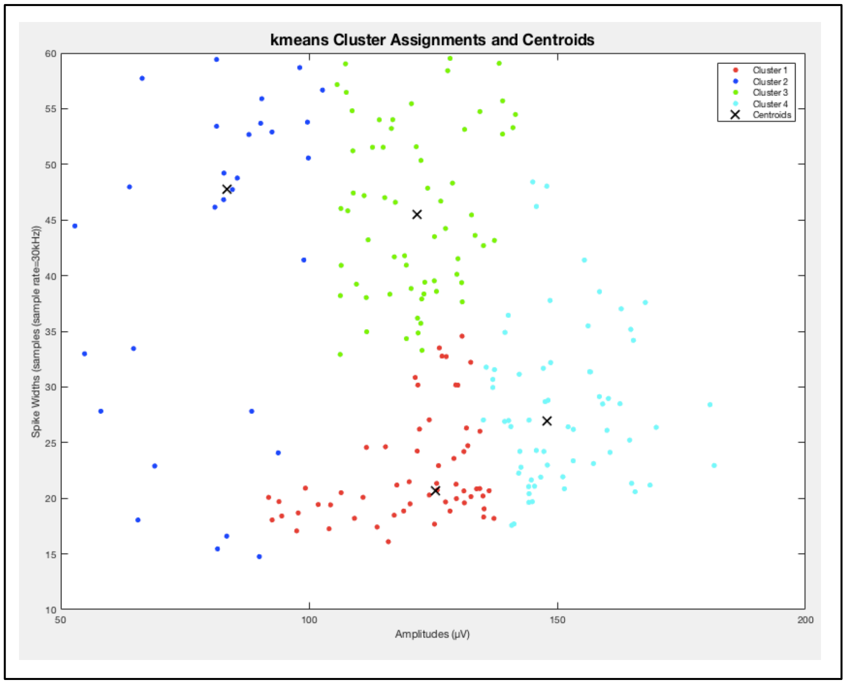

Figure 2.24 k-means clustering based on spike width and amplitude. Cluster centers are marked with black crosses.

the k-means algorithm (Figure 2.24). In this particular example, the spikes were divided into four clusters. The cluster number, four, was found as optimum number for the mentioned data set based on reduction of the standard deviations and the distinctiveness of the cluster shapes after trying to group them into 4±2 clusters. Clustered spikes indicate possible recording from several sources. However in Figure 2.25 cluster 1 and 4 may be merged into the same cluster.

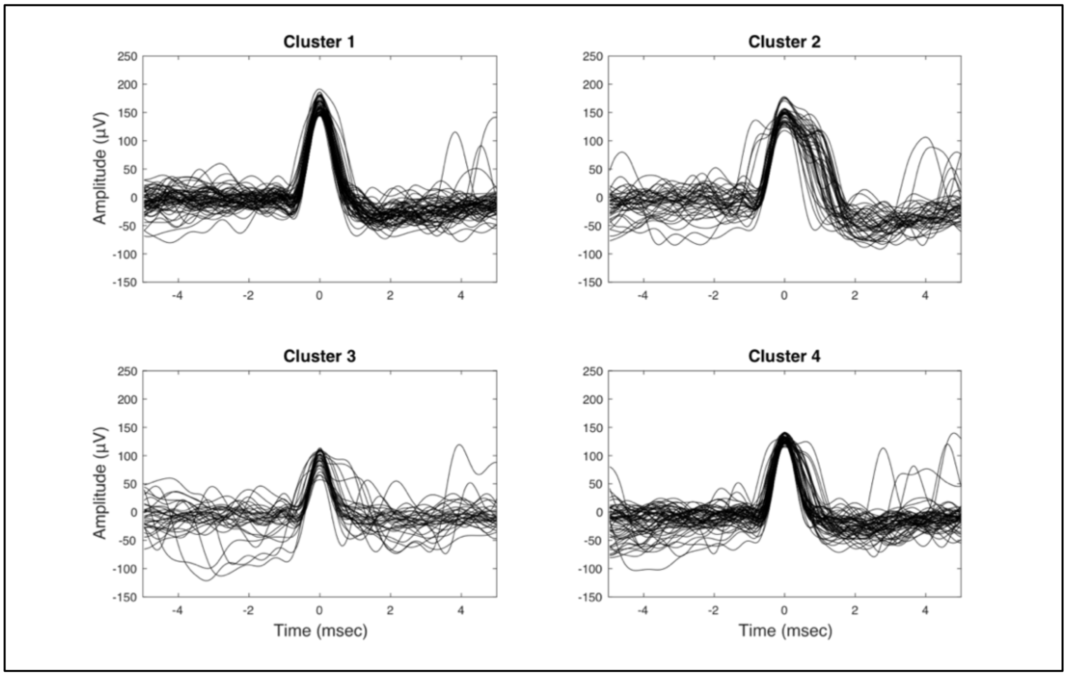

Figure 2.25 Spike sorting data.

2.3.2.3 Signal Quality.

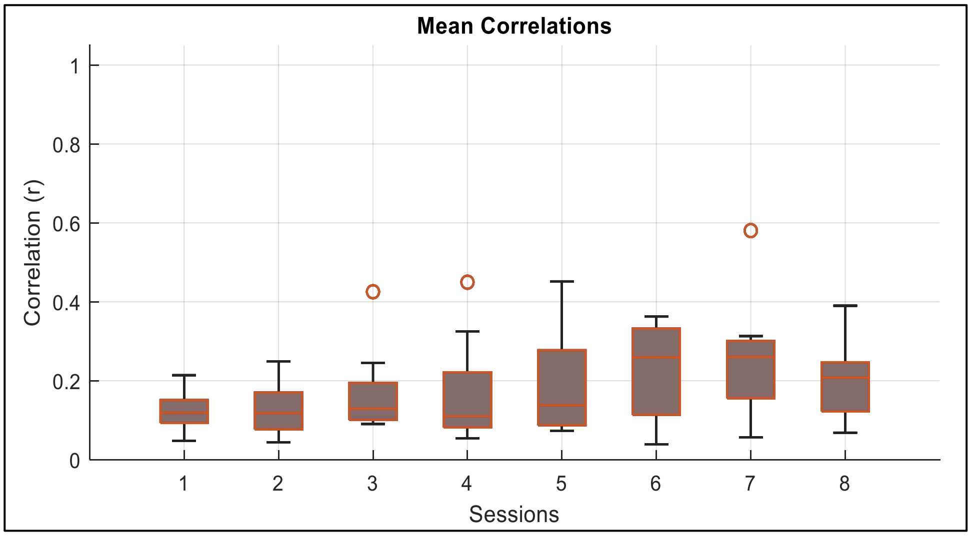

Figure 2.26 Mean of absolute value of the correlations between the neural channels after taking their differentials. Red dots: outliers; top edge of the bar: 75th percentile; bottom edge of the bar: 25th percentile; central red line: median; whisker ends: extreme data points.

2.3.2.3.1 Cerebellum Electrode As a measure of common-mode signals in the raw neural data , the correlations between the channels were calculated. After taking the differentials of the neural channels, their correlations with each other were decreased from above 0.6 to around 0.2 on average consistently over sessions (Figure 2.26).

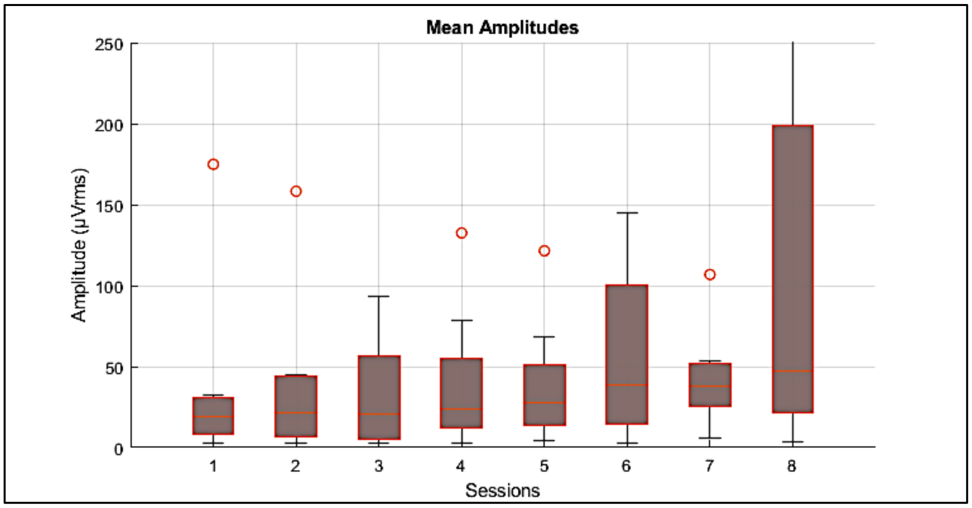

Figure 2.27 The variation of the mean amplitudes of neural data averaged for all animals and plotted across sessions. Red dots: outliers; top edge of the bar: 75th percentile; bottom edge of the bar: 25th percentile; central red line: median; whisker ends: extreme data points.

Average amplitudes of the neural data (calculated as the RMS (root-mean-square)) increased over sessions from a median of ~20 μVrms to ~50 μVrms (Figure 2.27).

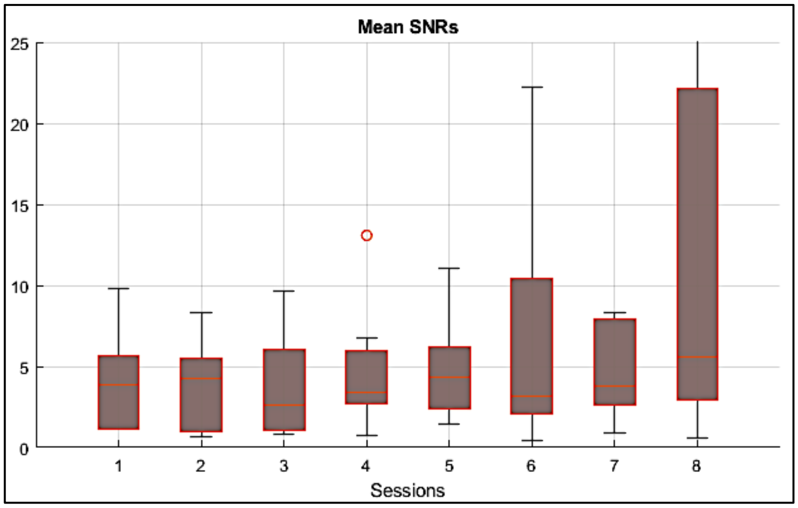

Figure 2.28 Average SNR values of neural channels of 6 animals. Red dots: outliers; top edge of the bar: 75th percentile; bottom edge of the bar: 25th percentile; central red line: median; whisker ends: extreme data points.

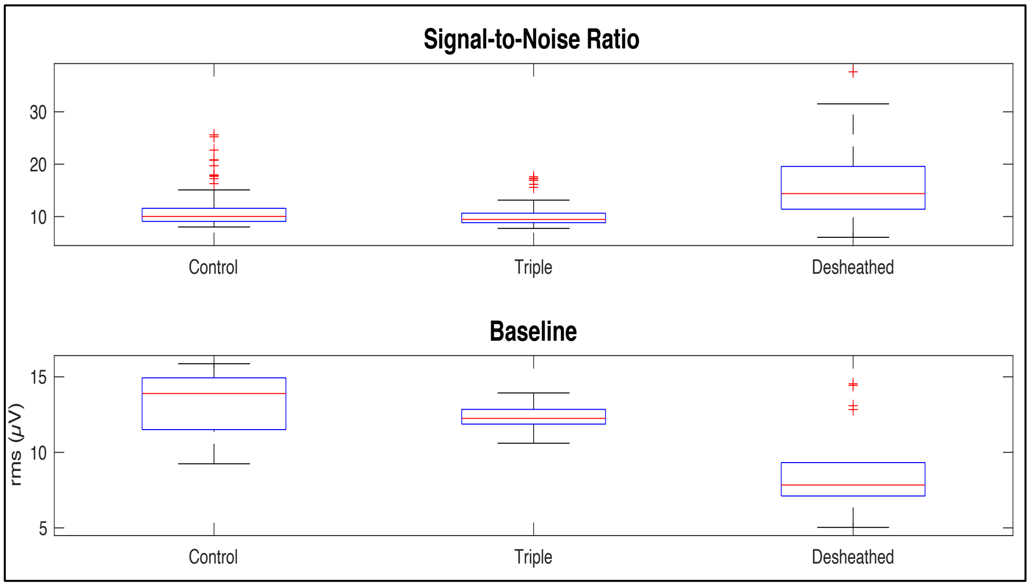

Figure 2.29 SNR values of spinal cord electrode. In 'triple' electrode design, three carbon fibers were connected to the same contact. SNR was calculated as the RMS of the signal divided by the RMS of the baseline.

The SNR (signal-to-noise ratio) values calculated as RMS of neural data over the RMS of the baseline noise (~10 μV). From the first session to the last, the SNR values increased, except in some sessions in the middle where SNRs were lower, which can be due to transient increases in the baseline activity (Figure 2.28).

2.3.2.3.2 Spinal Cord Electrode: In the data presented by Figure 2.29 and 2.30 the “control” group is composed of electrodes where the electrode tips were created with blunt cut only and single carbon fibers connected to each terminal; the “triple” group is composed of electrodes where three carbon fibers were connected to each connector terminal and the tips were simply blunt cut; finally the “desheathed” group is composed of electrodes that were generated with single carbon fibers with desheathed electrode tips on each terminal. The purpose of this analysis was to determine the effect of the exposed area on signal quality parameters like the SNR and spike counts. Both method of using triple carbon fibers and desheathing the tips increase the total exposed electrode area.

SNR Comparisons: Figure 2.30 summarizes the data analysis results from

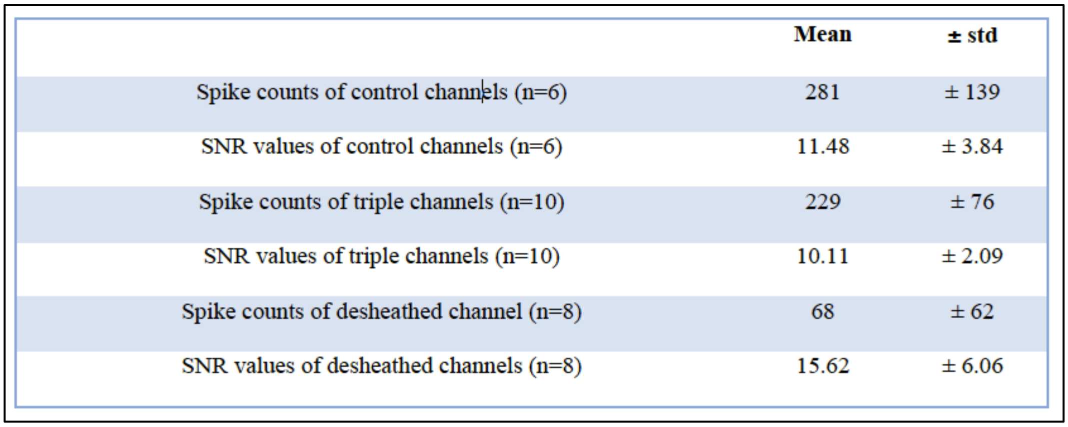

	Mean	**± std**
Spike counts of control channels (n=6)	281	± 139
SNR values of control channels (n=6)	11.48	± 3.84
Spike counts of triple channels (n=10)	229	± 76
SNR values of triple channels (n=10)	10.11	± 2.09
Spike counts of desheathed channel (n=8)	68	± 62
SNR values of desheathed channels (n=8)	15.62	± 6.06

Figure 2.30 Some parameters calculated on compared electrode types.

Rat2. For each group, simultaneously-collected data was used to calculate the spike count, SNR, and baseline RMS (root-mean-square) values. As expected, exposing a larger area of the recording tip by desheathing electrode tips (Figure 2.29, “desheathed” group) decreased the number of spikes that were recorded, but increased the SNR. No substantial difference was observed between the single filament and triple filament configurations.

2.3.3 Histology

Histology results were evaluated as a measure of electrode quality. Limited

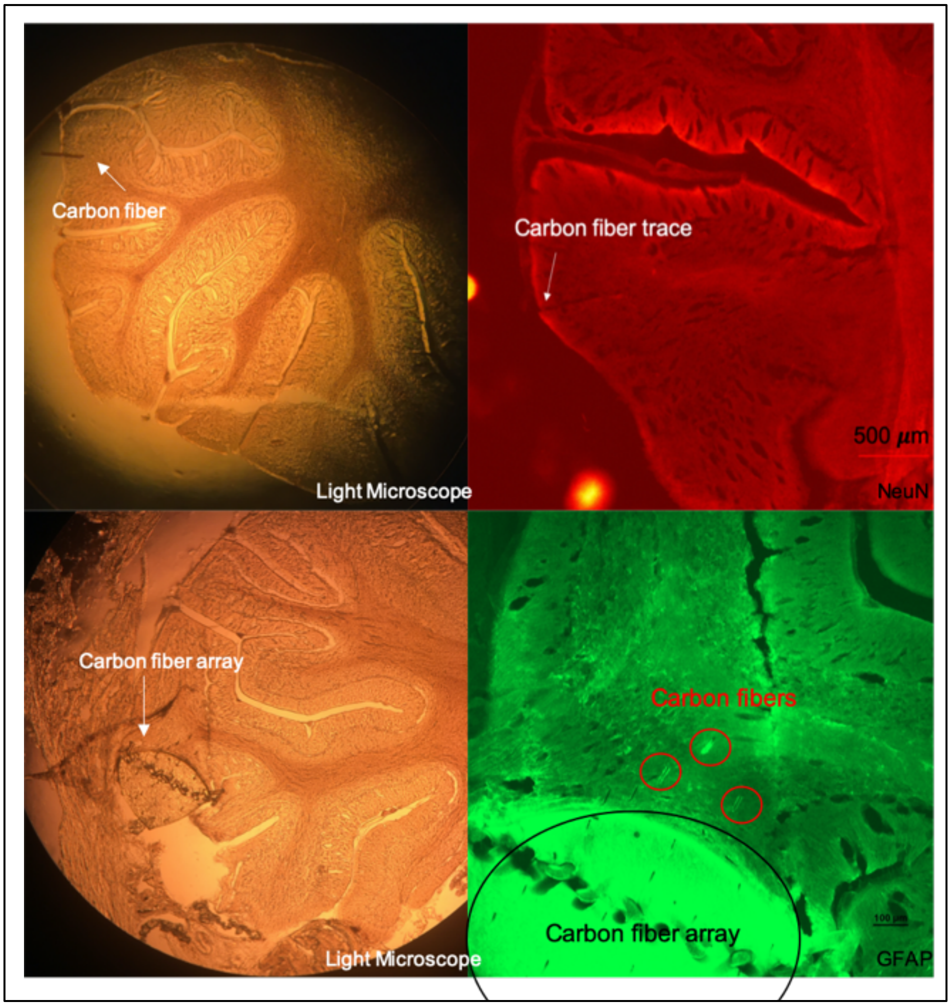

Figure 2.31 Left: Cerebellar tissue section with CFMEA. Right: Cerebellar section with a carbon fiber trace (NeuN staining).

encapsulation around the electrode footprint is a desirable outcome in terms of electrode technology.

2.3.3.1 Cerebellum Electrode. Single carbon fiber electrodes (Figure 2.31 A) and arrays (Figure 2.31 C) were observed in tissue sections. Sagittal histology images showed minimal tissue damage in NeuN staining. GFAP staining showed hardly detectable glial sheath around carbon fiber electrodes..

2.3.3.2 Spinal Cord Electrode. Luxol fast blue (LFB) image from Rat1 (Figure 2.32-A) showed that even though electrodes were bundled together before the implantation, they still stayed apart as small groups in the tissue after implantation as suggested by the empty circles marked by the arrows. Since LFB

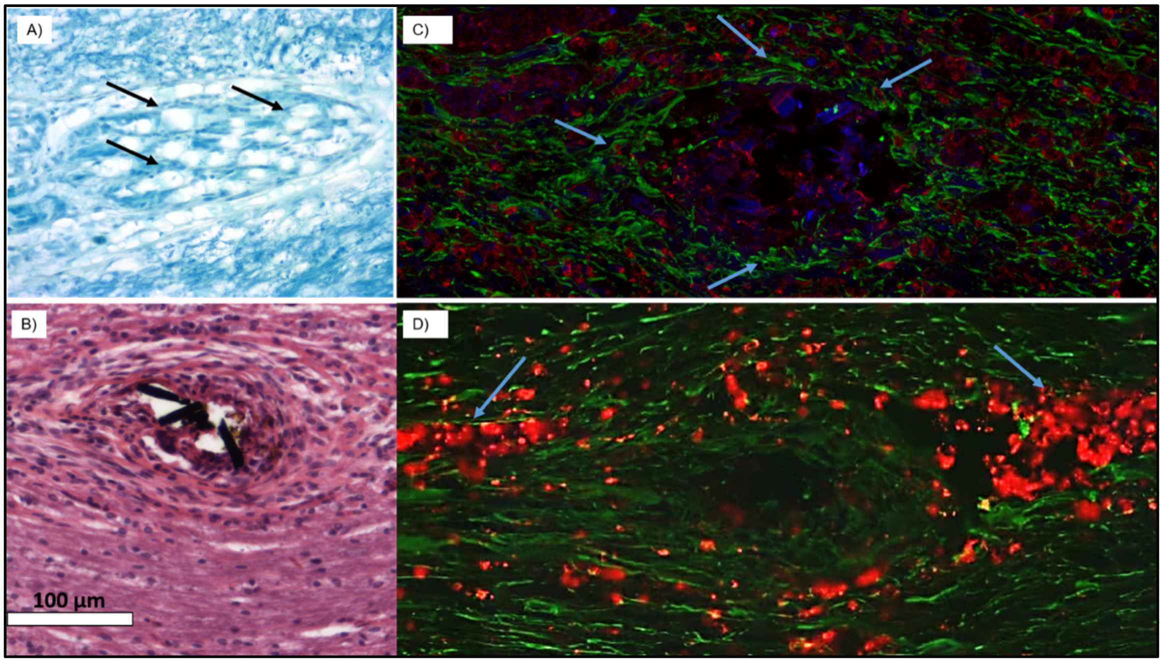

Figure 2.32 Immunohistochemistry coronal sections A) LFB image from the first animal tissue. B) H&E image of the second animal tissue. C) GFAP (green), CD68 (red), and DAPI (blue) images from a sample of Rat2 above the electrode tip and D) around the electrode tip.

stains mainly the myelin sheath around the axons, the larger empty strip encircling the footprint is more likely due to the encapsulation tissue that consisted of astrocytes and macrophages. Figure 2.32-B includes an H&E stained section from Rat2. The fragments of carbon fibers can be recognized inside the electrode cleft, which has a diameter of ~50 µm. Microglial formation was observed around the cleft along the rostro-caudal axis. The tissue reaction was more prominent around the electrode tip, and it gradually became milder as we approached the dorsal surface. Figure 2.32-C shows a sample that is closer to dorsal surface and exhibits very mild astrocytosis and almost no microglia migration. The glial sheath around the bundle was approximately ~20 µm thick in this section. However, Figure 2.32-D belongs to a sample that is closer to the electrode tip and exhibits a stronger response. The glial sheath around the bundle was approximately 50 µm thick in this section. (Cell counting was not performed due to difficulty in counting cells in 50 µm sections in which they appear clustered.)

2.4 Discussion

2.4.1 Cerebellum Electrode

Laser cut: Laser cut played an important role in CFMEA manufacturing. Cutting the carbon fibers manually, which are very fragile, when they are separated as single fibers in the array, is very challenging without breaking them. Laser system made this possible. Also, it lowered the electrode impedances for the range of frequencies that we are interested in recording. Furthermore, it gave a tapering profile to the tips of the carbon fibers that helped with insertion during surgical implantation into the cerebellar cortex through the pia.

Data: Most of the data collected with CFMEAs contained MUA but included some single unit activity.

Bubble test: This was used for testing the quality of parylene-C coating on the carbon fibers before using them in an array. During development stage of the electrodes, we determined that even though the bubble test is a reliable method to confirm proper connection and intactness of the carbon fibers, the injected current causes the tip of the electrodes to be chemically dissolved quickly. Thus, we avoided using this method on the carbon fibers to be implanted into the animals.

Impedances: *In vitro* impedances which were measured in saline after fabrication and prior to implantation, showed that they were mostly in the 2-2.5 MOhm range, which again was achieved with laser cutting. *In vivo* impedances increased over time as expected.

Dissection: During dissection we were able to visually confirm that carbon fiber bundle outside the tissue was intact.

Histology: It was confirmed that carbon fibers caused minimal tissue damage owing to their very small size. But this also imposes a problem during histology. It is hard to detect the mark left by the carbon fibers during sectioning or staining (washing step especially) and thus locate where the fibers were.

Soak test: Soaking the entire arrays helped to confirm if electrodes were ready to be exposed to *in vivo* conditions. We realized that medical epoxy could become deformed *in vivo*. Also using a wood piece instead of a printed circuit board between the terminals can cause problems due to water absorption and swelling (Figure 2.33).

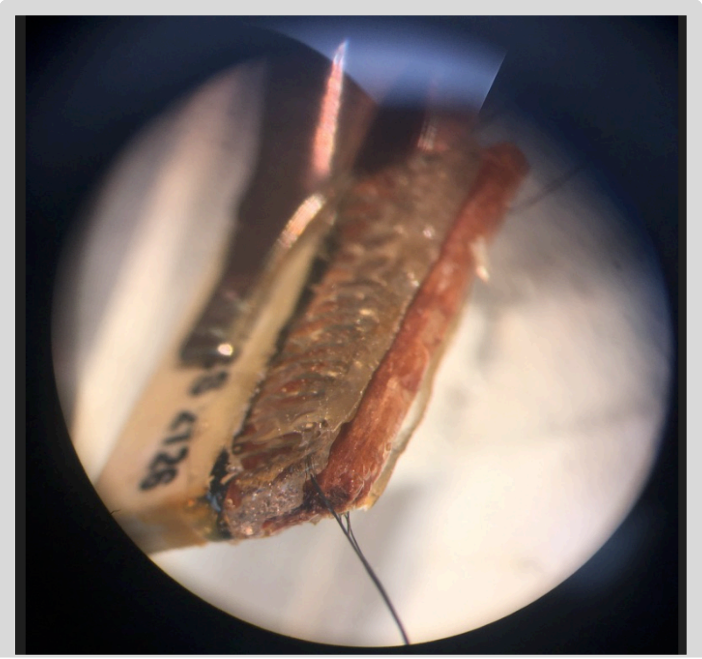

Figure 2.33 Example of an electrode that failed the soak test.

Signal Quality: Average correlations between differential channels were very low and they stayed low over sessions, which shows differential configuration helps to get rid of the common mode signals, presumably from the mechanical and electrical sources. Most of the mechanical artifacts must have been eliminated by the bandpass filter used (30-2000Hz) prior to forming the differential signals. On the other hand, there is always a risk of losing some important data by differentiating the channels. However, the fact that the prediction correlations with different orientations and inter-channel distances did not change much indicates that the loss of neural information by subtracting the activity of adjacent electrodes was not substantial.

Impedances: Electrode impedances increased over time as expected from chronic electrodes. The increase was higher after 4th session, on average in about one month, which may mean possible electrode failure. But based on regression results, it can be said that half of the regressions showed increased success after the middle time point (about 4 weeks) in the study.

2.4.2 Spinal Cord Electrode

The results of the present study demonstrated the suitability of carbon fiber electrodes for chronic neural signal recording. The SEM images indicate that parylene-C coating was successfully removed by our custom-made heating apparatus. We showed that CFs can record single units in behaving rats. Spike amplitudes ranged between 100-200 µVpeak and the spike durations were <2 ms. The presence of bursting activities that were captured by two different electrodes might indicate simultaneous firings of distinct neurons or firing of a single neuron that induced signals on both electrodes. Performing a principal component analysis based on the signal waveforms induced on each electrode can determine if these spikes are from one or two different neurons. Signal-to-noise ratio was notably higher in desheathed electrodes than that of undesheathed and blunt-cut ones. Immunohistochemistry results in Figure 2.32(A) demonstrated that even though electrodes were bundled together before implantation, they splayed in the tissue after implantation, which was preferred in terms of recording from different neurons or units simultaneously. Limited microglial encapsulation around the electrode cleft indicates mild tissue response against the CFME, a desirable characteristic for a chronic neural electrode.

CHAPTER 3

SENSORIMOTOR CONTENT OF MULTI-UNIT ACTIVITY IN THE PARAMEDIAN LOBULE OF THE CEREBELLUM

3.1 Introduction

The primary motor cortex and the associated areas have been the brain site of choice for extraction of volitional information in the past. Philips and Porter (Phillips and Porter 1977) showed the limitations of the classical Fritsch-Hitzig maps (G.Fritsch and E.Hitzig 1870) and somatotopical maps (Woolsey 1958) that were used for the cerebral cortex regions and their respective functions based on their electrical stimulation studies. Primary motor cortex, M1, projects to several regions and the contribution of motor cortex to the total cortical input is reported to be around forty percent (Schwartz 2007). Recent imaging studies (e.g.(Grafton et al. 1991)) are quickly replacing the classical Fritsch - Hitzig maps of the brain to a much more intensely connected view of the brain, which challenges the validity of classical BCI approaches (Schwartz 2007). Therefore, our group has been testing alternative sites for tapping into the volitional signals: the spinal cord descending corticospinal tracts towards a spinal cord-computer interface((Prasad and Sahin 2012),(Gok and Sahin 2019a),(Guo et al. 2014)) and now the cerebellum in this study.

In 1993, Llinas (Llinas and Welsh 1993) claimed that the cerebellum is actually involved in the execution of the movements (Llinas and Welsh 1993). Later reports showed the correlations between the licking movements and the

Purkinje cell (PC) complex spike (CS) activity in rats (Welsh et al. 1995). Then, the contribution of the cerebellar outputs to motor control and timing of muscle contractions were demonstrated (Heck and Sultan 2002). Alterations in the frequency of PC simple spike (SS) activity was observed in Crus I during volitional tactile whisker movements (Chen, Augustine, and Chadderton 2016). These studies expanded our knowledge on the cerebellar function, but the degree of its involvement in motor coordination and the anatomical functional mapping of the cerebellum are still mysteries. The cerebellar involvement in the forelimb kinematics is well-established but there is a need to show how much EMG representation is present in the cerebellar cortex and the localization of the forelimb motor functions (Ebner, Hewitt, and Popa 2011), specifically in the PML.

Purkinje cell (PC) axons form the only output projections from the cerebellar cortex. The PCs reside very close to the cerebellar surface at a depth ~300 μm in the rat allowing easier access to their activity with minimal disturbance to the neural tissue with short-shank electrodes. PCs organized in microzones together with their targeted cerebellar nuclei are responsible for processing of afferent activity from the periphery and the descending signals from the higher brain centers in motor coordination, learning, and cognitive functions. Moreover, the cerebellum offers a highly organized structure with parasagittally clustered zones and microzones that consist of only few neuronal subtypes.

Carbon fibers, with their small size and high flexibility, are one of the best electrode materials that can minimize the tissue response at implantation. Our previous work (Cetinkaya, Gok, and Sahin 2018) showed negligible tissue damage to carbon fibers implanted into the rat spinal cord, agreeing with the reports in the motor cortex (Patel et al. 2016). CFMEAs are designed to record from multi-zones/stripes of the cerebellum by taking advantage of carbon fiber`s micro-size (7 μm) while maintaining high strength (Young`s Modulus ~250 GPa) despite owning excellent flexibility in cross-sectional direction for an electrode material.

In this study, we investigated the feasibility of a BCI system that is based on accessing the volitional forelimb muscle activity from the cerebellar neural signals. Rats were implanted with CFMEAs and the PML activity was recorded during arm-reaching behavior. The muscle activities and force profiles were predicted using a linear regression model. The results suggest that the PML activity contains information that is correlated to the forelimb motor function.

3.2 Methodology

3.2.1 Carbon Fiber Microelectrode Array Fabrication

Carbon fibers (7 μm, Goodfellow Cambridge Ltd., England) were coated with 2 μm (±50%) parylene-C at a foundry (Specialty Coating Systems, Indianapolis) at room temperature. Thirty-two single carbon fiber filaments were cut to a length of 1.5-3 cm under microscope and ~250 μm of parylene-C coating was removed from one end of the filament using a soldering iron at 290˚C. Carbon filaments were connected to the pins on the micro-connector (A79022-001, Omnetics Connector Corporation, Minneapolis) individually using conductive silver epoxy

(EpoTek, Massachusetts) and cured in an oven at 150˚C for 10 min. A 10 by 9 matrix was cut off from a nylon woven mesh sheet with thread diameter of 31 µm and 21% open area (U-CMN-31, Component Supply, TN). Single carbon fibers were inserted through the holes in the mesh to form a 4x8 array with 100 µm caudal and 150 µm lateral direction pitch and fixed in place with medical epoxy (OJ 2116 EpoTek, MA). Teflon-coated multi-strand stainless steel wires (25.4 µm, 793200, A-M Systems, WA) were attached to the Omnetics connector as reference and ground electrodes with silver epoxy. Connector terminals were hermetically sealed using medical epoxy. Carbon fibers protruding from the mesh substrate were cut at ~450 µm using a 450 nm laser (4 W, Wercan Comp., China).

3.2.2 Testing the Coating and Electrodes

Electrode impedances were measured at 1 kHz and found to vary from 0.5 to 3 MΩ prior to implantation. In some cases, parylene-C insulation was tested by passing a small direct current (<1 µA anodic) for a few seconds through the electrode in saline that would produce bubbles if there were any pinholes in the insulation exposing the fiber.

3.2.3 Implantable Electromyogram Electrodes

Electromyogram (EMG) wire electrodes were prepared to record from four forelimb muscles: a wrist extensor on the dorsal forearm, a flexor on the ventral side of the forearm, the triceps, and the biceps. Five cm long Teflon-coated multi-strand stainless steel wire pairs were connected to an Omnetics connector (A79022-001, Omnetics Connector Corporation, Minneapolis), two for each muscle for differential recording, and coated with clear medical epoxy (code, company) for hermetic sealing. The tips of the wires were desheathed for ~2 mm and staggered by 4 mm, and medical epoxy was applied to the very end forming a small bead to provide an anchor for suturing to the muscle belly.

3.2.4 Animal Training

Eight Long Evans male rats were trained for a reach-to grasp task. Food restriction of animals began 3 days prior to training to boost animals` attentiveness to training and appetite for sugar pellets. During food restriction, animals were fed 3 pellets/day based on the protocol. Animals were about 175 g when they arrived at the facility. During training and recording, the animals' weights were monitored and feeding was adjusted if necessary to keep the weight ±20 percent of the baseline (175 g). Animals weights were generally ranging between 180-250 g during data collection.

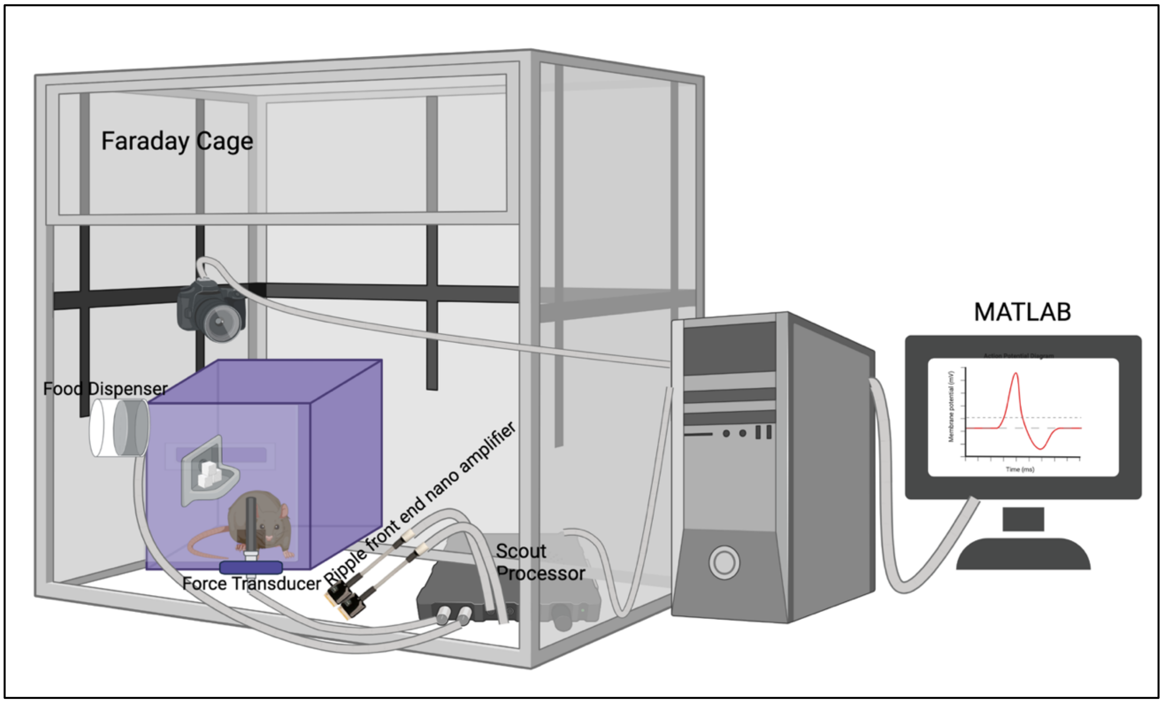

Figure 3.1 Animal training and recording setup.

Animals were trained in a clear plexiglass box that was equipped with a force and torque transducer (Nano 17, ATI Industrial Automation) fixed outside a window opening of the box at 1 cm distance and a computer-controlled food dispenser. The behavior was to reach and pull the force bar attached to the transducer in order to receive a sugar pellet as a reward. The average training time was about one week. The animal was rewarded only when it pulls the force bar with a force above a certain threshold. Animal`s behavior was shaped to use a single paw and reach the force threshold only in one attempt (Figure 3.1 and 3.2).

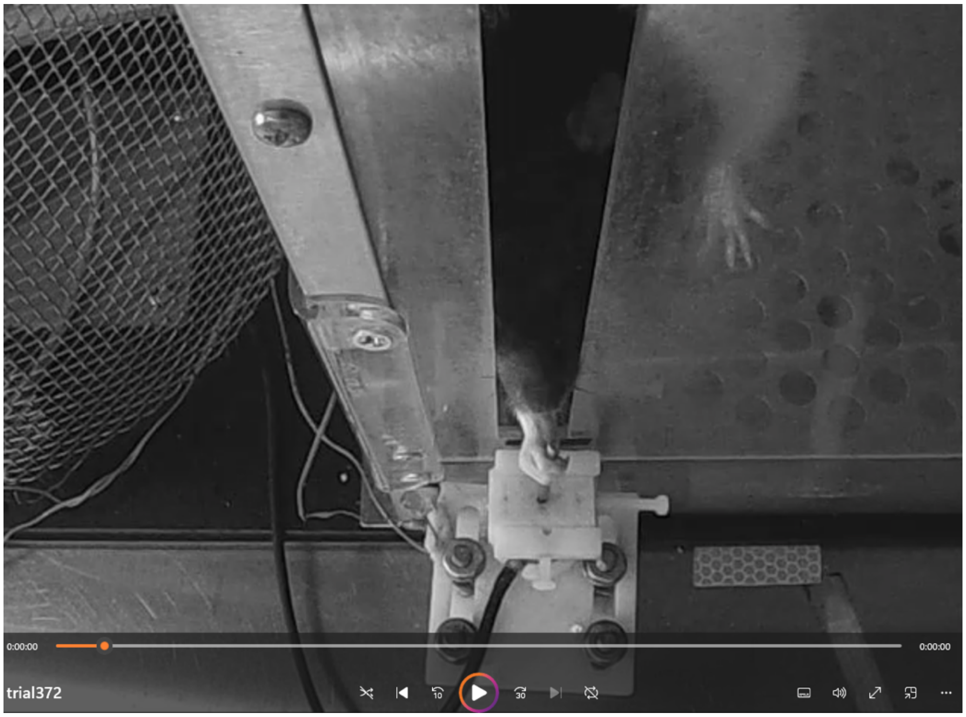

Figure 3.2 Animal training and recording setup. Top view of the animal while grasping the force bar.

3.2.5 Animal Surgery

All procedures are approved by the Institutional Animal Care and Use Committee (IACUC), Rutgers University, Newark, NJ. Anesthesia is induced with 5% isoflurane and maintained with 2.0-2.5% isoflurane (v/v) in 100% oxygen throughout the surgery. Animal`s head is fixed in a stereotaxic frame and the fur in the surgical area is shaved. Ointment is applied to the eyes to prevent dehydration. Blood oxygenation level and heart rate are monitored with pulse-oximeter attached to the hind paw. Body temperature is regulated at 36.5ºC using a heating pad underneath the animal and a rectal temperature probe. Salix (0.5 mL/kg, IM) is given to avoid brain edema and bulging of the cerebellum during surgery. Local analgesic (Marcaine, 0.5 mg) was injected into the neck and head muscles around the incision areas as pre-emptive anesthesia. After making an incision to expose the skull from bregma to the lambda and removing the periosteum completely, five or six holes are drilled into the skull using a fine drill bit. Metal screws (0-80 X 1/16, 1.6 mm, PlasticsOne Medical Design and Manufacture, VA) are screwed into the holes with a little amount of cyno acrylate (Gluture, WPI). The skull is dried completely by applying 3% hydrogen peroxide followed by rinsing with normal saline. The skull top and the screw heads are covered with dental acrylic mixed with Gluture before Omnetics connectors are attached.

EMG electrode implantation: The EMG connector is then fixed atop the skull using dental acrylic. Four small skin incisions are made to expose the muscles of interest in the forelimb that was most frequently used by the animal during training. Each muscle is electrically stimulated with bipolar electrodes under direct vision to confirm their location and function. Electrode wires are tunneled subcutaneously from the Omnetics connector to the respective muscle with the help of a stainless steel tube. Finally, the EMG wires are sutured with 8-0 non-absorbable sutures to the muscles epimysially, and the skin incisions are closed with 6-0 absorbable sutures.

CFMEA implantation: For the CFMEA implantation, a cranial hole (2 x 2 mm) is opened over the paramedian lobule (PML) and Crus II in posterior cerebellum (Figure 3.3) using ophthalmic rongeurs. The dura is resected medio laterally along the midline over the PML.

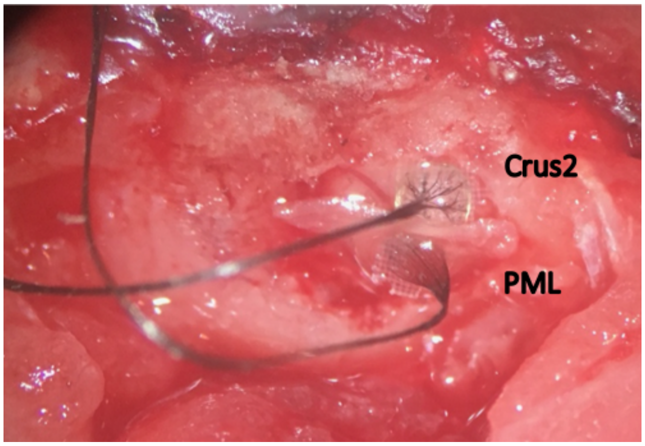

Figure 3.3 The rat cerebellum with implanted carbon fiber arrays in the PML and Crus II.

CFMEA Implantation: The 4x8 carbon fiber array is implanted by slowly inserting it into the PML cortex with the medial edge being ~1.0 mm from the paravermal vein (Figure 3.4). The carbon fibers extending from the Omnetics connector are covered with dental acrylic except the last 5 mm near the array. Then, the array is covered with connective tissue excised from the neck muscles to secure it in position. The reference and ground wires are fixed to the skull bone using dental acrylic. Finally, the skin incisions are closed with absorbable sutures and the skin edges around the connectors were sealed using dental acrylic.

3.2.6 Data Collection

Neural and EMG signals are collected at 30 kHz sampling rate during trained behavior using a multi-channel head-stages (Grapevine front end nano2, Ripple, UT) and amplifier (Scout Processor, Ripple, UT), and a data acquisition card (PCI 6071, National Instruments) controlled through MATLAB (MathWorks, Inc.). Forearm movements are captured at 100 frames/s using a video camera (1080p

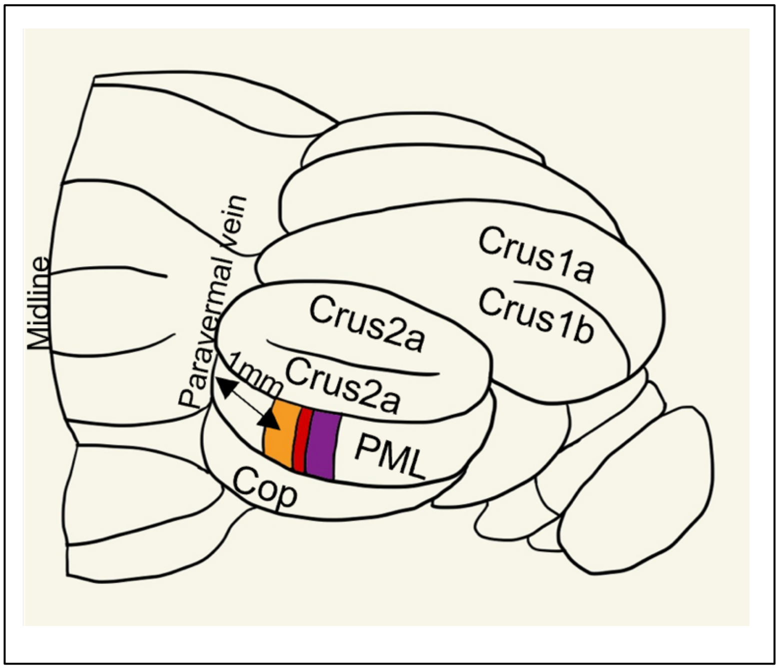

Figure 3.4 The PML regions where the electrodes were implanted: C1, CX, C2.

HD Webcam C018, TeckNet, UK) and synchronized with electrophysiological and force signal from the transducer. *In vivo* electrode impedances are measured and stored with Trellis software (Ripple Inc.). Each session consisted of a set of recordings that contained 50-100 4 s episodes collected during behavior on the same day. Two sessions were conducted each week for ~4 weeks in each animal after they completely recovered from the surgery.

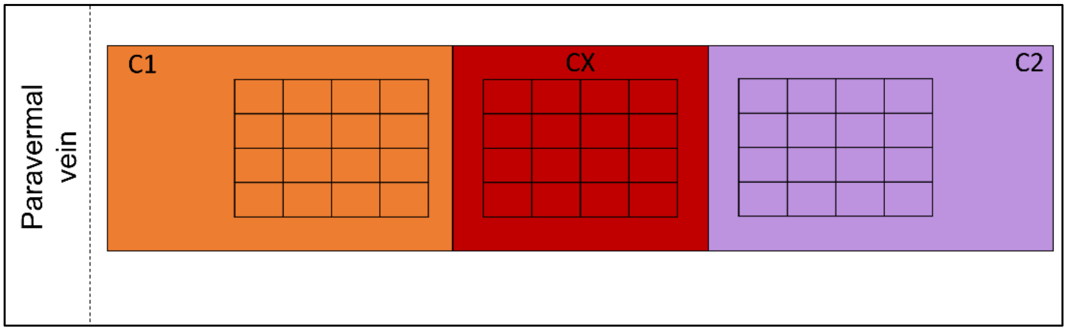

Figure 3.5 The zones of the PML to which electrodes were implanted: C1, CX, C2. (2 implants to C1, 3 implants centered around CX, and 1 implant to C2).

3.2.7. Data Analysis

3.2.7.1 Electromyogram Prediction via Linear Regression.

3.2.7.1.1 Preprocessing All data processing was performed in MATLAB. Each session was divided into 80% training and 20% test sets for cross-validation of the reconstruction coefficients. The force data was 5 Hz-lowpass filtered and was synched to neural and EMG signals. The maximum amplitude time point of the force data was marked as the center and +/- 0.75 s window around this point was used to analyze the neural and EMG data. Neural data was filtered with a 60 Hz band-stop notch filter and was then further cleared of any movement artifacts by removing the episodes that exceeded a threshold mark (1000 μV). considering extracellular neural activity recordings cannot normally exceed this threshold in a typical extracellular recording.

3.2.7.1.2 Generating Electromyogram and Neural Envelopes EMG signals were band-pass filtered between 20-2000 Hz using 4th order Butterworth filters. For each dataset (each session of each electrode data (10 electrodes x 8 sessions x 4 EMGs = 320 datasets)) ±1, 1.5, or2 standard deviations of EMG envelopes were computed. Standard deviations of EMGs were calculated for each data point in the entire signal length from EMG envelopes in all trials of the dataset. The outliers were calculated as any EMG envelope that falls above or below the STDs of the signal for any data point. Once a trial is tagged as an outlier, any corresponding data whether it is neural, EMG or force, is excluded from the regression. The algorithm was designed to pick either one of the four options (No Outlier, 1 STD, 1.5 STD, 2 STD) to eliminate some of the outliers or not eliminate at all (No Outlier) based on the success of the prediction. From “No Outlier” to “2 STD” to “1.5 STD” to “1 STD” the number of trials remained in the dataset

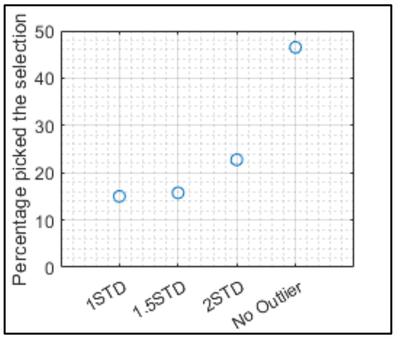

Figure 3.6 Out of 320 datasets how many datasets (in percentage) required the outlier elimination.

decreases but also the success of the regression increased. The algorithm was forced to pick next highest option when the dataset is too small (<25 trials total and <5 trials test set) after outlier eliminations. The percentages of all datasets (not the number of trials, but out of 320 datasets how many of them required outlier elimination) that picked every specific option are shown in Figure 3.6.

Neural signals from 32-electrodes were paired to obtain 16 differential channels based on their positions in the array as the closest neighboring channels in the medio lateral direction. Following a 60 Hz band-stop notch filtering, neural signals were divided into five different frequency bands (30-100 Hz, 100-300 Hz, 300-1000 Hz, 1000-1500 Hz, and 1500-2000 Hz) using 4th order Butterworth filters, resulting in 80 neural envelopes (16 differential channels * 5 bands). Then they were full-wave rectified and low-pass filtered at 5 Hz for generating envelopes. Transient filter responses at the start and end of the signals were removed by truncating 0.35 s of the data and all the trials in a session were concatenated to form continuous time signals. The neural and EMG envelopes were down sampled from 30 kHz to 1 kHz to reduce computer processing time.

3.2.7.1.3 Regression Linear regression is used to predict the EMG signals from the neural signal envelopes after randomly separating the trials into training and test sets for cross validation. As a measure of goodness of estimation, the Pearson's correlation (r) between predicted and measured EMG signals were calculated in each session. Several criteria were added to the prediction algorithm to increase the rigor in the results. The session was excluded if the test set size is too small (<5 trials), the p-value of correlation did not reach significance ($p > 0.05$), or the kinematics, i.e. the force profile, did not show repeatability which was treated as an outlier . Around 50% of the data required one of the outlier elimination options to be used.

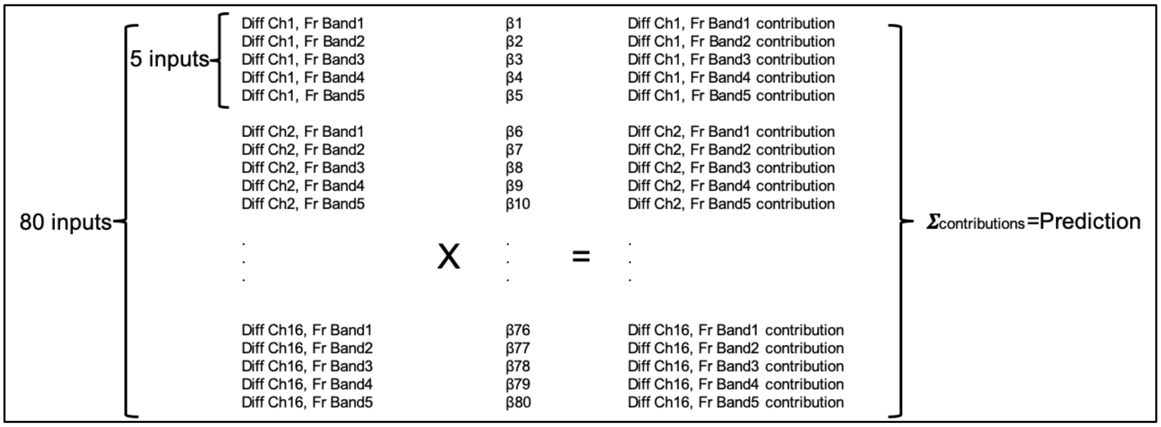

Figure 3.7 All neural inputs and their contributions to the prediction diagram.

3.2.7.2 Shifts: Analyzing Data with Different Neural Delays. The regression procedure was repeated for different shifts (±10, ±50, ±100, and ±200 ms) of neural data with respect to EMG signals to determine if the cerebellar signals primarily contain motor or sensory information.

3.2.7.3 Regression in Different Phases of the Behavior. The 0.8 s behavior

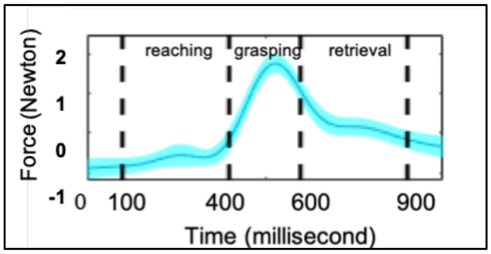

Figure 3.8 Phases of the behavior based on the force profile (average of multi-animal, multi-session data).

data were divided into three time-windows based on the average force profile from all the trials (N=~1000 trials), which indicated that the first ~0.3 s of the data is ‘reaching’, the next ~0.2 s in the middle is ‘grasping’, and the last ~0.3 s of the behavior is ‘retrieval’ (Figure 3.8). Because the average force profile had a smaller standard deviation, we relied on the force profile for determining the phase durations. In human trials, reaching takes around 800 ms on average(Wang et al. 2016; Coats et al. 2018). Mice complete reaching movement in 0.5-0.8 second with normal speed in freely behaving animals (Becker et al. 2020). In Gok`s study (Gok and Sahin 2019b), he divided the behavior window into two phases as “reaching” (-0.2 second from the center of the behavior) and “grasping” (+0.2 second from the center of the behavior). However, here we considered either the onset or the peak of the force as the beginning of grasping. The regression algorithm was applied in each one of the three time windows separately, and as a whole as well, to investigate which segment of the behavior has a stronger representation in the neural signals.

3.2.7.4 Configurations: Regression for Different Configurations of Differential Neural Channels. Differential electrode configuration is chosen here in order to suppress the common mode signals that may potentially be injected into the signals through the reference electrode. However, some of the neural information sampled locally by each electrode may also be lost while subtracting the channels from each other, depending on how much the volumes of recording overlap by adjacent electrode channels. In order to minimize the loss of useful neural data and maximize the information content, five different combinations of

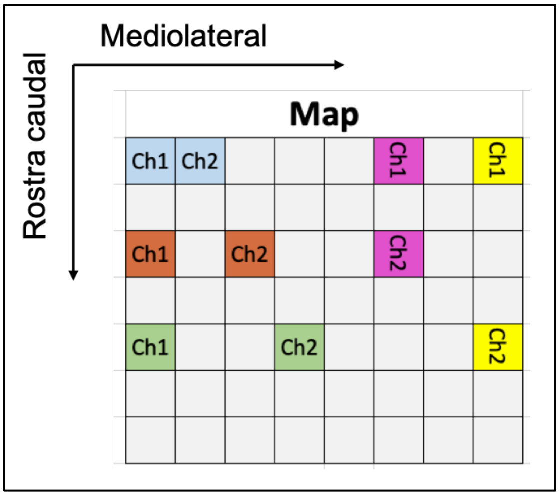

Figure 3.9 Configurations that were analyzed. Differentials between the same color channels were taken (for each of the 16 pairs). Blue: medio lateral-short, orange: medio lateral-medium, green: medio lateral long, pink: rostra caudal-medium, and yellow: rostra caudal long.

channel pairs were tested as differential configurations. Principal components of 32 single-ended channels were computed as an alternative. The first differential configuration was formed by pairing the neighboring channels in the medio lateral direction (blue in Figure 3.9). The pitch between channels in this direction is 68-100 µm, which is smaller than reported distances between microzones, ~200 µm. The second (orange in Figure 3.9) and the third configurations (green in Figure 3.9) were again differentials in medio lateral direction but now by skipping one and two channels respectively, and thus the distances were 136-200 and 204-300 µm. In the two remaining configurations (pink and yellow in Figure 3.9) the channels were paired in the rostra caudal direction.

3.2.7.5 Clustering Signals and Detecting the Patterns of Neural, Electromyogram, and Force Data. Force signals, and neural and EMG envelopes were clustered using the k-means algorithm in MATLAB using the entire time signals as vectors. The purpose of this analysis was to investigate if there are any typical patterns in the neural signals that may correlate with the shape of the corresponding force or EMG signal.

3.2.7.6 Contributions of Different Frequency Bands to Prediction. Raw neural signals were divided into five different frequency bands by filtering them with nonoverlapping bandpass filters and used in regression as distinct input channels. Regression coefficients from the training set belonging specifically to a given frequency band were multiplied by the input data in the test set to find the contribution of that frequency band only. RMS value of the resulting time signals were calculated, and its relative contribution was found as a percentage of all the frequency bands. The frequency bands were chosen: 30-100 Hz (low frequency LFP signals), 100-300 Hz (high frequency LFP signals), 300-1000 Hz (low frequency band of MUA), 100-1500 Hz (high frequency band of MUA and spike activity), 1500-2000 Hz (harmonics of spike activity).

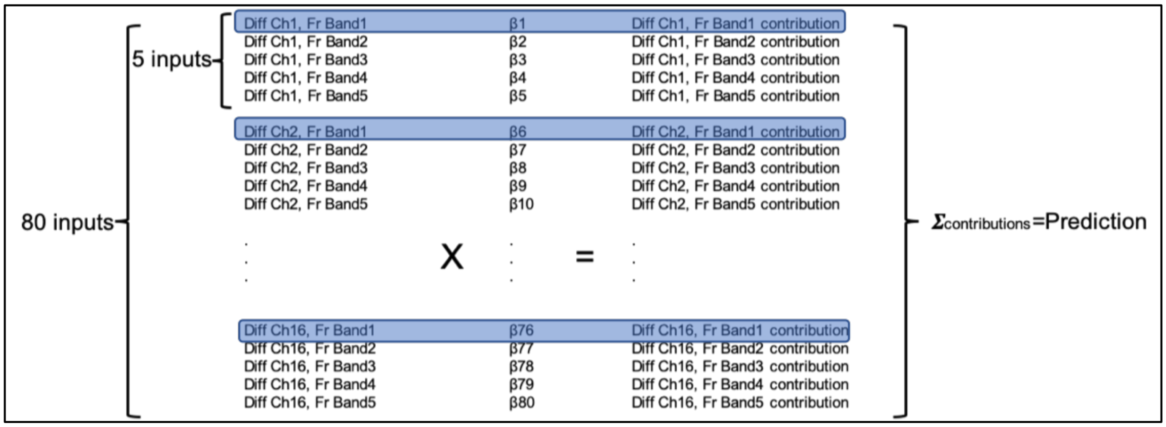

Figure 3.10 A schematic diagram of how frequency band contribution inputs were selected.

3.2.7.7 Contributions of Different Channels to Predicted Signals Based on Topography. The contributions of individual neural channels were calculated in the same way as in frequency band contributions. Briefly, for each channel, the RMS value of the sum of all the five frequency band contributions of a channel were calculated. Then the percentage contribution of the channel to the final prediction was calculated.

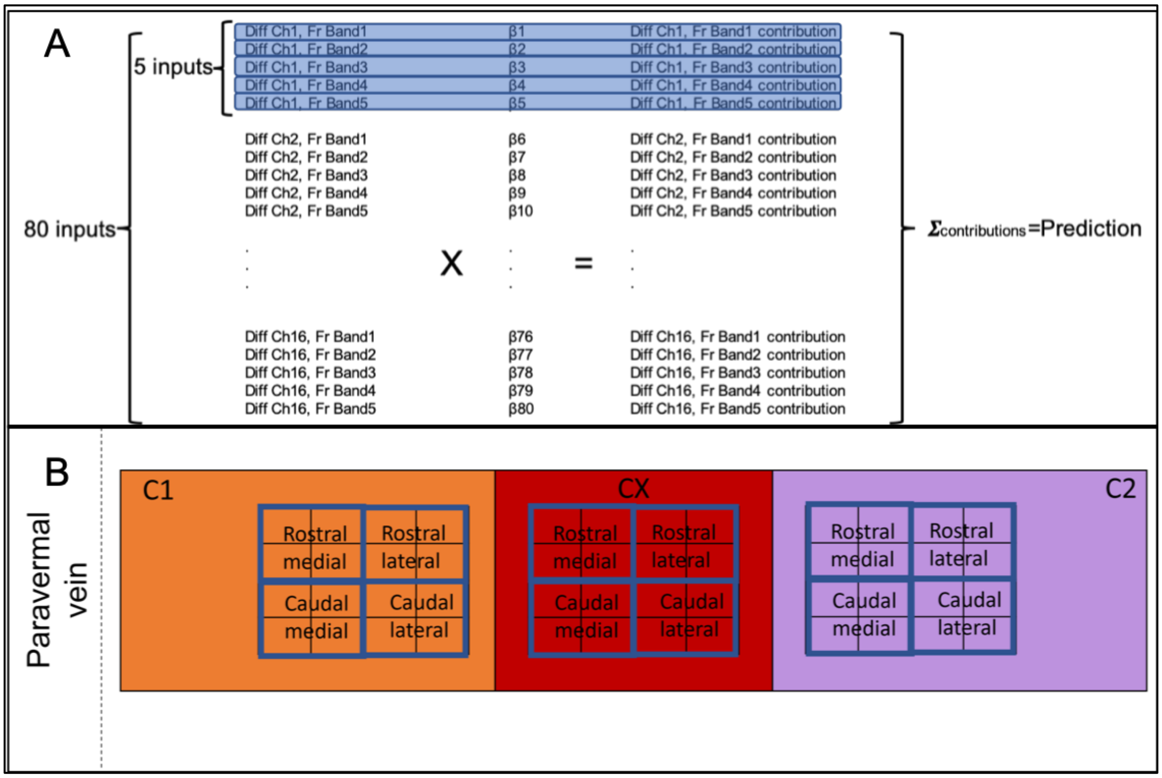

Figure 3.11 A) A schematic diagram of how input channel contributions were selected and B) how arrays were divided into quadrants.

The results of this analyses were statistically tested with z-score for each quadrant of the array matrix. The differential channels in the four quadrants were named as ‘rostral medial’, ‘rostral lateral’, ‘caudal medial’, and ‘caudal lateral’. In each animal the electrode array implanted to one of the three regions (approximately C1, CX, and C2) was analyzed separately following this approach.

3.2.7.8 Principal Component Analysis. Principal Component Analysis (PCA) was used for reduction of dimensionality in the neural data. First few principal components (PCs) account for most of the variation in the data. As an alternative to taking the differentials of the neural data, the principal components were used but as mentioned in section 3.3.2.6, it resulted in lower success rates in regression compared to differentials. PC1 was removed from the signals with the assumption that it may represent the common mode signal injected through the reference electrode, and the next several components (4-17 PCs depending on the dataset (Figure 3.33) that are representing 80% of variance in the data were included in reconstruction. If a large number of PCs are required to account for 80% of variance, this indicates multiple neural sources and thus richer information content in the signals and *vice versa*. The smallest components were left out of the analysis assuming that they were representing the noise components that had insignificant contributions to the behavior, which was measured here as low variances. Common-mode signals were also considered as contamination and eliminated from the signals by taking the difference between the recording channels. The reasoning behind this assumption is that any mechanical perturbation due to animal's movement would affect all electrodes similarly as a common-mode signal. Also any electrical noise near the recording electronics, including the biological ones such as the ECG and the activity from the nearby muscles, would induce artifacts in all the recording channels simultaneously, which is also a form of common-mode signal. Thus, the signals that appear in all the channels simultaneously would mostly contain undesired mechanical or electrical artifacts.

3.2.7.9 Finding the Center Point in the Behavioral Window. The behavior center was used to determine where the grabbing of the force bar was taking place and the +/- 0.4 s time window around it was included into the data analysis to capture the behavior. The center point of behavior was determined with three different methods to see if the selection of window affects the results. In Force-Max method, the force profile's maximum amplitude time point was selected as the center of the behavior. In Force-Onset method, a square trigger signal that is ~10 ms long was generated when animal pulled the force bar above threshold and its midpoint was selected as the center. Force threshold by default was set to 0.4 N in the y-direction (animal`s rostra caudal direction) at the beginning of

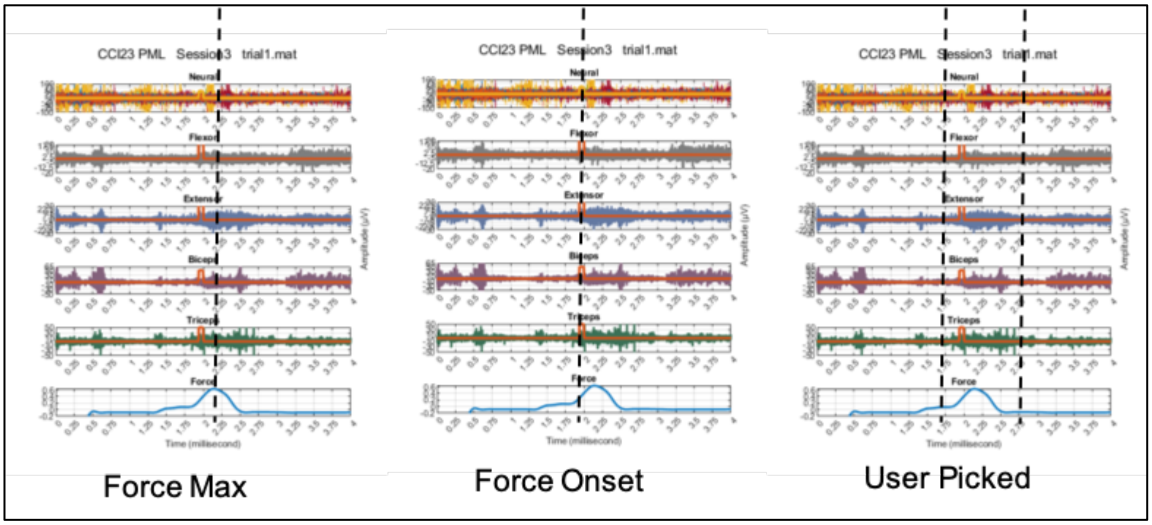

Figure 3.12 Three different methods of determining the center of the behavior.

training, then optimized for each animal to 0.4 ± 0.15 N to achieve a firm grasping behavior as the animal learned the behavior. The same threshold was used during data collection. In User-Picked method, the center was marked by the user based on the EMG profiles (Figure 3.12).

3.3 Results

3.3.1 Regression on Entire Dataset

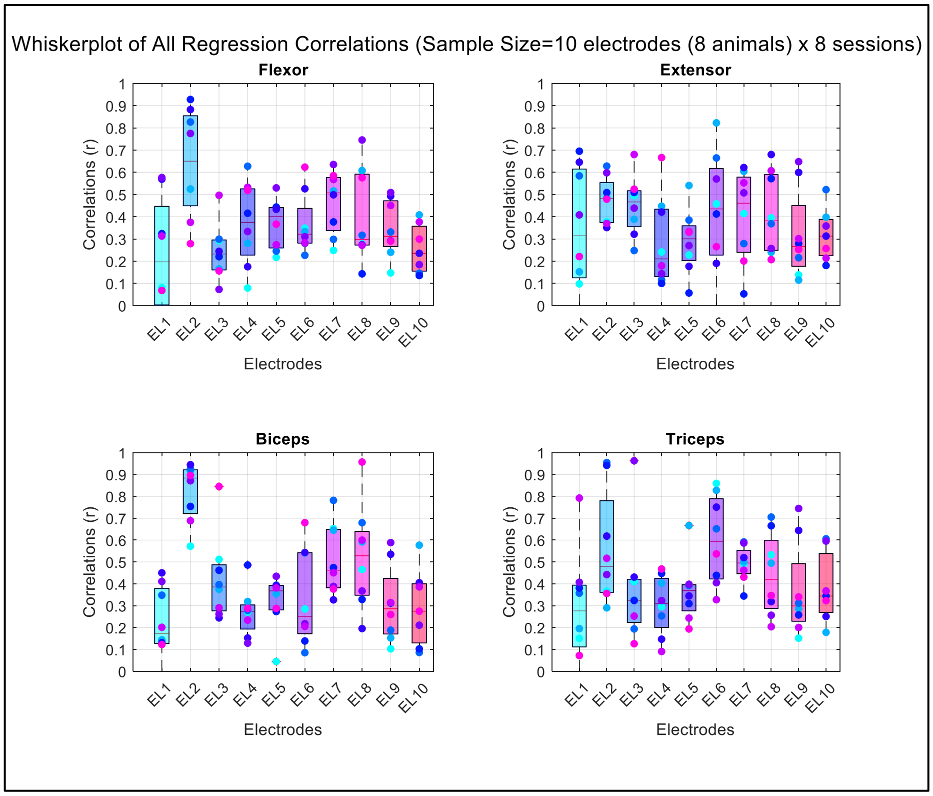

Figure 3.13 Correlation (r) values between neural and EMG envelopes in the test set for 10 electrodes implanted in 8 animals, each with 8 sessions.

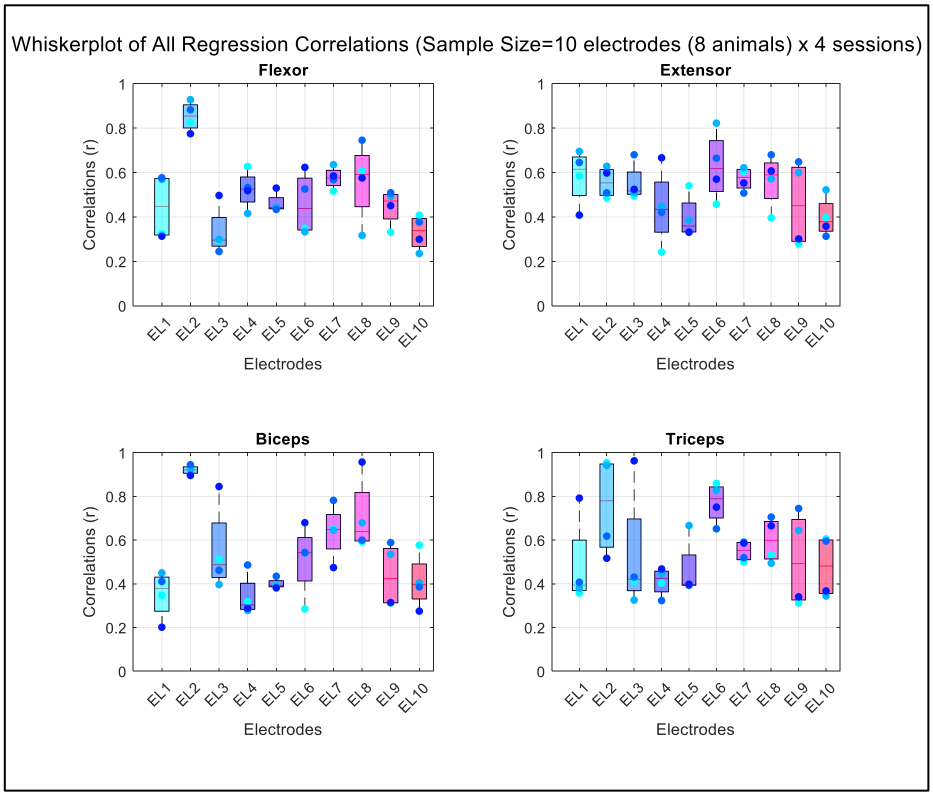

Figure 3.14 Correlation (r) values between neural and EMG envelopes in the test set for 10 electrodes implanted in 8 animals, only 4 sessions with signals of good quality are included from each electrode.

3.3.2 Data Analysis on Subset

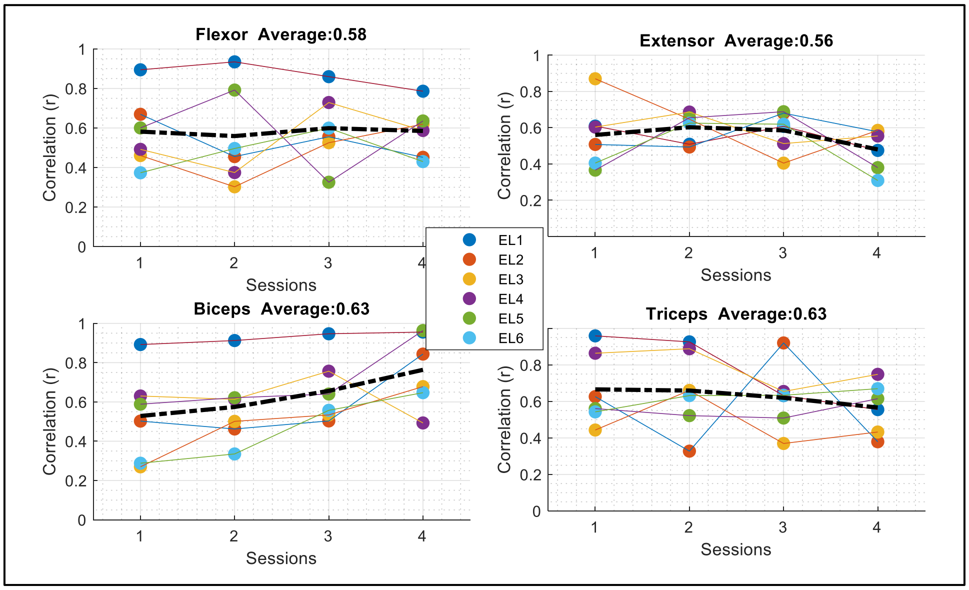

Figure 3.15 Correlation measures between the actual and predicted EMGs in 6 animals, encoded in different colors, over 4 sessions.

Since the signal quality was poor in earlier implants (Figure 3.13 and 14), future

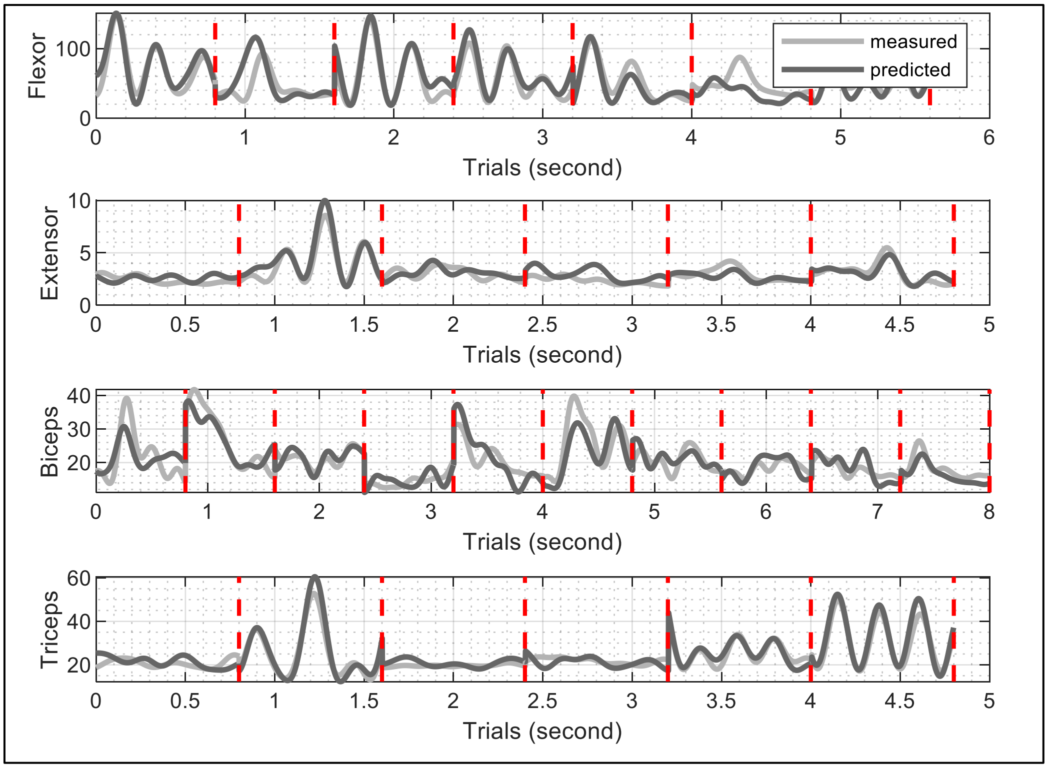

Figure 3.16 Sample EMG predictions with average correlation of 0.85. Vertical dash bars delineate data from separate trials.

analyses were performed on a selected data set as described. The size of this subgroup was 6 electrodes and 4 sessions in each. The change in correlations over sessions can be seen in the figure (Figure 3.15).

The average regression correlations between measured and predicted EMGs were around 0.6 in these 6 animals. In some sessions median values were as high as ~0.78. In animal1 data predicted flexor, biceps, and triceps EMGs with high success (r=~0.9). Biceps' median value reached to 0.76 in session 4. The correlations values were in the 0.8-0.9 range in some other

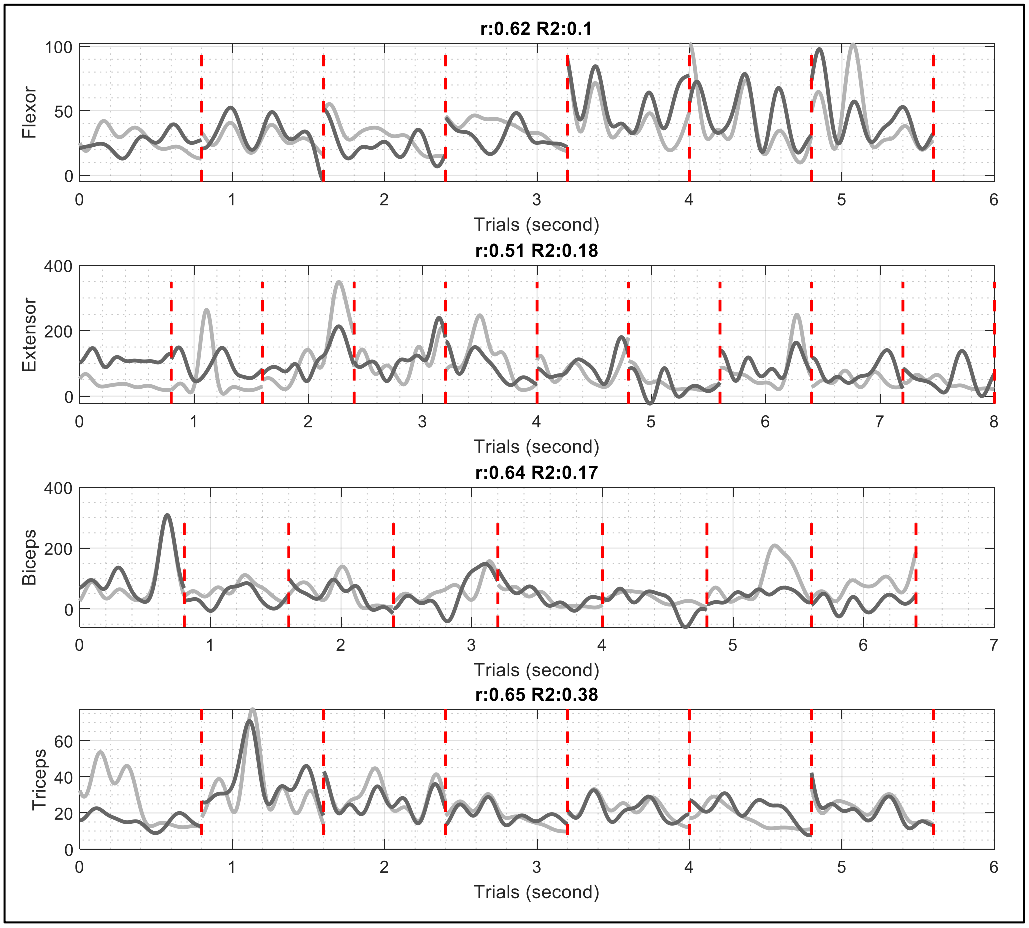

Figure 3.17 Sample EMG predictions with average correlation of 0.6. Compare with previous figure.

sessions also (Animal1, r= 0.93, for flexor in session 2; Animal3, r=0.85, for extensor in session 2; animal5 and animal1, r= 0.96, in session 4; animal1, r= 0.95, and animal4, r= 0.86, for triceps in session 1.)

Even though the group data from all animals and sessions did not yield high correlation values between measured and predicted EMG envelopes, in some data sessions, the predictions were outstandingly successful (Figure 3.16).

3.3.2.1 Regression and Mutual Information with Varying Shifts.

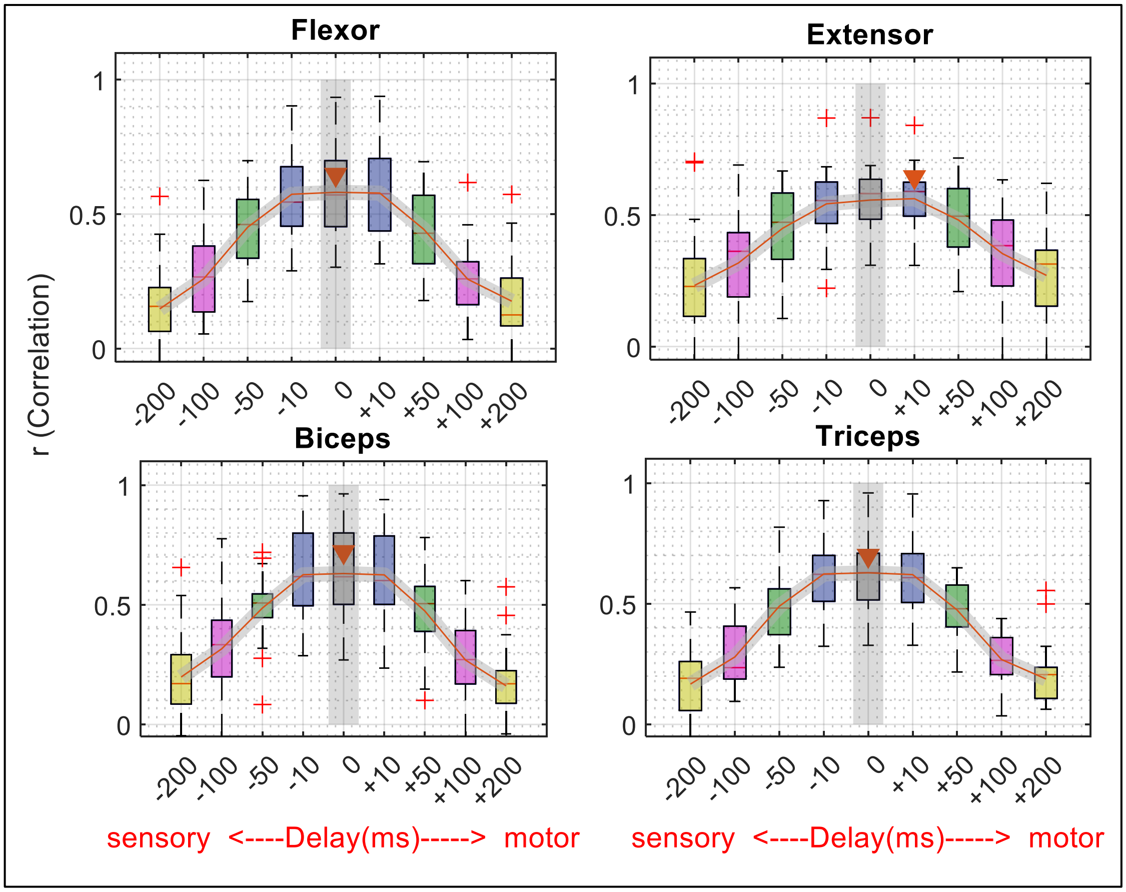

Figure 3.18 Group correlations from linear regression for forward and backward shifting of neural data with respect to the EMG signals to determine the sensory and motor nature of the neural signal. 5 Hz filter is used to obtain the neural and EMG signal envelopes.

3.3.2.1.1 Using Regression The success of the regression (r values) decreased

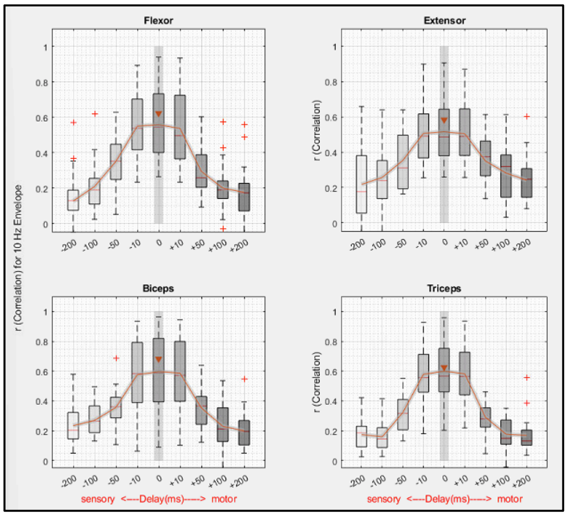

Figure 3.19 Group correlations from linear regression for forward and backward shifting of neural data with respect to the EMG signals to determine the sensory and motor nature of the neural signals using 10 Hz filter.

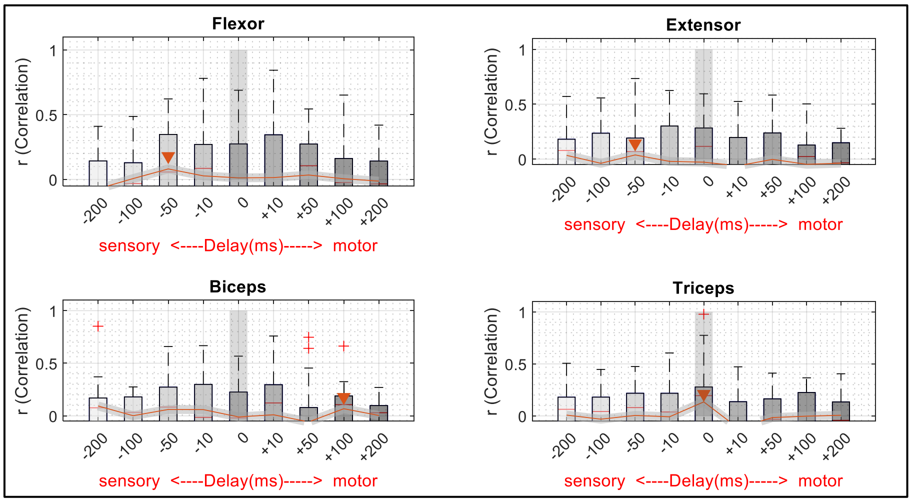

Figure 3.20 Chance level correlations from linear regression for forward and backward shifting using white noise. For most shifts correlations around ~ 0.1. shows the correlations found in the previous figure (Figure3.19) were above chance level.

for shifts in either direction (Figure 3.18) and the maxima ocurred at 0 ms shift except for the extensor muscle where the peak was at +10 ms (marked with red arrow tips). However, the fact that there is still correlation above the chance level for significant delays in either direction suggests that the PML signals contain both sensory and motor related information. The regression analysis was repeated for a lighter filtering (corner frequency is 10 Hz instead of 5 Hz) on the rectified neural and EMG signals to find their envelopes. The results in Figure 3.19 is similar to those in Figure 3.18 in general except that the peak correlations are a little smaller and the decline on each side of the peak is a little sharper for time shifts larger than ±10 ms with the 10 Hz filter. This suggests that the memory effect introduced by the envelope filter has a small effect on the

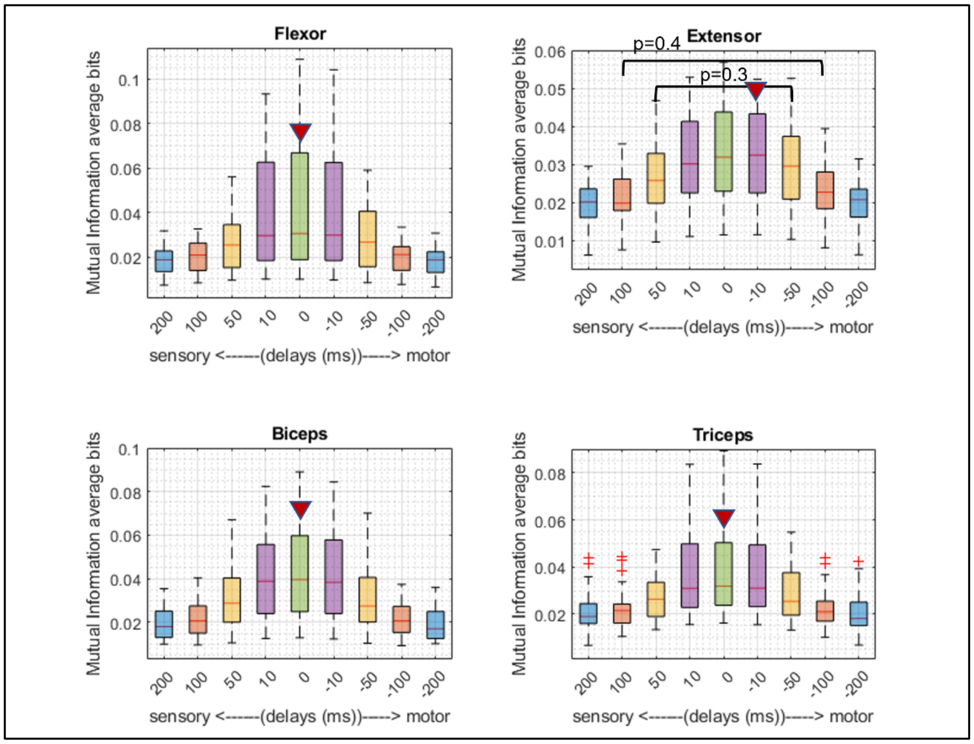

Figure 3.21 Effect of shifting the neural data in time on the mutual information between the neural and EMG signal envelopes.

regression results and the correlations plot is not smeared by it giving a rise to correlations fictiously for non-zero time shifts.

3.3.2.1.2 Using Mutual Information Mutual Information plots agreed with the correlation results. The neural data contained both motor and sensory information, although there is a slight increase for positive delays (Purple and yellow bars in Figure 3.21 (+/- 10 ms shifts) suggesting a stronger motor component).

3.3.2.2 Phases: Regression in Different Phases of the Behavior. The regression was most successful for the reaching part of the behavior. For the flexor, extensor, and triceps muscles, the retrieval phase was also predicted with

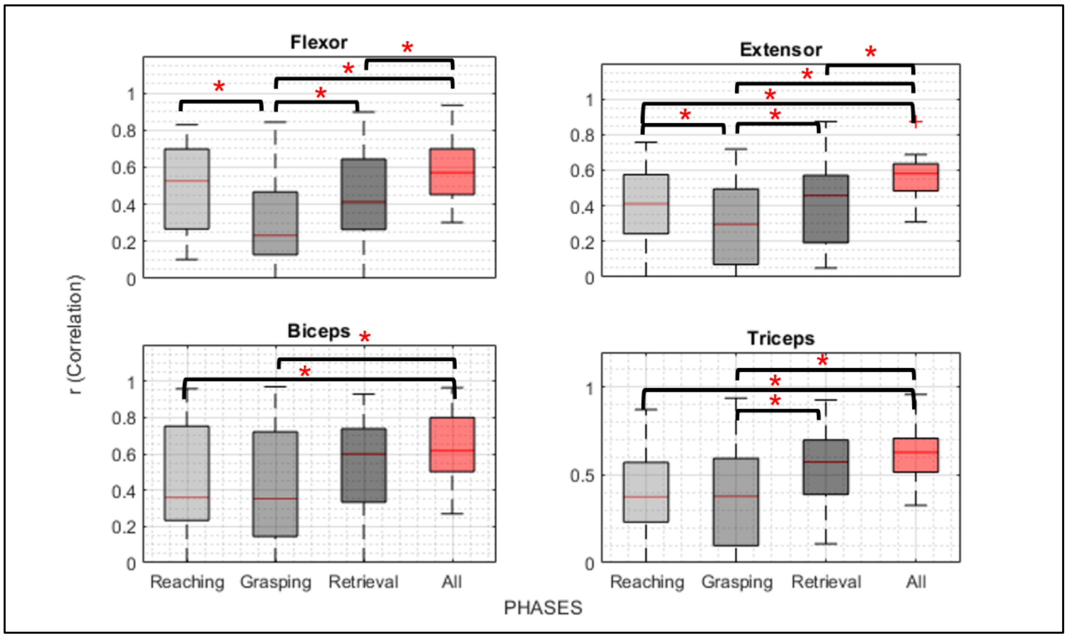

Figure 3.22 Regression for individual phases of the behavior and the entire behavioral window (“all”).

better than the grasping phase (paired t-test, for flexor, for extensor p=0.04, p=0.03, and for triceps p=0.02). For the biceps, the median values of retrieval was higher than the other two phases, but the distribution was not statistically different (paired ttest for reaching vs retrieval p=0.66; for grasping vs retrieval p=0.43) . For flexor and extensor, the difference between reatrieval and grasping phases were also significant (paired t-test, p=0.02 and p=0.05 respectively). However, in general, the best regression results were achieved when all the phases were included in the prediction. For the biceps and triceps, the difference between the reaching and including “all” phases were significant (paired t-test, p=0.01 and p=0.003, respectively), so was grasping and “all” for both muscles (paired t-test p=0.01 and p=0.001). For extensor, “all” was significantly higher than each of phases (reaching vs. “all”, paired t-test, p=0.003; grasping vs. “all”, paired ttest, p=4.6e-05; and retrieval, paired ttest, p=0.01). Lastly, for the flexor muscle, “all” was higher than both grasping and retrieval, again significantly (paired t-test p=0 and p=0.03).

3.3.2.3 Regression Using Different Pairing of Differential Channels. The regressions of the flexor showed the highest success with the configuration in

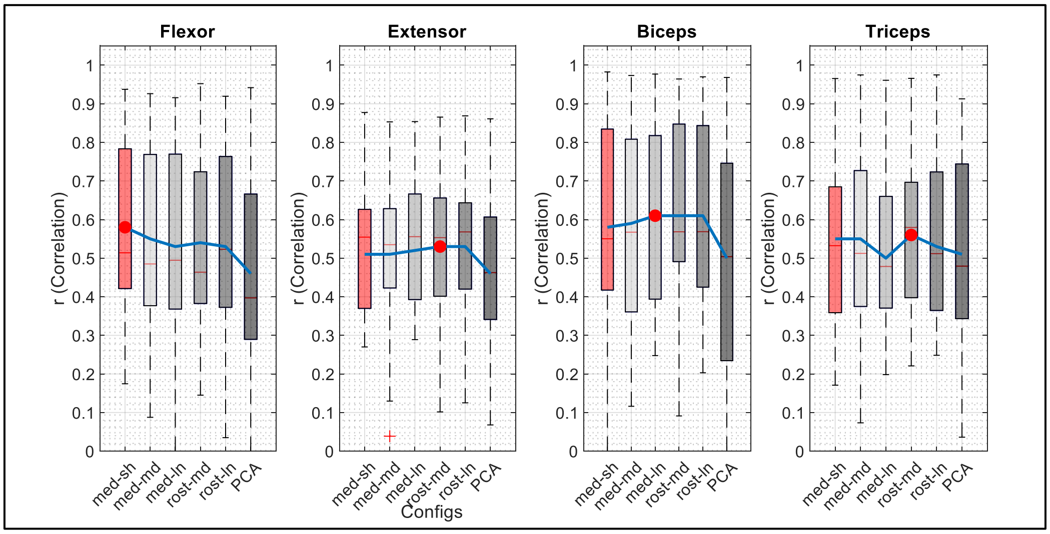

Figure 3.23 Comparison of differential channel configurations pairing the neural channels in different orientations and by varying pitch. Red bar (medio lateral-short) is the configuration used in all other analysis. (med-sh: medio lateral-short; med-md: medio lateral-medium; med-ln: medio lateral-long; rost-md: rostra caudal-medium; rost-ln: rostra caudal-long).

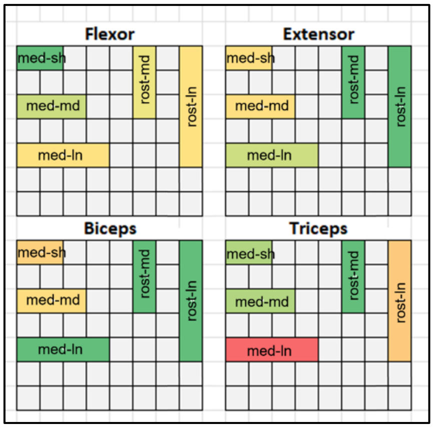

Figure 3.24 Heat map visual representation of the differences in configurations based on their topographical alignment. Red to yellow to green representing respectively lowest to highest.

which differentials of neural channels were taken in the medio lateral direction with the shortest distance (one inter-electrode pitch). For other muscles *rostra caudal- short* resulted in slightly higher values even though the differences in general were not significant. For all muscles, the results were lowest for PCA, except for the triceps in which it was the second lowest. For the biceps, the difference between PCA and *rostra caudal* was trending to be significant (t-test p=0.1).

3.3.2.4 Clustering for Detection of Patterns in Neural, Electromyogram, and Force Data. When the average of EMG envelopes from the entire data set (10 animals with 8 sessions, over 1000 trials) was taken, the overall EMG pattern showed a surge in the reaching phase in all four muscles. The EMGs declined in the grasping phase and reescalated in retrieval, but this second increase was

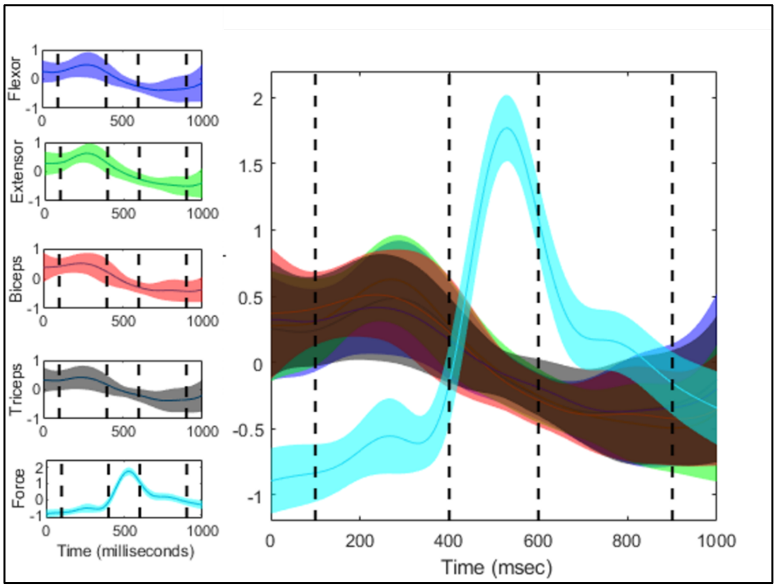

Figure 3.25 Averages and standard deviations of force, EMG, and neural data from all animals and sessions are shown for detection of dominant patterns.

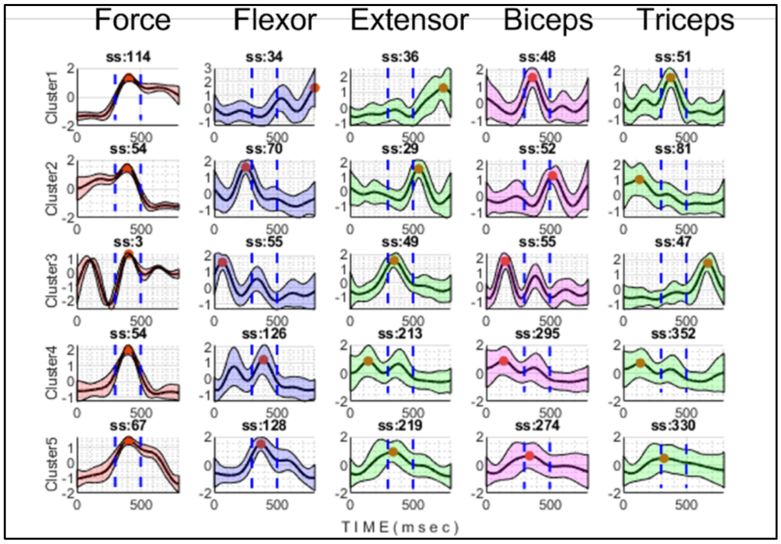

Figure 3.26 Force and 4 EMG envelopes clustered in 5 clusters each. Each has a unique pattern during the behavior. Number of trials in each cluster is shown above the plots.

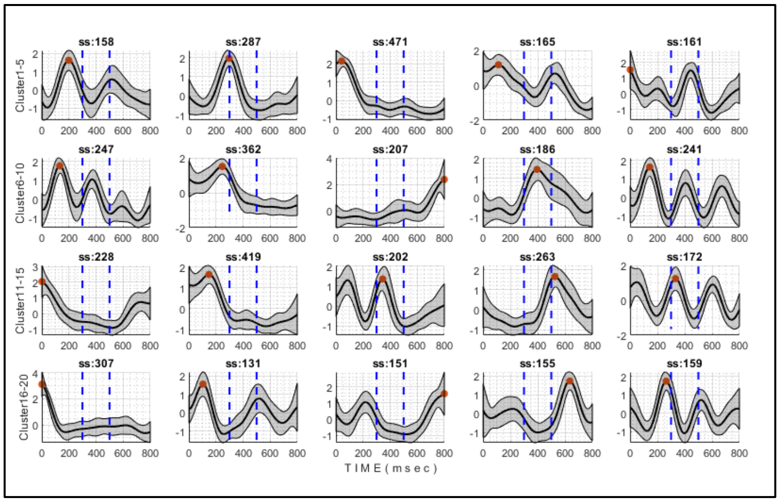

Figure 3.27 Neural envelopes clustered into 20 groups to determine repeated neural patterns.

lower compared to the first surge in reaching (Figure 3.25).

The envelopes of neural, EMG, and force signals were grouped (clustered) based on the similarity of their temporal waveforms using the *kmeans* algorithm in MATLAB. For the neural and EMG signals, rather a large number of clustered had to be used in order to keep the standard deviations low in each cluster. This is due to large variations in the neural and EMG patterns across trials and animals. However, some patterns emerged, when the data from the best performing animal (r= ~0.9) were clustered.

All EMG (Figure 3.26 columns 2-5) and neural signal envelopes (Figure 3.27) had clusters in which 3 surges in activity in each phase could be seen. Each of these clusters represent the activity change (increased or decreased activity) in the respective signal (neural/force/EMG) in a specific phase of the behavior.

Force data followed a rising and falling trajectory centered around grasping time as expected (Cluster4). But due to inter-animal variations, some differences were seen. Cluster1 and Cluster2 possibly represent the behaviors in which animals keep holding the force bar longer than average, which happened because the animals were not conditioned to a cue (e.g., sound) to release the bar. Cluster5 may represent the animals that were slow performers. Cluster3 represents multiple attempt trials that happened only in 3 trials in 292 trials.

For each muscle, there were clusters that had peaks in each phase.

Out of 20 neural clusters, interestingly 10 of the clusters peaked during reaching, 2 at the beginning of grasping window, 2 during grasping, 2 at the end of the grasping, and the last 2 during retrieval.

3.3.2.5 Contributions of Different Frequency Bands to Electromyogram Prediction and Mutual Information.

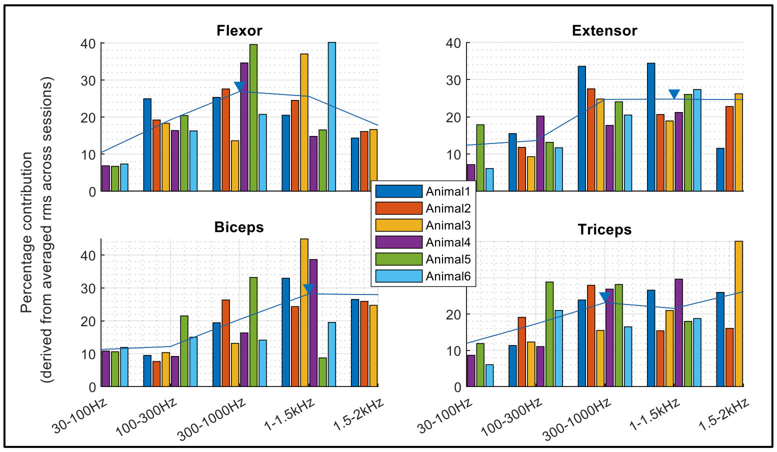

Figure 3.28 Contributions of neural signals in different frequency bands to the predicted EMG envelope signals. All four sessions are included in the data.

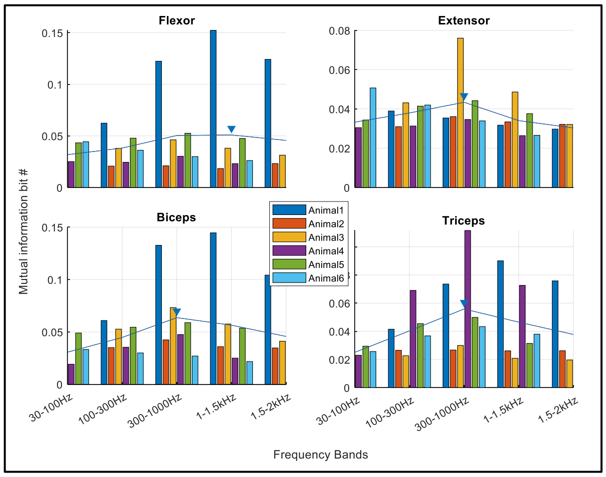

Figure 3.29 Frequency band contributions by using mutual information between EMG and neural envelopes.

3.3.2.5.1 Using Regression In general, the 30-100 Hz band was in most cases the least contributing. The 300-1000 Hz and 1000-1500 Hz bands made higher contributions.

3.3.2.5.2 Using Mutual Information Mutual information (MI) results are consistent with regression results. Again, 300 Hz to 1500 Hz frequency bands showed higher MI between the neural and EMG envelopes. Overall, the 300-1000Hz frequency band was the most prominent for all four muscles.

3.3.2.6 Topography: Contributions of Different Channels Based on Regression. Even though differences were not statistically significant (z-scores<1.25), some regions showed weak trends. For all muscles in C2 one of

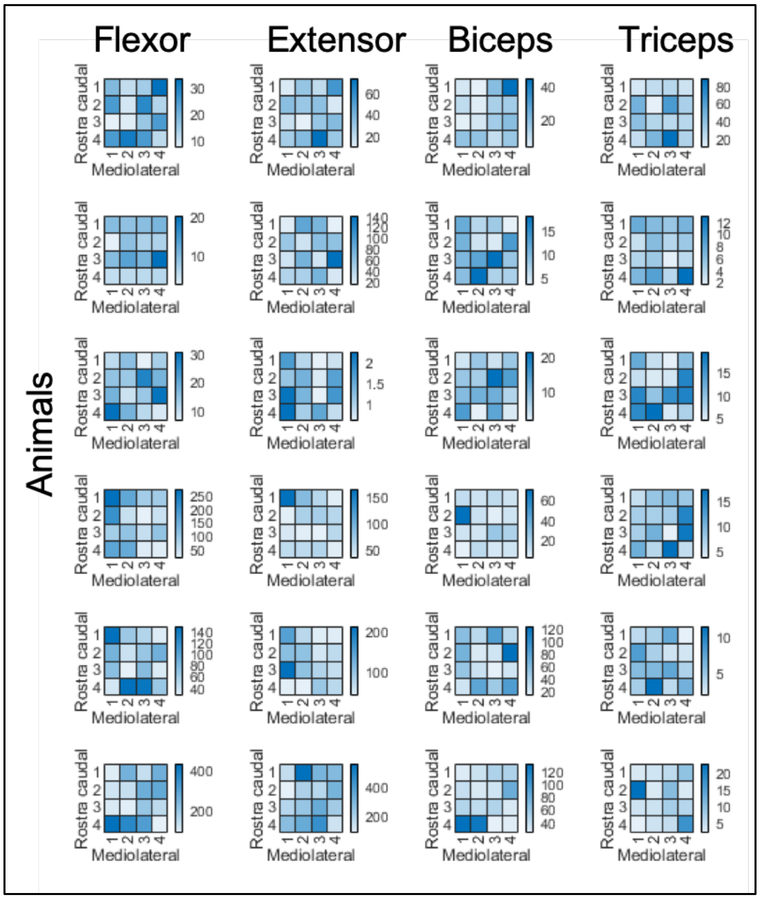

Figure 3.30 Heat maps of mean channel contributions of all animals and sessions. Scale bars show the mean (averaged over sessions) RMS values for each channel`s contribution in microvolts.

medial regions showed highest z-score compared to other three regions of the zone that imply highest contributions. Also, again in C2, there has been lowest z-scores on lateral regions of flexor and triceps muscles, which indicate lowest contributions. For all muscles the electrodes those were implanted in CX didn`t show much preference. Compared to CX, C1 had slightly higher variations in contributions among 4 quarters for extensor and triceps muscles.

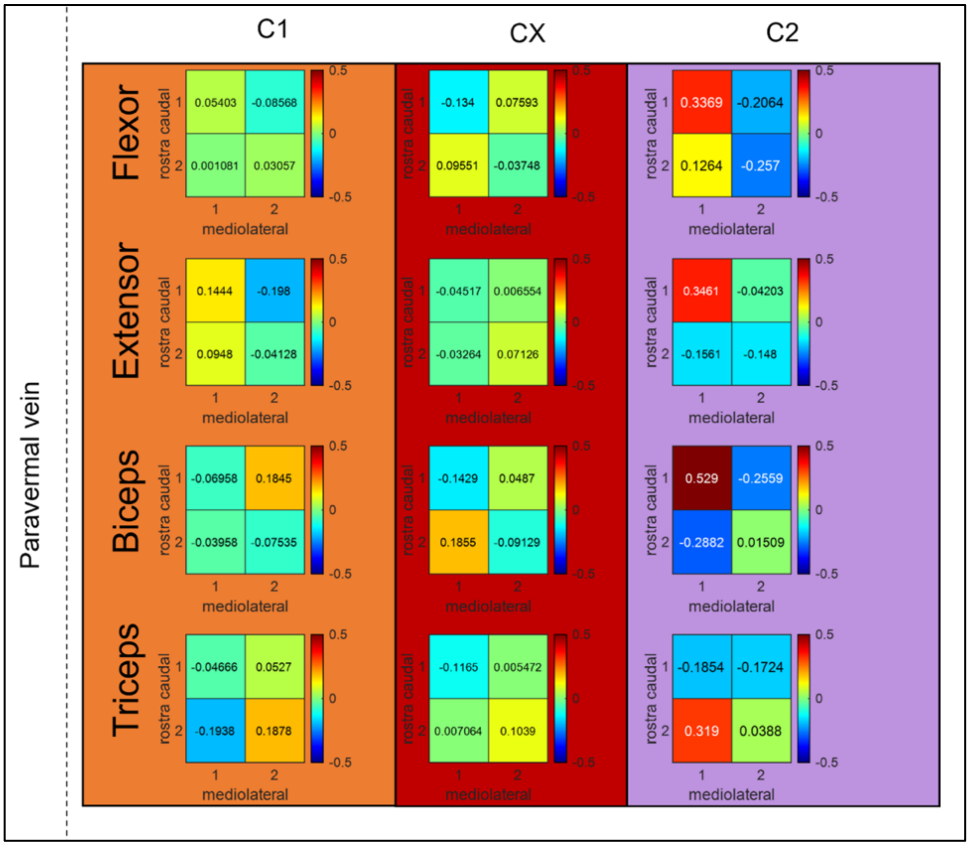

Figure 3.31 Heatmaps of z-scores for the neural signal contributions to EMG predictions in each quadrant of the arrays. From the 1st row to the last row: flexor, extensor, biceps, and triceps.

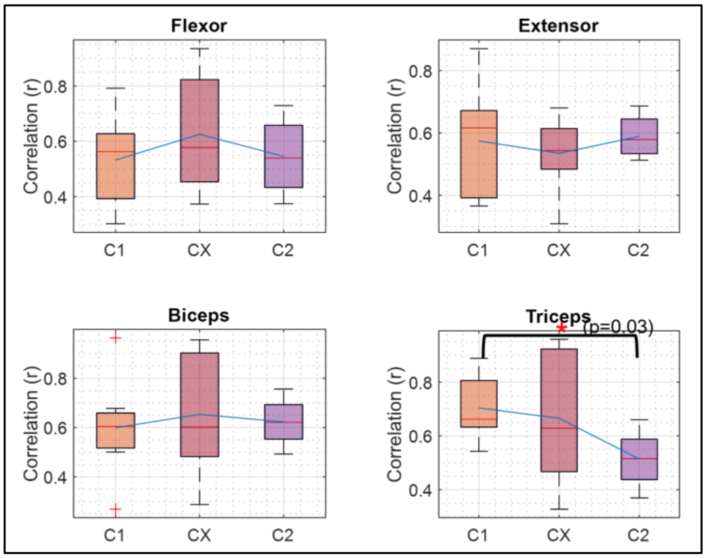

Figure 3.32 Comparisons of different zones in terms of their success (correlation in prediction). Only for the triceps muscle, C1 showed significantly higher success than C2.

3.3.2.7 Principal Component Analysis. The number of PCs that were representing the 80% variance in the data ranged from 4 to 17. But for most of the cases the first three PCs had the largest variances (Figure 3.33).

3.3.2.8 Finding the Center of Behavioral Window. Using the time point at which the force reaches its maximum as the center of the behavioral window produced the best predictions. For extensor and triceps muscles, the correlations with Force-Max were significantly higher than the Force-onset and User-Picked methods (paired t-test p=0.04 and p=0.05).

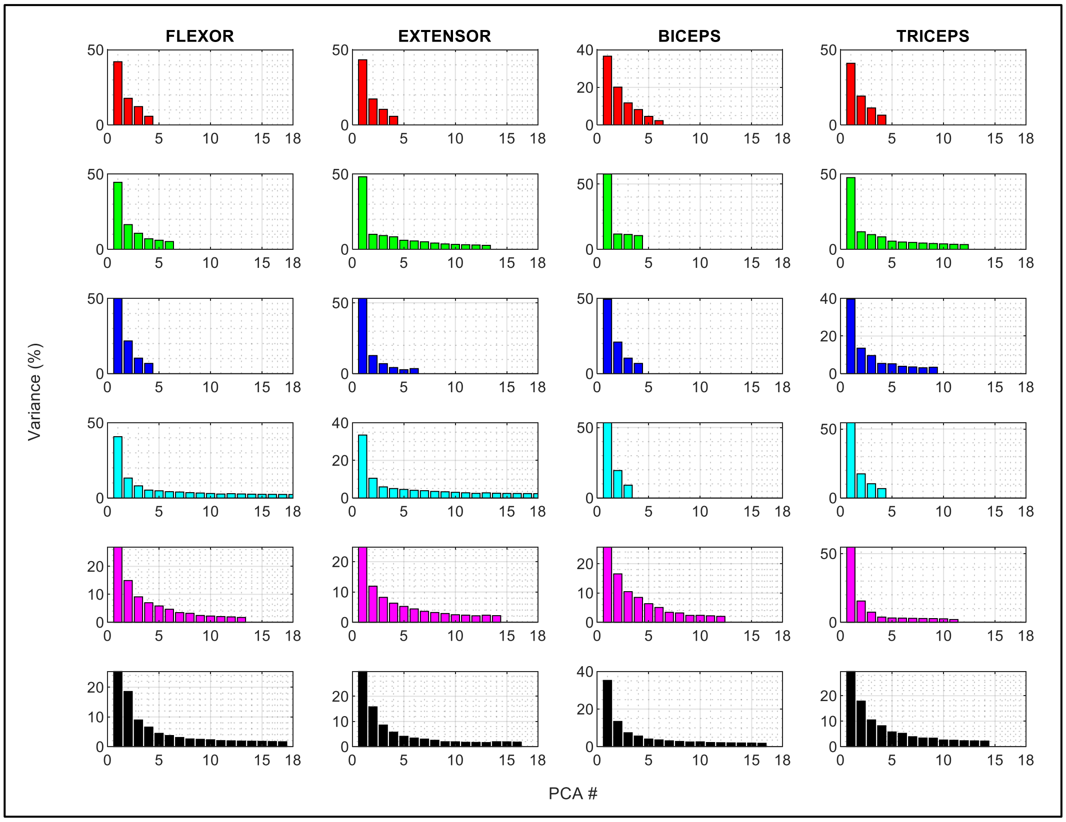

Figure 3.33 The principal components of the neural signals that accounted for 80% of the variance in the EMG data. 1st PC was removed, PCs are shown starting from the second PC.

3.4 Discussion

In this study, we recorded the neural data with multi-channel electrode arrays with the motivation that a higher sample size can reveal and add new information to our knowledge of the cerebellar involvement in behavior. Rather than targeting spiking activity from single cells, we recorded MUA with these arrays to sample activity from a larger population of neurons. This study in that respect is unique compared to most other work in the past that primary recorded from a small number of individual cells in each animal subject. It should be noted that the recorded signals may contain activity not only from PCs but also from other neuronal types in the cerebellar cortex. The electrode lengths were made such that most of the electrode tips would end up in or near the PC layer. Considering that most of the interneurons are closer to the pia mater, and that the PCs are the largest cells in the cerebellar cortex, we expect that the recorded signals to primary contain the PC activity.

3.4.1 Predictions

The correlations between the predicted and the measured muscle signals

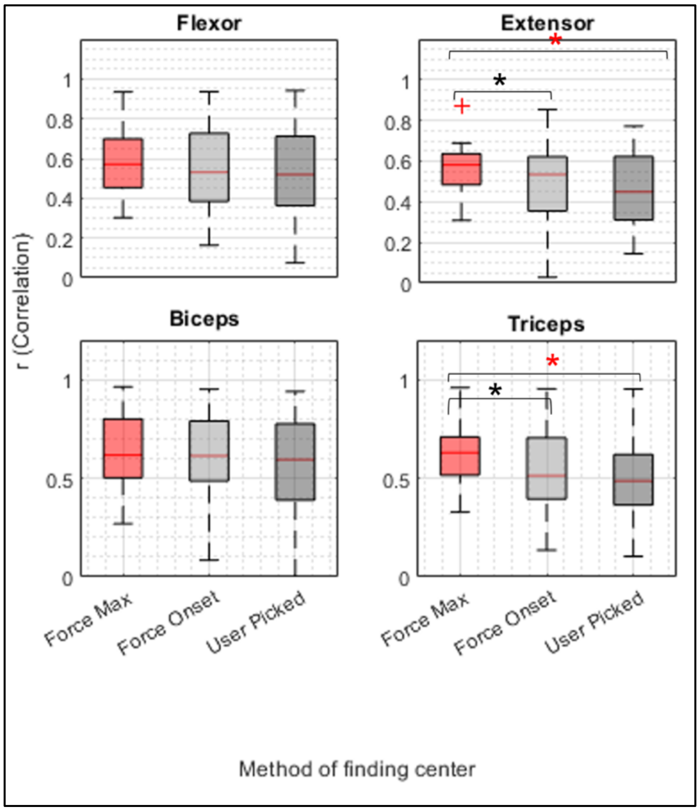

Figure 3.34 The effect of using different methods to determine the center of the behavior. The differences between Force Max were significantly higher than User Picked for extensor and triceps muscles. For the same muscles Force Max`s difference from Force Onset were not significant but trending to be significant (paired t-test p=0.1 for extensor and p=0.1 for triceps).

suggest presence of forelimb related information in the PML cortex of the cerebellum. For some animals the regression algorithm predicted signals with correlations as high as 0.8 on average in multiple sessions/days, however some others showed poor correlation results. The low prediction performance can be attributed to the possible involvement of the multizonal cerebellar activity for the same function (Aoki, Coulon, and Ruigrok 2019) or the neural trauma induced by the implant surgery.

3.4.2 Time Shifts

Shifts the neural signal in time with respect to EMG in both motor and sensory directions lowered the performance but stayed above the chance level. This was shown by regression and also with mutual information between the neural and EMG signals. To test if there was any effect of the 5 Hz envelope filter on the correlations, the analysis was repeated with 10 Hz and confirmed that the correlations observed with time shifts were not simply due to the smearing of data in time (memory effect) by the low-pass filter.

These results can be interpreted as PML carrying both sensory and motor information, which agrees with reports on cerebellar neuroanatomy.

The cerebellar cortical region implanted in this study included the intermediate zones of the cerebellum that is involved in integration of sensory inputs with motor commands to coordinate execution of motor function (Knierim 2020). Hence, correlations in the predicted signals showing both motor and sensory contents is in agreement with this information.

The intermediate cerebellum that projects to the interpositus nucleus has been shown to have a closed-loop circuits with the motor cortex and help correct the error in movement execution while the lateral cerebellum, projecting to the lateral nucleus, is involved rather in movement planning. However, studies later showed that multiple cortical areas may have parallel projections to the cerebellum and the functional distinction between the interpositus and lateral nuclei is not so clear (for review see (Lang 2015)). The findings of our study as well suggest that intermediate cerebellum in PML may receive both sensory signals ascending from the periphery and descending signals from various sensorimotor areas of the cerebrum.

Additionally, Richard Apps` 2018 study (Apps et al. 2018) points out the fact that most of the cerebellar C zones have projections to somatosensory cortex besides the primary and secondary motor cortices. Especially the CX zone, where most of our electrodes were implanted, has strong connections with both primary and somatosensory cortex in the cited study.

3.4.3 Phases of Forelimb Reaching

This analysis revealed that the algorithm can predict the reaching and retrieval behaviors in general better than grasping. But, all EMGs were predicted more successfully when the entire behavioral window was used.

The cerebellum is known to represent timing information for volitional motor movements. It has been shown that the cerebellum is involved mostly in initiation and termination phases of the movement (Gaffield, Sauerbrei, and Christie 2022). Our findings in the PML support this idea since the correlation of prediction for initial and termination segments of the behavior is higher than the middle.

Even though earlier studies mostly assigned a role to the lateral cerebellum for initiation of the behavior and intermediate cerebellum for termination, later studies have actually shown more widespread and overlapping assignments of the cerebellar regions to the timing of the behavior (Lang 2015). Our findings showed increased regression success at both initiation (reaching) and termination (retrieval) phases for flexor and extensor muscles, while for triceps muscle only increased its activity in the termination phase.

The highest correlations seen when all phases of the behavior are included in the analysis can be due to the fact that inclusion of the entire behavior provides more information to the regression algorithm including some repeated patterns that are not captured in smaller sections of the behavior.

3.4.4 Alternative Contact Configurations

Our current understanding of the cerebellar circuits suggests that the information between different zones that are aligned in sagittal planes should be correlated less compared to the activities sampled within the same sagittal plane. Thus, one can expect to observe richer information from an electrode array when differentials of the recording channels are taken in the medio lateral direction, which should also lead to higher success in behavioral prediction. For one of the muscles (flexor), predictions were most successful in the medio lateral (shortest pitch) configuration, in agreement with the statement above.

However, interestingly, for all other muscles differentials in rostra caudal direction performed higher, although the difference between any configuration pair was not significant. This result suggests that the effect of electrode pair selection was not important for the success of predictions. Thus, the smallest inter-electrode pitch, about 68-100 μm, in this study was sufficient to sample the cortical activity from non-overlapping regions in terms of their content related to the forelimb function.

Additionally the synchrony between different microzones is a transient activity which takes place for only about a few tens of milliseconds (Zeeuw and Romano 2022). This short-lived activity may not reflect on the MUA when their envelopes are taken. This can be the reason for the differential neural signals in the medio lateral direction not producing more successful prediction results.

PCA produced slightly lower correlations, but again, not significantly different than the differential channels. This lack of higher success with PCA may be due to exclusion of the first PC or the channels that accounted for the remaining 20% of variance in the neural signals that could contain some useful neural components. The synchrony in the cerebellum is proposed as the key mechanism for timing of the motor output (Gruijl, Hoogland, and Zeeuw 2014). There is a possibility that the synchronous activity between the channels is contained in the PCs that were excluded from the predictions.

3.4.5 Clusters of Patterns

Clustering of force traces was useful to separate the behavior into classes with different patterns, as in some cases the animal released the force bar later than usual, while in others the force reached the threshold slower. But, at the same time, these variations in the reaching behavior probably made the regression analysis more robust by expanding the parameter space visited. As a result, the correlations were not very high, but insensitive to transient outliers in the data.

All four EMG traces had at least one cluster (grouped using the kmeans algorithm in MATLAB) with a surge in activity in at least one of the three phases. This implies that each one of the forelimb muscles may become active in different phases of the behavior in different trials. This suggests a large variability in recruitment of these four muscles in a restricted and relatively a simple behavior in a highly trained animal.

It has been reported that Purkinje cell activity shows variability and also some variable patterns during locomotion (Sauerbrei, Lubenov, and Siapas 2015). The population activity of PML neural signals as well shows various patterns, some mainly encoding the beginning of the behavior, some the middle, and some the end. Very interestingly all EMGs and neural data had some clusters with three bumps showing activity in multiple phases. These multiple surges in activity are in agreement with the Purkinje cell activity patterns observed during walking (Sauerbrei, Lubenov, and Siapas 2015).

Another interesting outcome about neural clusters was that 50% of the clusters (10 in 20 clusters) had their maximum points in the reaching segment of the data, six around grasping, while only two in the retrieval. This suggests that PML is much active during reaching than grasping or retrieval phases of the behavior. This may be because a fine control of the movement requires the involvement of the cerebellum as it is needed during reaching while the animal is targeting the force bar, more so than the other two phases. Since the cerebellum is seen as a timing device in sensorimotor control in the sub second range (Spencer and Ivry 2013), it makes sense that it increases its activity in the part of the behavior when precise timing is needed in the recruitment of the muscles.

In a study published in Nature (Yeom, Kim, and Chung 2020), brain mechanisms in motor control during reaching movement was analyzed and interestingly the connectivities (measured by magnetoencephalography) between most motor related regions were decreased but only cerebellum and basal ganglia connectivities were increased during reaching movement. Our study as well showed increased neural activity during reaching, suggesting the importance of cerebellar involvement in this ballistic movement

3.4.6 Frequency Band Contributions

The 300-1000 Hz frequency band, the frequency band of the multi-unit activity (MUA), contributed most to the EMG predictions, which is the targeted type of neural signals with our chronic implants. Higher frequency components (1000-1500 Hz) that are also within the MUA band contributed to the predictions also even though their contributions were not as high as that of the 300-1000 Hz band. Lower contributions from the 100-300 Hz band suggest that most of the information is contained in the spiking activity of the neurons rather than the local field potentials that contain synaptic signals.

3.4.7 Channel Contributions

The C zones in the PML projects to the interposed nuclei (IPN) (Apps et al. 2018). And IPN contributes to the spatial and temporal characteristics of coordination to execute the function in trained forelimb reach movements (Milak et al. 1997). In our study, the activity captured from C zones during a trained behavior showed correlations with biceps and triceps muscle activity, confirming previous studies. However, higher resolution conclusions require more intense work.

3.4.8 Principal Component Analysis Variance

The results of PCA show that in some datasets it was as many as 17 PCs that represent the data. This suggests that the data had multiple neural sources and thus a rich content. On the other hand, these cases may also show no neural source at all, and only uncorrelated noise sources from different contacts. However, this should not be the case since these signals predicted EMG signals with correlations higher than the change level. In most cases, however, only two or three components accounted for 80% variation in the data. This suggests that removing the first PC effectively eliminated the common mode signal and the neural sources were contained in the few PCs after the first.

3.4.9 Method of Finding Behavior Center

Based on results, using the maximum time point of the force was a better choice than using the other two methods. Moreover, the User-picked method potentially has human errors in deciding the behavioral phased based on visual inspection of the EMGs. That is, EMG signals do not always appear to be very reproducible and it is hard to predict in which part of the behavior they should normally appear.

CONCLUSION

The nature of the cerebellar information processing and the localization of different functions on the cerebellar cortex are still not well understood, which is also the reason why the cerebellar contribution to motor function is underappreciated. In this study, we aimed to collect data with multi-channel electrode arrays, with the motivation that a higher sample size can reveal and add new information to our knowledge of the cerebellar involvement in behavior.

The highest correlation values were not always generated from the first sessions, but rather in later sessions in some subjects. This shows electrodes were not deteriorating, but rather they were stabilizing over time, suggesting electrode longevity. CFMEAs offer comparably small electrode sizes to the PC somas. This enables neural recordings with minimum disturbance to the cells.

The cerebellum`s unique position between the cerebrum and the spinal cord, and also some of the ascending information from the spinal cord to the cerebrum relaying on the cerebellum via spinocerebellar tract before projecting onto higher order brain regions like motor and somatosensory cortices, highlights its importance in transformation and generation of information.

From our results, we conclude that volitional information can be extracted from the PML cortex of the cerebellum and this information is present in the MUA frequency band of the signals recorded with carbon microelectrode arrays in chronically implanted subjects.

REFERENCES

Aoki, S., P. Coulon, and T. J. H. Ruigrok. 2019. 'Multizonal Cerebellar Influence Over Sensorimotor Areas of the Rat Cerebral Cortex', *Cerebral Cortex*, 29: 598-614.

Apps, R., and M. Garwicz. 2005. 'Anatomical and Physiological Foundations of Cerebellar Information Processing', *Nature Reviews Neuroscience*, 6: 297-311.

Apps, R., R. Hawkes, S. Aoki, F. Bengtsson, A. M. Brown, G. Chen, T. J. Ebner, P. Isope, H. Jorntell, E. P. Lackey, C. Lawrenson, B. Lumb, M. Schonewille, R. V. Sillitoe, L. Spaeth, I. Sugihara, A. Valera, J. Voogd, D. R. Wylie, and T. J. H. Ruigrok. 2018. 'Cerebellar Modules and Their Role as Operational Cerebellar Processing Units', *The Cerebellum*, 17: 654-82.

Armstrong, D. M., and T. Drew. 1980. 'Responses in the Posterior Lobe of the Rat Cerebellum to Electrical Stimulation of Cutaneous Afferents to the Snout', *Journal of Physiology*, 309: 357-74.

Averbeck, B. B., P. E. Latham, and A. Pouget. 2006. 'Neural Correlations, Population Coding and Computation', *Nature Reviews Neuroscience*, 7: 358-66.

Becker, M., D. Calame, J. Wrobel, and A. L. Person. 2020. "Quantification of Mouse Reach Kinematics as a Foundation for Mechanistic Interrogation of Motor Control." In. bioRxiv.

Breatnach, C. S. 1975. "Sir Goldon Holmes." In *Cambridge University Press*, 194-200.

Brookhart, J. M., G. Moruzzi, and R. S. Snider. 1950. 'Spike Discharges of Single Units in the Cerebellar Cortex', *Journal of neurophysiology*, 13: 465-86.

Cajal, R. 1911. *Histologie du Système Nerveux de l'homme & Des Vertébrés* (France: Maloine).

Carlson, C., and O. Devinsky. 2009. 'The Excitable Cerebral Cortex', *Epilepsy and Behavior*, 15: 131-32.

Centers for Disease Control and Prevention, National Center for Injury Prevention and Control. 2016. "Summary Health Statistics: National Health Interview Survey, 2016." In, edited by U.S. Department of Health and Human Services.

Cetinkaya, E., S. Gok, and M. Sahin. 2018. "Carbon Fiber Electrodes for In Vivo Spinal Cord Recordings." In *40th Annual International Conference of the IEEEE Engineering in Medicine and Biology Society*. Hawai, USA.

Chen, S., G. J. Augustine, and P. Chadderton. 2016. 'The Cerebellum Linearly Encodes Whisker Position During Voluntary Movement', *Elife*, 5: e10509.

Coats, R. O., R. J. Holt, G. P. Bingham, and M. A. Mon-Williams. 2018. 'Predicting the Duration of Reach-to-Grasp Movements to Objects with Aymmetric Contact Surfaces', *Public Library of Science One*, 13.

D’Angelo, E., and S. Casali. 2012. 'Seeking a Unified Framework for Cerebellar Function and Dysfunction: From Circuit Operations to Cognition', *Frontiers in Neural Circuits*, 6: 116.

Ebner, T. J., A. L. Hewitt, and L. S. Popa. 2011. 'What Features of Limb Movements are Encoded in the Discharge of Cerebellar Neurons?', *Cerebellum*, 10: 683-93.

Fernández-Guardiola, A., E. Manni, J. H. Wilson, and R. S. Dow. 1962. 'Microelectrode Recording of Cerebellar and Cerebral Unit Activity During Convulsive After Discharge', *Experimental Neurology*, 6: 48-69.

G.Fritsch, and E.Hitzig. 1870. 'Electric Excitability of the Cerebrum (Über die Elektrische Erregbarkeit des Grosshirns)', *Epilepsy & Behavior*, 15: 123-30.

Gaffield, M. A., B. A. Sauerbrei, and J. M. Christie. 2022. 'Cerebeelum Encodes and Influences the Initiation, Performance, and Termination of Discontinuous Movements in Mice', *Elife*.

Glickstein, M., P. Strata, and J. Voogd. 2009. 'Cerebellum: History', *Neuroscience*, 162: 549-59.

Gok, S., and M. Sahin. 2019a. 'Prediction of Forelimb EMGs and Movement Phases from Corticospinal Signals in the Rat During the Reach-to-Pull Task', *International Journal of Neural Systems*, 29(7).

Gok, Sinan, and Mesut Sahin. 2019b. 'Prediction of Forelimb EMGs and Movement Phases from Corticospinal Signals in the Rat During the Reach-to-Pull Task', *Int J Neural Syst.*, 29(7).

Grafton, S. T., R. P. Woods, J. C. Mazziotta, and M. E. Phelps. 1991. 'Somatotopic Mapping of the Primary Motor Cortex in Humans: Activation Studies with Cerebral Blood Flow and Positron Emission Tomography', *Journal of neurophysiology*, 66.

Grill, W. M., S. E. Norman, and R. V. Bellamkonda. 2009. 'Implanted Neural Interfaces: Biochallenges and Engineered Solutions', *Annual Review of Biomedical Engineering*, 11: 1-24.

Gruijl, J. R. De, T. M. Hoogland, and C. I. De Zeeuw. 2014. 'Behavioral Correlates of Complex Spike Synchrony in Cerebellar Microzones', *The Journal of Neuroscience*, 34: 8937-47.

Guitchounts, G., W. A. Liberti, T. J. Gardner, and J. E. Markowitz. 2013. 'A Carbon-Fiber Electrode Array for Long-Term Neural Recording', *Journal of Neural Engineering*, 10.

Guo, Y., R. A. Foulds, S. V. Adamovich, and M. Sahin. 2014. 'Encoding of Forelimb Forces by Corticospinal Tract Activity in the Rat', *Frontiers in Neuroscience*, 8.

Han, S., J. Chu, H. Kim, J. W. Park, and I. Youn. 2017. 'Multiunit Activity-Based Real-TimeLimb-State Estimation from Dorsal Root Ganglion Recordings', *Nature Scientific Reports*.

Harmon, T. C., U. Magaram, D. L. McLean, and I. M. Raman. 2017. 'Distinct Responses of Purkinje Neurons and Roles of Simple Spikes During Associative Motor Learning in Larval Zebrafish', *Elife*.

Hebb, D. 1949. *The Organization of Behavior a Neurophysiolocal Theory* (Mahwah, N.J. : L. Erlbaum Associates).

Heck, D. H., and F. Sultan. 2002. 'Cerebellar Structure and Function: Making Sense of Parallel Fibers.', *Human Movement Science*, 12(3): 411-21.

Heck, D. H., W. T. Thach, and J. G. Keating. 2007. 'On-beam Synchrony in the Cerebellum as the Mechanism for the Timing and Coordination of Movement', *Proceedings of the Natlonal Academy of Sciences*, 104: 7658-63.

Herculano-Houzel, S. 2010. 'Coordinated Scaling of Cortical and Cerebellar Numbers of Neurons', *Frontiers in Neuroanatomy*, 4: 12.

Herndon, R. M. 1963. 'The Fine Structure of the Purkinje Cell', *The Journal of Cell Biology*, 18: 167-80.

Hewitt, A. L., L. S. Popa, and T. J. Ebner. 2015. 'Changes in Purkinje Cell Simple Spike Encoding of Reach Kinematics During Adaption to a Mechanical Perturbation', *Journal of Neuroscience*, 35: 1106-24.

Hochberg, L. R., D. Bacher, B. Jarosiewicz, N. Y. Masse, J. D. Simeral, J. Vogel, S. Haddadin, J. Liu, S. S. Cash, P. van der Smagt, and J. P. Donoghue. 2012. 'Reach and Grasp by People with Tetraplegia Using a Neurally Controlled Robotic Arm', *Nature*, 485: 372-77.

Holmes, G. 1917. 'The Symptoms of Acute Cerebellar Injuries due to Gunshot Injuries', *Brain*, 40: 461-535.

Huffman, M. L., and B. J. Venton. 2009. 'Carbon-Fiber Microelectrodes for In Vivo Applications', *Analyst*, 134: 18-24.

Khorasani, A., R. Foodeh, V. Shalchyan, and M. R. Daliri. 2018. 'Brain Control of an External Device by Extracting the Highest Force Related Contents of Local Field Potentials in Freely Moving Rats', *IEEE Transactions on Neural Systems and Rehabilitation Engineering*, 26.

Kitazawa, S., T. Kimura, and P. Yin. 1998. 'Cerebellar Complex Spikes Encode Both Destinations and Errors in Arm Movements', *Nature*, 392: 494-97.

Knierim, J. 2020. "Cerebellum." In, edited by J. Knierim. Neuroscience Online.

Kozai, T. D. Yoshida, N. B. Langhals, P. R. Patel, X. Deng, H. Zhang, K. L. Smith, J. Lahann, N. A. Kotov, and D. R. Kipke. 2012. 'Ultrasmall Implantable Composite Microelectrodes with Bioactive Surfaces for Chronic Neural Interfaces', *Nature Material*, 11.

Lang, E. J. 2015. 'Coordination of Reaching Movements: Cerebellar Interactions with Motor Cortex.' in D. H. Heck (ed.), *The Neuronal Codes of The Cereebllum* (Elsevier).

Lang, E. J., I. Sugihara, J. P. Welsh, and R. Llinas. 1999. 'Patterns of Spontaneous Purkinje Cell Complex Spike Activity in the Awake Rat', *The Journal of Neuroscience*, 19: 2728-39.

Llinas, R., and J. P. Welsh. 1993. 'On the Cerebellum and Motor Learning', *Current Opinion in Neurobiology*, 3(6): 958-65.

Marr, D. 1969. 'A Theory of Cerebellar Cortex', *The Journal of Physiology*, 202: 437-70.

Milak, M. S., V. Bracha, and J. R. Bloedel. 1995. 'Relationship of Simulataneously Recorded Cerebellar Nuclear Neuron Discharge to the Acquisition of a Complex, Operantly Conditioned Forelimb Movement in Cats', *Experimental Brain Research*, 105: 325-30.

Milak, M. S., Y. Shimansky, V. Bracha, and J. R. Bloedel. 1997. 'Effects of Inactivating Individual Cerebellar Nuclei on the Performance and Retention of an Operantly Conditioned Forelimb Movement', *The Journal of Neurophysiology*, 78: 939-59.

Mirfathollahi, A., M. T. Ghodrati, V. Shalchyan, and M. R. Daliri. 2022. 'Decoding Locomotion Speed and Slope from Local Field Potentials of Rat Motor Cortex', *Elsevier Computer Methods and Programs in Biomedicine*, 223.

Napper, R. M. A., and R. J. Harvey. 1988. 'Number of Parallel Fiber Synapses on an Individual Purkinje Cell in the Cerebellum of the Rat', *The Journal of Comparative Neurology*: 168-77.

Orozco, E. A., R. B. Jiménez, J. L. C. Álvarez-Tostado, W. Vogt, and G. Rivera Silva. 2010. 'The Specific Origin of the Simple and Complex Spikes in Purkinje Neurons', *The Journal of Physiology*, 588: 3853-53.

Patel, P. R., N. A. Kotov, E. Yoon, C. A. Chestek, K. Na, H. Zhang, and T. D. Y. Kozai. 2015. 'Insertion of Linear 8.4 μm Diameter 16 Channel Carbon Fiber Electrode Arrays for Single Unit Recordings', *Journal of Neural Engineering*, 12.

Patel, P. R., M. T. Robbins, M. J. Kobylarek, N. A. Kotov, C. A. Chestek, H. Zhang, J. B. Nofar, S. P. Marshall, and T. D. Y. Kozai. 2016. 'Chronic In Vivo Stability Assessment of Carbon Fiber Microelectrode Arrays', *Journal of Neural Engineering*, 13.

Phillips, C. G., and R. Porter. 1977. 'Corticospinal Neurones. Their Role in Movement', *Monographs of the Physiological Society*: v-xii, 1-450.

Popa, I. S., M. L. Streng, and T. J. Ebner. 2017. 'Long-Term Predictive and Feedback Encoding of Motor Signals in the Simple Spike Discharge of Purkinje Cells', *eNeuro*, 4.

Potts, M. B., H. Adwanikar, and L. J. Noble-Haeusslein. 2009. 'Models of Traumatic Cerebellar Injury', *Cerebellum*, 8: 211-21.

Prasad, A., and M. Sahin. 2012. 'Can Motor Volition be Extracted from the Spinal Cord?', *Journal of NeuroEngineering and Rehabilitation*, 9: 41.

Rapoport, M. 2000. 'The Role of the Cerebellum in Cognition and Behavior: A Selective Review', *The Journal of Neuropsychiatry Clinical Neurosciences*, 12(2): 193-8.

Rolls, G. 2022. "An Introduction to Decalcification." In, edited by G. Rolls. Leica Biosystems.

Rylkova, D., A. R. Crank, and D. J. Linden. 2015. 'Chronic In Vivo Imaging of Ponto-Cerebellar Mossy Fibers Reveals Morphological Stability during Whisker Sensory Manipulation in the Adult Rat', *eNeuro*, 2.

Sauerbrei, B., E. Lubenov, and A. Siapas. 2015. 'Structured Variability in Purkinje Cell Activity During Locomotion', *Elsevier ScienceDirect Journals Complete*, 87: 840-52.

Schwartz, A. B. 2007. 'Useful Signals from Motor Cortex', *Journal of Physiology*, 579: 581-601.

Sedaghat-Nejada, E., J. S. Pia, P. Hagea, M. A. Fakhariana, and R. Shadmehra. 2022. 'Synchronous Spiking of Cerebellar Purkinje Cells During Control of Movements', *Proceedings of National Academy of Sciences of United States of America*, 119.

Spencer, R. M. C., and R. B. Ivry. 2013. 'Cerebellum and Timing.' in M. Manto, D. L. Gruol, J. D. Schmahmann, N. Koibuchi and RF. Rossi (eds.), *Handbook of the Cerebellum and Cerebellar Disorders* (Springer Science+Business Media: Dordrecht).

Strata, P. 2009. 'David Marr’s Theory of Cerebellar Learning: 40 years Later', *The Journal of Physiology*, 587: 5519-20.

Streng, M., L. S. Popa, and T. J. Ebner. 2017. 'Climbing Fibers Control Purkinje Cell Representations of Behavior', *The Journal of Neuroscience*, 37: 1997-2009.

Thach, W. T. 1968. 'Discharge of Purkinje and Cerebellar Nuclear Neurons During Rapidly Alternating Arm Movements in the Monkey', *Journal of neurophysiology*, 31(5): 785-97.

Therrien, A. S., and A. J. Bastian. 2019. 'The Cerebellum as a Movement Sensor', *Neuroscience Letters*, 688: 37-40.

Viswam, V., M. E. J. Obien, F. Franke, U. Frey, and A. Hierlemann. 2019. 'Optimal Electrode Size for Multi-Scale Extracellular-Potential Recording From Neuronal Assemblies', *Frontiers in Neuroscience*, 13.

Wang, C., TY. Xiao, E. Burdet, J. Gordon, and N. Schweighofer. 2016. 'The Duration of Recahing Movement is Longer than Predicted by Minimum Variance', *The Journal of Neurophysiology*, 116: 2342-45.

Welle, E. J., P. R. Patel, J. E. Woods, A. Petrossians, E. della Valle, A. Vega-Medina, J. M. Richie, D. Cai, J. D. Weiland1, and C. A. Chestek. 2020. 'Ultra-Small Carbon Fiber Electrode Recording Site Optimization and Improved In Vivo Chronic Recording Yield', *Journal of Neural Engineering*, 17.

Wellman, S. M., J. R. Eles, K. A. Ludwig, J. P. Seymour, N. J. Michelson, W. E. McFadden, A. L. Vazquez, and T. D. Y. Kozai. 2018. 'A Materials Roadmap to Functional Neural Interface Design', *Advanced Functional Materials*, 28: 1-1.

Welsh, J. P., E. J. Lang, I. Suglhara, and R. Llinas. 1995. 'Dynamic Organization of Motor Control Within the Olivocerebellar System', *Nature*: 453-57.

Woolsey, C. N. 1958. 'Organization of Somatic Sensory and Motor Areas of the Cerebral Cortex. In: The Biological and Biochemical Bases of Behavior.' in H. F. Harlow and C. N. Woolsey (eds.) (University of Wisconsin Press: Madison, WI).

Yeom, H. G., J. S. Kim, and C. K. Chung. 2020. 'Brain Mechanisms in Motor Control During Reaching Movements: Transition of Functional Connectivity According to Movement States', *Nature Scientific Reports*, 10.

Zeeuw, C. I. De, F. E. Hoebeek, L. W. J. Bosman, M. Schonewille, L. Witter, and S. K. Koekkoek. 2011. 'Spatiotemporal Firing Patterns in the Cerebellum', *Nature Reviews Neuroscience*, 12: 327-44.

Zeeuw, C. I. De, and V. Romano. 2022. 'Time and Tide of Cerebellar Synchrony', *Proceedings of National Academy of Sciences of United States of America*, 119.